Quantum Multiple Scattering:

Correspondence between Particle and Photon Scattering

A thesis presented

by

Sheng Li

to

The Department of Chemistry and Chemical Biology

in partial fulfillment of the requirements

for the degree of

Doctor of Philosophy

in the subject of

Chemical Physics

Harvard University

Cambridge, Massachusetts

June, 2003

Abstract — **Quantum Multiple Scattering:**

Correspondence between Particle and Photon Scattering

Sheng Li, June 2003

Thesis advisor: Prof. Eric J. Heller

This thesis discusses the quantum multiple scattering theory of both particle and photon scattering. Chapter 1 provides the outline. Chapter 2 discusses particle scattering by a group of s-wave point scatterers. We present the eigenchannel expansion method, which is based on the Green's function between scatterers and takes into account all orders of multiple scattering effects. Its application to particle scattering by small samples of scatterers, especially the proximity resonance phenomenon, is discussed. Chapters 3 and 4 discuss superradiance — collective spontaneous emission by a group of atoms in radiation field. The discussion is based on the effective dissipative Hamiltonian, which includes the generalized dipole-dipole interaction between atoms. Chapter 5 discusses photon scattering by a group of point two-level atoms in ground state. It can be formulated under either the multiple scattering view or the effective Hamiltonian view. The two views are

equivalent, because the Green's function between atoms is closely related to the generalized dipole-dipole interaction. Particle scattering by scatterers can also be formulated under these two equivalent views. There is one-to-one correspondence between particle scattering by a group of s-wave point scatterers and photon scattering by a group of point two-level atoms in ground state. In Chapter 5, we also discuss proximity resonance in photon scattering by small samples of atoms. Chapter 6 explores both particle and photon scattering by large random lattices of scatterers and atoms.

To my grandma

To be a sailor of the world, bound for all ports,

. . .

— Walt Whitman

"A Song of Joys", *Leaves of Grass*

To be a photon coherent, bound for all atoms.

Acknowledgments

This thesis would not be possible without my advisor, Rick Heller, who has led me to many hidden beauties of the quantum world and is always a great source of inspiration. I thank Jesse Hersch, a previous member of the Heller group, for helping me get started on multiple scattering. I also thank Susanne Yelin at the Institute for Theoretical Atomic and Molecular Physics (ITAMP), for many fruitful conversations on atom-photon interactions. I would also like to thank Profs. Misha Lukin and S.-T. Yau for discussions. As my thesis committee members, Prof. Roy Gordon has given many insightful comments on my thesis, and Prof. David Reichman has always tended to my research. I remember Suse Broyde, my previous advisor at New York University, for understanding my choice of career path.

I am grateful to many previous and current Heller group members, who together make this group vibrant and diversified. Being in this group, I have also been able to take advantage of resources from many places, such as the Harvard Physics and Chemistry Departments, ITAMP, and the Harvard-MIT Center for Ultracold Atoms (CUA). I am happy to share the work space with my officemates, many of whom are from other research groups.

Friends, new and old, have made my life colorful and have shared my high and low times here. To this vein, Xiaohui Lü, my best friend at Harvard, deserves special mention. Friendships are always cherishable, not to mention that my old friends from China and now all over the world have made my travels more memorable. A good part of my leisure time is spent on volleyball. I am proud to be a member of the Intermetallics team, speaking of both the team-spirit and the competence level.

Lastly, a special thank you to my parents, who, at the other side of the Pacific, are always supportive of me.

Works Published Elsewhere

Parts of this thesis have been and will be published elsewhere.

S. Li and E.J. Heller, *Quantum multiple scattering: eigenmode expansion and its applications to proximity resonance*, Phys. Rev. A **67** 032712 (2003).

S. Li and E.J. Heller, *Title to be decided — On the correspondence between particle and photon scattering*, to appear in Phys. Rev. A.

Contents

List of Figures

List of Tables

Chapter 1

Introduction

This thesis has been the fruit of two initially separate research topics.

One research topic is quantum scattering of a massive particle by a group of scatterers. Examples are electron or phonon scattering by defects or impurities in crystal. When neighboring scatterers are proximate, i.e., distances between them are much smaller than the wavelength of incident particle in resonance, we cannot neglect multiple scattering effects — scattered wave from one scatterer can be scattered again by another scatterer. Green's functions between different scatterers can be used to take into account multiple scattering effects.

In Chapter 2, we present the eigenchannel expansion method for the

particle multiple scattering problem, which is based on Green's function, and its applications to proximity resonance. Proximity resonances occur in scattering by small samples, where all scatterers are proximate to each other.

The other research topic is quantum coherent interaction between a group of atoms (or molecules) and radiation field. In the past few years, there have been significant advances in the cooling and trapping of atoms. In high density atomic clusters, neighboring atoms are proximate, i.e., distances between them are much smaller than the wavelength of a photon in resonance with a particular atomic transition. Atoms in the cluster interact coherently with the radiation field.

Chapters 3 and 4 discuss one particular phenomenon of coherent interaction — superradiance, which means coherent spontaneous emission by a group of atoms. In Chapter 3, we derive the master equation for the evolution of atomic variables in vacuum radiation field. The evolution of atoms is governed by an effective Hamiltonian, which includes generalized dipole-dipole interactions between different atoms. Implications of the master equation, including its relation to the Dicke model of superradiance, are discussed. In Chapter 4, we further derive the spontaneous emission spectrum, i.e., the final distribution of photons. A large portion of the contents in Chapters

Table 1.1: Two problems, each in two views, discussed in this thesis.

	particle scattering by scatterers	photon scattering by atoms
multiple scattering view	I	III
effective Hamiltonian view	IV	II

3 and 4 do not go much beyond known literature by other authors. These contents are necessary to establish context for our new results in these two and later chapters.

Chapter 5 discusses photon scattering by a group of atoms. A resonant photon scattering process can be thought of as absorption followed by spontaneous emission. Its formulation can be similar to that of Chapters 3 and 4. Together with Chapter 2, we have discussed the problems of particle scattering by a group of scatterers in multiple scattering point of view, and photon scattering by a group of atoms in effective Hamiltonian point of view. These two problems in two different views, originated separately from two research topics, form the diagonal elements (I and II) in Table 1.1.

The two problems, or more generally the two research topics, become

linked when we start discussing the offdiagonal elements (III and IV) in Table 1.1. Also in Chapter 5, we present the multiple scattering view for photon scattering by atoms (III). It is equivalent to the effective Hamiltonian view, because Green's function and generalized dipole-dipole interaction are closely related. By the same token, we present the effective Hamiltonian view for particle scattering by scatterers (IV). Thus, we have drawn a complete picture of correspondence between particle scattering by scatterers and photon scattering by atoms, which is the central theme of this thesis. We also discuss proximity resonance of atoms, in parallel to Chapter 2.

Throughout this thesis for consistency, we use the word "scatterer(s)" for target(s) of massive particle scattering, and the word "atom(s)" for target(s) of photon scattering. The reader should bear in mind that a "scatterer" in fact can be an atom or something else, and that an "atom" in fact can be a photon scatterer.

In Chapter 6, we discuss both particle and photon scattering by large samples, where the largest distance between scatterers/atoms are larger than the resonant wavelength of incident particle/photon. We still cannot neglect multiple scattering effects if neighboring scatterers/atoms are proximate.

Because the central theme of this thesis is correspondence between two

different topics, substantial cross references between chapters are unavoidable. Thus said, efforts have been made to make each chapter as self-contained as possible. Readers with limited time or interest should understand the relevant contents reasonably well by reading one or several chapters only. Throughout this thesis, we set $\hbar = 1$, $c = 1$, and the mass of incident particle $m = 1$.

Chapter 2

Particle Scattering by s-wave Point Scatterers

There are lots of physical processes involving scattering of waves by a group of scatterers. Examples are electrons or phonons scattering by defects or impurities in crystals and light scattering by conjugated molecules or biological complexes. Many interesting phenomena arise from multiple scattering effects — waves scattered by one scatterer can be scattered again by another scatterer, especially when neighboring scatterers are proximate.

This chapter is on quantum multiple scattering by a group of s-wave point scatterers. We introduce the s-wave point scatterer model, present the

eigenchannel expansion method for particle scattering by a group of such scatterers, and discuss its applications to proximity resonance.

2.1 Basic Quantum Scattering Theory

To begin, we briefly review some basic results in quantum scattering theory. These results can be found in standard textbooks, e.g., [1, 2].

2.1.1 Wave Matrix, S-matrix, T-matrix, and Eigenchannel

For a particle with no internal degrees of freedom, the free space Hamiltonian

$$H_0 = -\frac{1}{2}\nabla^2. \tag{2.1}$$

The total Hamiltonian

$$H = H_0 + V, \tag{2.2}$$

where V is the potential due to the presence of scatterer(s). The general equation

$$|\psi\rangle = |\phi\rangle + |\phi_s\rangle \tag{2.3}$$

describes a scattering process of the particle. $|\phi\rangle$ is the incident wave, eigenstate of H_0, also referred to as unperturbed state. $|\phi_s\rangle$ is the scattered wave. $|\psi\rangle$ is the total wave, eigenstate of H. The wave operator or wave matrix Ω is defined as $|\psi\rangle \equiv \Omega|\phi\rangle$, or

$$|\phi_s\rangle = (\Omega - 1)|\phi\rangle. \tag{2.4}$$

The scattering operator or scattering matrix or S-matrix $\mathcal{S}$ gives the transition amplitude between eigenstates of H_0 due to the influence of V:

$$\mathcal{S} \equiv \lim_{T\to\infty} e^{iH_0\frac{T}{2}} U(T) e^{iH_0\frac{T}{2}}, \tag{2.5}$$

where $U(T)$ is the time evolution operator:

$$U(T) \equiv e^{-iHT}. \tag{2.6}$$

S-matrix is unitary and only connects eigenstates of H_0 with the same energy E. Eigenstates of S-matrix are eigenchannels of the scattering potential V. Their corresponding eigenvalues are $e^{i2\delta(E)}$'s, where $\delta(E)$'s are eigen-phase angles. At each energy, eigenchannels are orthogonal to each other.

The S-matrix within the subspace of energy E can be written as

$$\mathcal{S}_E = 1 - 2\pi i\delta(E - H_0)\mathcal{T}, \tag{2.7}$$

where $\mathcal{T}$ is the transition operator or transition matrix or T-matrix. In fact,

$$\mathcal{T} = V\Omega. \tag{2.8}$$

For a plane incident wave $\phi(\boldsymbol{r}) = e^{i\boldsymbol{k}\cdot\boldsymbol{r}}$, the asymptotic form of the total wave is

$$\psi(\boldsymbol{r}) \cong e^{i\boldsymbol{k}\cdot\boldsymbol{r}} + f(\boldsymbol{k}, \hat{\boldsymbol{r}})\frac{e^{ikr}}{r} \text{ for } r \to \infty. \tag{2.9}$$

At distance r large compared to the force range of V, the scattered wave is an outgoing spherical wave with some angular dependent scattering amplitude $f(\boldsymbol{k}, \hat{\boldsymbol{r}})$. $f(\boldsymbol{k}, \hat{\boldsymbol{r}})$ satisfies the optical theorem

$$\frac{4\pi}{k}\mathrm{Im}f(\boldsymbol{k}, \hat{\boldsymbol{r}} = \hat{\boldsymbol{k}}) = \sigma(\boldsymbol{k}), \tag{2.10}$$

where the total cross section

$$\sigma(\boldsymbol{k}) \equiv \int |f(\boldsymbol{k}, \hat{\boldsymbol{r}})|^2 \, d\hat{\boldsymbol{r}}. \tag{2.11}$$

Within the subspace of energy

$$E = \frac{1}{2}k^2, \tag{2.12}$$

$f(\boldsymbol{k}, \hat{\boldsymbol{r}})$ can be regarded as the transition amplitude between the incident direction $\hat{\boldsymbol{k}}$ and the scattered direction $\hat{\boldsymbol{r}}$.

The asymptotic form of T-matrix within the subspace of energy E, T_E, can be defined as an operator acting on functions of $\hat{\boldsymbol{r}}$:

$$T_E y(\hat{\boldsymbol{r}}) \equiv \frac{k}{4\pi} \int f(k\hat{\boldsymbol{r}}', \hat{\boldsymbol{r}}) y(\hat{\boldsymbol{r}}')\, d\hat{\boldsymbol{r}}'. \tag{2.13}$$

The asymptotic form of $\mathcal{S}_E$, S_E, is related to T_E by

$$S_E = 1 + 2iT_E. \tag{2.14}$$

Note the sign convention of T_E is opposite to $\mathcal{T}$ (compare (2.7) and (2.14)). Asymptotically, eigenchannels are also eigenfunctions of T_E, with eigenvalues $\sin\delta(E)e^{i\delta(E)}$'s.

2.1.2 Partial Wave Expansion

For spherically symmetric V, e.g., by an elastic spherically symmetric scatterer placed at $\boldsymbol{r} = 0$, it is useful to expand the incident wave into spherical harmonic partial waves:

$$\begin{aligned} e^{i\boldsymbol{k}\cdot\boldsymbol{r}} &= \sum_{l=0}^{\infty} \sum_{m=-l}^{l} 4\pi i^l j_l(kr) Y_{lm}^*(\hat{\boldsymbol{k}}) Y_{lm}(\hat{\boldsymbol{r}}) \\ &\cong \sum_{l,m} 4\pi Y_{lm}^*(\hat{\boldsymbol{k}}) \frac{e^{ikr} - e^{-i(kr-l\pi)}}{2ikr} Y_{lm}(\hat{\boldsymbol{r}}), \end{aligned} \tag{2.15}$$

where we have used the asymptotic form of spherical Bessel functions:

$$j_l(kr) \cong \frac{e^{i(kr-l\pi/2)} - e^{-i(kr-l\pi/2)}}{2ikr} \text{ for } r \to \infty. \tag{2.16}$$

Each term in (2.15) is an eigenfunction of H_0. We also expand $f(\boldsymbol{k}, \hat{\boldsymbol{r}})$ into $Y_{lm}(\hat{\boldsymbol{r}})$'s:

$$f(\boldsymbol{k}, \hat{\boldsymbol{r}}) = \sum_{l,m} 4\pi f_l(E) Y^*_{lm}(\hat{\boldsymbol{k}}) Y_{lm}(\hat{\boldsymbol{r}}), \tag{2.17}$$

so the asymptotic total wave function is:

$$\psi(\boldsymbol{r}) \cong \sum_{l,m} 4\pi Y^*_{lm}(\hat{\boldsymbol{k}}) \frac{[1 + 2if_l(E)k]e^{ikr} - e^{-i(kr - l\pi)}}{2ikr} Y_{lm}(\hat{\boldsymbol{r}}). \tag{2.18}$$

Each term in (2.18) is an eigenfunction of H. Compare (2.15) and (2.18), we see that for the same incoming part of the wave function $Y_{lm}(\hat{\boldsymbol{r}})e^{-i(kr-l\pi)}/r$, the only difference in the outgoing part $Y_{lm}(\hat{\boldsymbol{r}})e^{ikr}/r$ is the factor of $1 + 2if_l(E)k$.

Each $j_l(kr)Y_{lm}(\hat{\boldsymbol{r}})$ is an eigenfunction of S-matrix with eigenvalue $1 + 2if_l(E)k = e^{i2\delta_l(E)}$. $j_l(kr)Y_{lm}(\hat{\boldsymbol{r}})$'s, or asymptotically, $Y_{lm}(\hat{\boldsymbol{r}})$'s are eigenchannels of the scatterer. In eigenchannel basis, T_E has a diagonal form:

$$\begin{aligned} T_E \;\; = \;\; & \mathrm{diag}\{\sin\delta_0(E)e^{i\delta_0(E)}, \cdots, \sin\delta_l(E)e^{i\delta_l(E)} \\ & (\text{repeat } 2l+1 \text{ times}), \cdots\}. \end{aligned} \tag{2.19}$$

The total cross section is

$$\sigma(E) = \frac{4\pi}{k^2} \sum_l (2l+1) \sin^2\delta_l(E), \tag{2.20}$$

a sum of contributions from each eigenchannel.

2.2 Scattering by a Single s-wave Point Scatterer

2.2.1 s-wave Point Scatterer Model

If the force range of the scatterer is small compared to the wavelength of the incident particle, we can assume it only scatters the s-wave component $j_0(kr)Y_{00}$: $f(\boldsymbol{k}, \hat{\boldsymbol{r}}) = f(E) = f_0(E)$. There is only one non-0 phase angle $\delta(E) = \delta_0(E)$ left and T_E is reduced to a rank 1 matrix

$$T_E = \text{diag}\{\sin\delta(E)e^{i\delta(E)}, 0, \cdots\}. \tag{2.21}$$

Note that $|f(E)|$ is of order $\sqrt{\sigma(E)}$ and can be regarded as the effective radius of the scatterer.

We further assume the force range of the scatterer is so small that it can be considered as existing only at one point. In this point scatterer model, (2.9) holds not only asymptotically, but over all space except at the position of the scatterer. Since any incident wave of energy E can be written as a superposition of plane waves $e^{i\boldsymbol{k}\cdot\boldsymbol{r}}$ with $|\boldsymbol{k}| = k$, the total wave function can be written as

$$\psi(\boldsymbol{r}) = \phi(\boldsymbol{r}) + \phi(0)f(E)\frac{e^{ikr}}{r}. \tag{2.22}$$

$\phi(0)$ is the amplitude of incident wave at the point scatterer.

2.2.2 T-matrix of a Single s-wave Point Scatterer

For a single s-wave point scatterer i positioned at $\boldsymbol{r}_i$, similar to (2.22), the total wave is

$$\psi(\boldsymbol{r}) = \phi(\boldsymbol{r}) + \phi(\boldsymbol{r}_i) f_i k G_i(\boldsymbol{r}), \tag{2.23}$$

where f_i is the scattering amplitude,

$$G_i(\boldsymbol{r}) = \frac{e^{ik|\boldsymbol{r}-\boldsymbol{r}_i|}}{k|\boldsymbol{r}-\boldsymbol{r}_i|}, \tag{2.24}$$

and for simplicity we have omitted all implicit energy dependence. $G_i(\boldsymbol{r})$ is free space Green's function:

$$(E - H_0) G_i(\boldsymbol{r}) = -\frac{4\pi}{k} \delta(\boldsymbol{r}-\boldsymbol{r}_i), \tag{2.25}$$

where the extra factor of $-4\pi/k$ is introduced so

$$\lim_{\boldsymbol{r}\to\boldsymbol{r}_i} \mathrm{Im} G_i(\boldsymbol{r}) = 1. \tag{2.26}$$

Since we know the wave function everywhere, we have the explicit form of wave operator Ω_i according to (2.4):

$$(\Omega_i - 1)\phi(\boldsymbol{r}) = f_i k G_i(\boldsymbol{r}) \phi(\boldsymbol{r}_i). \tag{2.27}$$

It can be written as

$$\Omega_i - 1 = t_i |O_i\rangle\langle I_i|. \tag{2.28}$$

$t_i = f_i k = \sin\delta_i e^{i\delta_i} = (\cot\delta_i - i)^{-1}$ is the eigenvalue of asymptotic T-matrix T_i. $|I_i\rangle$ is the eigenchannel of the scatterer:

$$|I_i\rangle = j_0(k|\boldsymbol{r} - \boldsymbol{r}_i|)Y_{00} = \frac{1}{\sqrt{4\pi}} \frac{G_i(\boldsymbol{r}) - G_i^*(\boldsymbol{r})}{2i}. \tag{2.29}$$

$|O_i\rangle$ is the outgoing part of $|I_i\rangle$:

$$|O_i\rangle = \frac{1}{\sqrt{4\pi}} G_i(\boldsymbol{r}). \tag{2.30}$$

Since

$$G_i(\boldsymbol{r}) \cong e^{-ik\hat{\boldsymbol{r}}\cdot\boldsymbol{r}_i} \frac{e^{ikr}}{kr} \text{ for } r \gg |\boldsymbol{r}_i|, \tag{2.31}$$

$$y_i(\hat{\boldsymbol{r}}) \equiv \frac{1}{\sqrt{4\pi}} e^{-ik\hat{\boldsymbol{r}}\cdot\boldsymbol{r}_i} \tag{2.32}$$

is the eigenfunction of T_i.

(2.28) is consistent with (2.27) because for any $|\phi\rangle$,

$$\langle I_i|\phi\rangle = \sqrt{4\pi}\phi(\boldsymbol{r}_i). \tag{2.33}$$

(2.23) can be rewritten as

$$|\psi\rangle = |\phi\rangle + t_i |O_i\rangle\langle I_i|\phi\rangle. \tag{2.34}$$

We can easily see the scatterer picks out only s-wave component centered at $\boldsymbol{r}_i$, $|I_i\rangle$, from the incident wave and the rank of T-matrix is 1.

2.2.3 Resonance

An s-wave scatterer whose potential V is a well with one quasibound state (Fig. 2.1) has one internal Breit-Wigner type resonance. It can be modeled as

$$f_i(E) = -\frac{1}{k}\frac{\gamma_i}{E - E_i + i\gamma_i}, \tag{2.35}$$

or

$$\cot \delta_i(E) = -\frac{E - E_i}{\gamma_i}. \tag{2.36}$$

E_i is the energy of quasibound state and γ_i is related to coupling between the quasibound state and the continuum. The total cross section has a Lorentzian shape:

$$\sigma(E) = \frac{4\pi}{k^2}\frac{\gamma_i^2}{(E - E_i)^2 + \gamma_i^2}. \tag{2.37}$$

The point scatterer model is the limit of force range (width of potential well) going to 0 while keeping E_i and γ_i constant (by adjusting the depth of the well accordingly). Discussions on zero range potentials can be found in, e.g., [3, 4, 5].

Resonance corresponds to the pole of $f_i(E)$ on complex E plane, at

$$E = E_i - i\gamma_i, \tag{2.38}$$

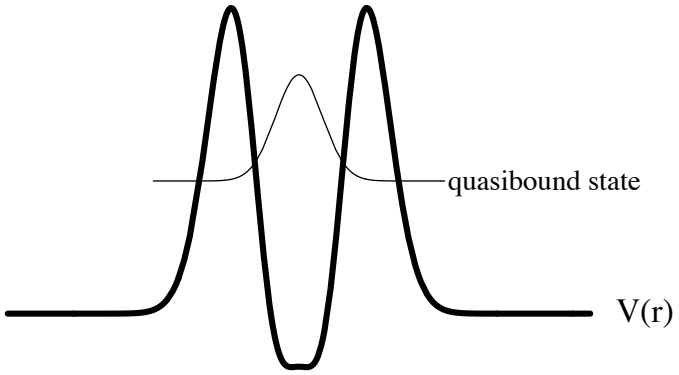

Figure 2.1: Example of a potential well which has one quasibound state and gives one internal Breit-Wigner type resonance.

where the "scattered wave" can exist without the incident wave. E_i and γ_i correspond to position and half width of the resonance peak. In phase shift picture, the phase angle monotonically increases from 0 to π as the energy increases. The position of the peak is at where $\delta_i = \pi/2$, or $\cot \delta_i = 0$. The width is determined by how fast δ_i passes through $\pi/2$ as a function of energy, or

$$\gamma_i = -1 \Big/ \left(\frac{\partial \cot \delta_i(E)}{\partial E} \Big|_{E=E_i} \right). \tag{2.39}$$

Fig. 2.2 shows σ and $\cot \delta_i$ as a function of energy for the model scatterer. Near resonance, the effective radius of the scatterer can be much larger than

the physical size (force range) of it.

2.3 Scattering by a Group of s-wave Point Scatterers

2.3.1 Green's Function and Multiple Scattering

We are now ready to tackle the problem of scattering by a group of N s-wave point scatterers fixed at positions $\boldsymbol{r}_1$, $\boldsymbol{r}_2$, $\cdots$, $\boldsymbol{r}_N$. The method used in this subsection is previously described in [5, 6]. The total wave is:

$$|\psi\rangle = |\phi\rangle + \sum_{i=1}^{N} t_i |O_i\rangle\langle I_i|\psi_i\rangle, \tag{2.40}$$

The $|\phi\rangle$ in (2.34) is replaced by $|\psi_i\rangle$ — the effective incident wave. $\psi_i(\boldsymbol{r})$ is the sum of the incident wave plus waves scattered by all other scatterers except the ith scatterer itself:

$$|\psi_i\rangle = |\phi\rangle + \sum_{j\neq i} t_j |O_j\rangle\langle I_j|\psi_j\rangle. \tag{2.41}$$

(2.41) multiplied by $\langle I_i|$ on the left provides a system of linear equations for $\langle I_i|\psi_i\rangle$. We can express them explicitly in matrix form. Define vector for

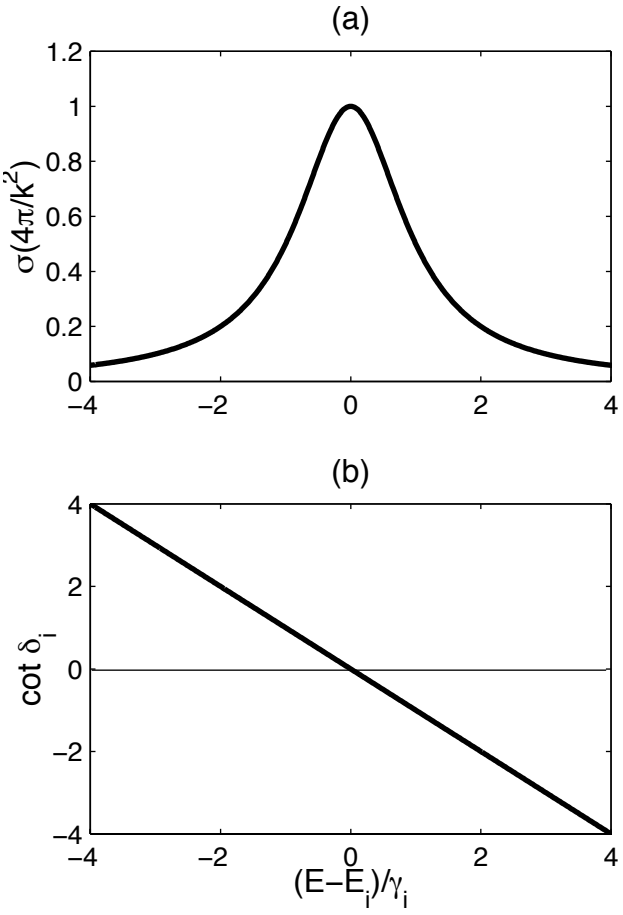

Figure 2.2: (a) Total cross section σ and (b) cotangent of phase angle δ_i as a function of energy E for an s-wave scatterer with one internal Breit-Wigner type resonance.

incident wave $\vec{\phi}$ as

$$\phi_i \equiv \langle I_i|\phi\rangle = \sqrt{4\pi}\phi(\boldsymbol{r}_i)\ (i = 1, \cdots, N) \tag{2.42}$$

and vector for effective incident waves $\vec{\psi}$ as

$$\psi_i \equiv \langle I_i|\psi_i\rangle = \sqrt{4\pi}\psi_i(\boldsymbol{r}_i)\ (i = 1, \cdots, N). \tag{2.43}$$

Define the $N \times N$ free space Green's matrix G as

$$G_{ij} \equiv \begin{cases} 0 & \text{for } i = j, \\ \langle I_i|O_j\rangle = G_j(\boldsymbol{r}_i) = \frac{1}{x_{ij}}e^{ix_{ij}} & \text{for } i \neq j, \end{cases} \tag{2.44}$$

where $\boldsymbol{x}_{ij} \equiv k(\boldsymbol{r}_i - \boldsymbol{r}_j)$, and matrix T as

$$T \equiv \text{diag}\{t_1, t_2, \cdots, t_N\}. \tag{2.45}$$

(2.41) multiplied by $\langle I_i|$ on the left is equivalent to

$$\vec{\phi} = (1 - GT)\vec{\psi}, \text{ or } \vec{\psi} = (1 - GT)^{-1}\vec{\phi}. \tag{2.46}$$

The physical implication of (2.46) is clear. Formally

$$(1 - GT)^{-1} = 1 + GT + (GT)^2 + \cdots. \tag{2.47}$$

Each term $(GT)^l$ $(l = 0, 1, \cdots)$ means the incident wave is scattered l times, since T means scattering once by one scatterer, and G means free propagation from one scatterer to another. Therefore, this formalism takes into

account all orders of multiple scattering effects. An integral equation similar to (2.46) is known in general scattering theory as the Lippmann-Schwinger equation [7].

Resonances occur at poles of $(1 - GT)^{-1}$ on complex E plane, where the "scattered wave" can exist without the incident wave.

2.3.2 Eigenchannels

How do we find the eigenchannels of such a system of N scatterers, nonsymmetric in general? For a single scatterer, the eigenchannel is $|I_i\rangle$ and the scattered wave is proportional to $|O_i\rangle$. From (2.40) we see that the scattered wave from a group of scatterers is a superposition of $|O_i\rangle$'s, so we try to write the incident wave as a superposition of $|I_i\rangle$'s:

$$|\phi\rangle = \sum_i c_i |I_i\rangle, \tag{2.48}$$

or $\vec{\phi} = B\vec{c}$, where the $N \times N$ spherical Bessel matrix B takes into account the nonorthogonality of $|I_i\rangle$'s:

$$B_{ij} \equiv \langle I_i | I_j \rangle = \int y_i^*(\hat{\boldsymbol{r}}) y_j(\hat{\boldsymbol{r}}) d\hat{\boldsymbol{r}} = j_0(x_{ij}) = \begin{cases} 1 & \text{for } i = j, \\ \mathrm{Im}G_{ij} = B(x_{ij}) & \text{for } i \neq j. \end{cases} \tag{2.49}$$

Function B, defined as

$$B(x) \equiv \frac{\sin x}{x}, \tag{2.50}$$

is the imaginary part of Green's function. We have $\vec{\psi} = (1 - GT)^{-1}\vec{\phi} = (1 - GT)^{-1}B\vec{c}$, and from (2.40), $|\phi_s\rangle = \sum_i t_i \psi_i |O_i\rangle$, we get

$$|\phi_s\rangle = \sum_i [T(1 - GT)^{-1}B\vec{c}]_i |O_i\rangle. \tag{2.51}$$

Suppose λ_α's and $\vec{q}_\alpha$'s are eigenvalues and (right) eigenvectors of $T(1 - GT)^{-1}B$:

$$T(1 - GT)^{-1}B\vec{q}_\alpha = \lambda_\alpha \vec{q}_\alpha \ (\alpha = 1, \cdots, N, \text{ and } \vec{q}_\alpha = (q_{1\alpha}, \cdots, q_{N\alpha})^T). \tag{2.52}$$

If we choose $\vec{c} = \vec{q}_\alpha$, then the incident wave

$$|I_\alpha\rangle \equiv \sum_i q_{i\alpha}|I_i\rangle = \frac{1}{\sqrt{4\pi}} \sum_i q_{i\alpha} \frac{G_i(\boldsymbol{r}) - G_i^*(\boldsymbol{r})}{2i} \cong \frac{Y_\alpha(\hat{\boldsymbol{r}})e^{ikr} - Y'_\alpha(\hat{\boldsymbol{r}})e^{-ikr}}{2ikr}, \tag{2.53}$$

where

$$Y_\alpha(\hat{\boldsymbol{r}}) \equiv \sum_i q_{i\alpha} y_i(\hat{\boldsymbol{r}}) \tag{2.54}$$

and $Y'_\alpha(\hat{\boldsymbol{r}}) = \sum_i q_{i\alpha} y_i^*(\hat{\boldsymbol{r}})$, and the scattered wave

$$|\phi_s\rangle = \lambda_\alpha \sum_i q_{i\alpha}|O_i\rangle. \tag{2.55}$$

The total wave

$$\begin{aligned} |\psi\rangle &= |I_\alpha\rangle + |\phi_s\rangle = \frac{1}{\sqrt{4\pi}} \sum_i q_{i\alpha} \frac{(1+2i\lambda_\alpha)G_i(\boldsymbol{r}) - G_i^*(\boldsymbol{r})}{2i} \\ &\cong \frac{(1+2i\lambda_\alpha)Y_\alpha(\hat{\boldsymbol{r}})e^{ikr} - Y'_\alpha(\hat{\boldsymbol{r}})e^{-ikr}}{2ikr}. \end{aligned} \tag{2.56}$$

Compare (2.53) and (2.56), we see that for the same incoming part of the wave function $Y'_\alpha(\hat{\boldsymbol{r}})e^{-ikr}/r$, the only difference in the outgoing part $Y_\alpha(\hat{\boldsymbol{r}})e^{ikr}/r$ is the factor of $1+2i\lambda_\alpha$.

Therefore, each $\vec{q}_\alpha$ or $|I_\alpha\rangle$, asymptotically $Y_\alpha(\hat{\boldsymbol{r}})$, is an *eigenchannel* of the system. $q_{i\alpha}$ is the relative amplitude of the scattered wave from ith scatterer ((2.55)). The eigen-phase angle Δ_α can be found by

$$e^{i2\Delta_\alpha} = 1 + 2i\lambda_\alpha, \text{ or } \lambda_\alpha = \sin\Delta_\alpha e^{i\Delta_\alpha}. \tag{2.57}$$

$\vec{q}_\alpha$ is real due to time reversal symmetry. Plugging (2.57) back into (2.56), the total wave

$$\psi(\boldsymbol{r}) = \sum_i q_{i\alpha} \frac{e^{i2\Delta_\alpha}G_i(\boldsymbol{r}) - G_i^*(\boldsymbol{r})}{2i}. \tag{2.58}$$

Due to time reversal symmetry, if $\psi(\boldsymbol{r})$ is an eigenfunction of H, so is $e^{i2\Delta_\alpha}\psi^*(\boldsymbol{r})$. Therefore,

$$e^{i2\Delta_\alpha}\psi^*(\boldsymbol{r}) = \sum_i q_{i\alpha}^* \frac{e^{i2\Delta_\alpha}G_i(\boldsymbol{r}) - G_i^*(\boldsymbol{r})}{2i} \tag{2.59}$$

is also a valid total wave. Compare (2.58) and (2.59), we know $\vec{q}_\alpha$ and $\vec{q}_\alpha^*$ are eigenvectors of $T(1-GT)^{-1}B$ corresponding to the same eigenvalue, so $\vec{q}_\alpha$ can be chosen real.

2.3.3 Separation of Real and Imaginary Parts of Green's Function

With the knowledge that all eigenvalues of $T(1-GT)^{-1}B$ are of the form $\sin\Delta_\alpha e^{i\Delta_\alpha} = (\cot\Delta_\alpha - i)^{-1}$, we can simplify the eigensystem problem of (2.52) to

$$B^{-1}A\vec{q}_\alpha = \cot\Delta_\alpha \vec{q}_\alpha, \tag{2.60}$$

where matrix $A \equiv (T^{-1} - G + iB) = \mathrm{Re}(T^{-1} - G)$. Since B is related to the imaginary part of G by (2.49), explicitly we have

$$A_{ij} = \begin{cases} t_i^{-1} + i = \cot\delta_i & \text{for } i = j, \\ -\mathrm{Re}G_{ij} = A(x_{ij}) & \text{for } i \neq j. \end{cases} \tag{2.61}$$

Function A, defined as

$$A(x) \equiv -\frac{\cos x}{x}, \tag{2.62}$$

is the real part of Green's function. Fig. 2.3 shows real and imaginary parts of Green's function as a function of distance between two scatterers. For a

general system, matrices A and B do not commute. We will discuss its many implications in this thesis.

Both A and B are real symmetric matrices. The transpose of (2.60) multiplied by B on the right is

$$\vec{q}_\alpha^T A = \vec{q}_\alpha^T B B^{-1} A = \cot \Delta_\alpha \vec{q}_\alpha^T B. \tag{2.63}$$

Therefore, $\vec{q}_\alpha^T B$'s are left eigenvectors of $B^{-1}A$. By definition (2.49), B is positive definite. Upon normalization of $\vec{q}_\alpha$'s, the orthonormal relation of eigenchannels is

$$\vec{q}_\alpha^T B \vec{q}_\beta = \langle I_\alpha | I_\beta \rangle = \delta_{\alpha\beta}, \text{ or asymptotically, } \int Y_\alpha^*(\hat{\boldsymbol{r}}) Y_\beta(\hat{\boldsymbol{r}}) d\hat{\boldsymbol{r}} = \delta_{\alpha\beta}. \tag{2.64}$$

Sometimes it is convenient to normalize $\vec{q}_\alpha$ to $\vec{q'}_\alpha$ such that

$$\vec{q'}_\alpha^T \vec{q'}_\alpha = 1. \tag{2.65}$$

2.3.4 Eigenchannel Expansion

In this subsection, we expand the incident waves into eigenchannels to get the total cross section of a group of scatterers. From (2.40), the scattered wave

$$\phi_s(\boldsymbol{r}) \cong \left[\sum_i \psi_i f_i y_i(\hat{\boldsymbol{r}}) \right] \frac{e^{ikr}}{r}. \tag{2.66}$$

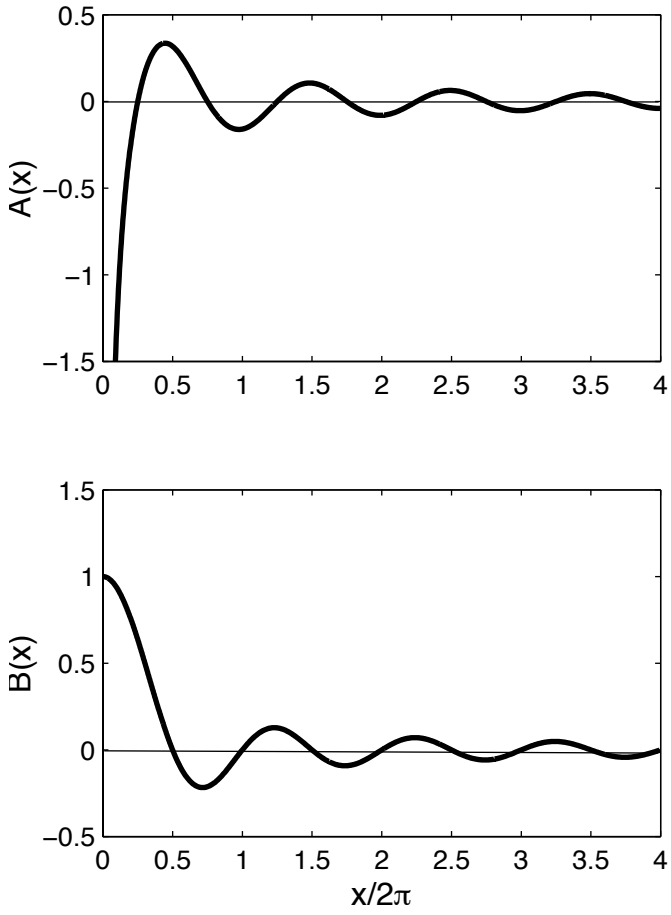

Figure 2.3: Real and imaginary parts of Green's function as a function of distance between two scatterers. $G_{ij} = -A_{ij} + iB_{ij} = -A(x_{ij}) + iB(x_{ij})$ for $i \neq j$.

If the incident wave is a plane wave $e^{i\boldsymbol{k}\cdot\boldsymbol{r}}$, the sum in the brackets of (2.66) is nothing else but the angular dependent scattering amplitude $f(\boldsymbol{k},\hat{\boldsymbol{r}})$. In this case,

$$\vec{\phi} = B\vec{c} = \sqrt{4\pi}(e^{i\boldsymbol{k}\cdot\boldsymbol{r}_1}, e^{i\boldsymbol{k}\cdot\boldsymbol{r}_2}, \cdots, e^{i\boldsymbol{k}\cdot\boldsymbol{r}_N})^T. \tag{2.67}$$

Expanding $\vec{c}$ into eigenchannels:

$$\vec{c} = \sum_{\alpha=1}^{N} a_\alpha \vec{q}_\alpha, \tag{2.68}$$

or $\vec{c} = Q\vec{a}$, where matrix

$$Q \equiv (\vec{q}_1, \vec{q}_2, \cdots, \vec{q}_N) \tag{2.69}$$

or $Q_{i\alpha} = q_{i\alpha}$, we get

$$\phi_s(\boldsymbol{r}) = \sum_\alpha a_\alpha \lambda_\alpha \left(\sum_i q_{i\alpha} \frac{1}{\sqrt{4\pi}} G_i(\boldsymbol{r}) \right) \cong \left[\frac{1}{k} \sum_\alpha a_\alpha \lambda_\alpha Y_\alpha(\hat{\boldsymbol{r}}) \right] \frac{e^{ikr}}{r}, \tag{2.70}$$

so

$$f(\boldsymbol{k},\hat{\boldsymbol{r}}) = \frac{1}{k} \sum_\alpha a_\alpha \lambda_\alpha Y_\alpha(\hat{\boldsymbol{r}}). \tag{2.71}$$

Therefore, the total cross section

$$\sigma(\boldsymbol{k}) = \frac{1}{k^2} \int |\sum_\alpha a_\alpha \lambda_\alpha Y_\alpha(\hat{\boldsymbol{r}})|^2 d\hat{\boldsymbol{r}} = \frac{1}{k^2} \sum_\alpha |a_\alpha|^2 \sin^2 \Delta_\alpha, \tag{2.72}$$

where we have used the orthonormal relation of $Y_\alpha(\hat{\boldsymbol{r}})$'s (2.64).

The total cross section not only depends on energy (or k), but also the direction of the incident wave $\hat{\boldsymbol{k}}$, since a_α's depend on $\hat{\boldsymbol{k}}$. This is what we would expect for a system without spherical symmetry. The average of total cross section over all possible incident directions for a given energy, $\frac{1}{4\pi}\int_{|\boldsymbol{k}|=k}\sigma(\boldsymbol{k})d\hat{\boldsymbol{k}}$, is a property of the system only, independent of $\hat{\boldsymbol{k}}$. From now on, "total cross section" σ means the average of $\sigma(\boldsymbol{k})$ over all possible $\hat{\boldsymbol{k}}$'s.

With the definition of Q (2.69), the orthonormal relation of $\vec{q}_\alpha$'s reads

$$Q^T B Q = 1. \tag{2.73}$$

Compare (2.67) with (2.32), we have $\phi_i(\hat{\boldsymbol{k}}) = 4\pi y_i^*(\hat{\boldsymbol{k}})$. And since $\vec{\phi}(\hat{\boldsymbol{k}}) = B\vec{c} = BQ\vec{a}(\hat{\boldsymbol{k}})$, $\vec{a}(\hat{\boldsymbol{k}}) = (BQ)^{-1}\vec{\phi}(\hat{\boldsymbol{k}}) = Q^T\vec{\phi}(\hat{\boldsymbol{k}})$, where we have used (2.73). Therefore,

$$a_\alpha(\hat{\boldsymbol{k}}) = 4\pi Y_\alpha^*(\hat{\boldsymbol{k}}). \tag{2.74}$$

Plugging (2.74) back into (2.71), we get the scattering amplitude

$$f(\boldsymbol{k}, \hat{\boldsymbol{r}}) = \sum_\alpha 4\pi \frac{\lambda_\alpha}{k} Y_\alpha^*(\hat{\boldsymbol{k}}) Y_\alpha(\hat{\boldsymbol{r}}), \tag{2.75}$$

analogous to (2.17). From (2.75) and (2.64) we can verify $Y_\alpha(\hat{\boldsymbol{r}})$'s are indeed eigenfunctions of the asymptotic T-matrix according to the definition

of (2.13):

$$T_E Y_\alpha(\hat{\boldsymbol{r}}) = \lambda_\alpha Y_\alpha(\hat{\boldsymbol{r}}). \tag{2.76}$$

From (2.74) and (2.64), the average of $|a_\alpha(\hat{\boldsymbol{k}})|^2$ over all possible $\hat{\boldsymbol{k}}$ is just 4π. Therefore, according to (2.72), the total cross section is

$$\sigma = \frac{4\pi}{k^2} \sum_\alpha \sin^2 \Delta_\alpha, \tag{2.77}$$

a sum of contributions from each eigenchannel, analogous to (2.20). From (2.72), (2.71), (2.74) and (2.57), we can verify that optical theorem (2.10) is also satisfied.

It is clear now that $Y_\alpha(\hat{\boldsymbol{r}})$'s here play the same role as spherical harmonics $Y_{lm}(\hat{\boldsymbol{r}})$'s in the case of spherically symmetric V.

2.3.5 T-matrix

Any incident wave can be written as $|\phi\rangle = \sum_i c_i |I_i\rangle + |\phi'\rangle$, where $|\phi'\rangle$ is orthogonal to each $|I_i\rangle$. Immediately we see the $|\phi'\rangle$ part does not scatter at all because $\langle I_i|\phi'\rangle = 0$ for all i. For a single scatterer, the T-matrix is of rank 1. For a group of N scatterers, if the scatterers are far apart so that $|I_i\rangle$'s do not overlap, the T-matrix of the system has N non-0 eigenvalues $\sin\delta_i e^{i\delta_i}$'s, so it is of rank N. If the scatterers are not far apart so multiple

scattering effects exist, the rank of the T-matrix is still N. The system scatters incident waves belonging to the N-dimensional space (2.48) spans.

There is a simpler explanation for the rank of T-matrix. Recall that the scattered wave depends only on $\vec{\phi}$, amplitudes of the incident wave at scatterers. For all the infinitely degenerate incident waves with the same energy, we can have a basis in which all but N waves have 0 amplitude at all $\boldsymbol{r}_i$'s. Consequently, the system only scatters the N waves which have non-0 amplitudes at $\boldsymbol{r}_i$'s, and does not scatter the rest at all. This is related to the previous paragraph because for any incident wave $|\phi\rangle$ orthogonal to $|I_i\rangle$, we must have $\phi(\boldsymbol{r}_i) = 0$ — 0 amplitude at the ith scatterer.

In eigenchannels $Y_\alpha(\hat{\boldsymbol{r}})$'s (plus all other linearly independent functions of $\hat{\boldsymbol{r}}$ orthogonal to all $Y_\alpha(\hat{\boldsymbol{r}})$'s) basis, the asymptotic T-matrix has a diagonal form

$$T_E = \mathrm{diag}\{\sin\Delta_1 e^{i\Delta_1}, \cdots, \sin\Delta_N e^{i\Delta_N}, 0, \cdots\}, \tag{2.78}$$

analogous to (2.19). $Y_\alpha(\hat{\boldsymbol{r}})$'s are eigenvectors of T_E corresponding to non-0 eigenvalues. In fact, matrix

$$BT(1 - GT)^{-1}B \tag{2.79}$$

is representation of asymptotic T-matrix in the nonorthogonal $y_i(\hat{\boldsymbol{r}})$ basis.

2.3.6 Resonances and Internal States

From (2.77), we know for each eigenchannel α, the position of resonance peak is at energy E_α where

$$\cot \Delta_\alpha(E_\alpha) = 0, \tag{2.80}$$

and the half width

$$\Gamma_\alpha = -1 \Big/ \left(\frac{\partial \cot \Delta_\alpha(E)}{\partial E}\bigg|_{E=E_\alpha} \right). \tag{2.81}$$

From (2.60), and because B is positive definite, one of the eigenvalues of A is 0 at E_α:

$$A(E_\alpha)\vec{q}_\alpha = 0. \tag{2.82}$$

This is consistent with the statement at the end of subsection 2.3.1 — resonances occur at poles of $(1 - GT)^{-1}$ or at where $T^{-1} - G = 0$ on complex E plane, because $A = \mathrm{Re}(T^{-1} - G)$.

If, for the energy range of our interest, we can neglect the energy dependence of Green's function between scatterers, then the only energy dependent elements in matrices A and B are diagonal elements of A, $\cot \delta_i(E)$'s. We refer to the approximation of neglecting the energy dependence of Green's function as the Markov approximation. As will be shown in Chapter 5, it

corresponds to the Markov approximation in interaction between atoms and the radiation field. We will discuss the validity of Markov approximation for different cases when we encounter them later.

After Markov approximation, differentiate (2.60) with respect to E, and with (2.80), at $E = E_\alpha$ we have

$$B^{-1}\frac{\partial A}{\partial E}\vec{q}_\alpha + B^{-1}A\frac{\partial \vec{q}_\alpha}{\partial E} = \frac{\partial \cot\Delta_\alpha}{\partial E}\vec{q}_\alpha. \tag{2.83}$$

Multiplying $\vec{q}_\alpha^T B$ on the left, we get

$$\vec{q}_\alpha^T\frac{\partial A}{\partial E}\vec{q}_\alpha = \frac{\partial \cot\Delta_\alpha}{\partial E}, \tag{2.84}$$

where we have used (2.64), (2.63) and (2.80). Therefore, from (2.81), the half width

$$\Gamma_\alpha = 1\Big/\sum_i\left(-\frac{\partial\cot\delta_i(E)}{\partial E}\right)_{E=E_\alpha} q_{i\alpha}^2\ . \tag{2.85}$$

We now focus on the case where each scatterer has one internal Breit-Wigner type resonance as specified by (2.35). Markov approximation is consistent with (2.35), which assumes E_i and γ_i are constants independent of k (or E). We introduce the internal state $\vec{\bar{q}}_\alpha$ for each eigenchannel at resonance $\vec{q}_\alpha(E_\alpha)$:

$$\bar{q}_{i\alpha} \propto \frac{1}{\sqrt{\gamma_i}}q_{i\alpha}(E_\alpha), \tag{2.86}$$

with normalization

$$\vec{\bar{q}}_\alpha^T \vec{q}_\alpha = 1. \tag{2.87}$$

(2.82) is equivalent to the statement that E_α's and $\vec{q}_\alpha$'s are eigenvalues and eigenvectors of the energy-independent $N \times N$ matrix $\bar{A}$:

$$\bar{A}\vec{q}_\alpha = E_\alpha \vec{q}_\alpha, \tag{2.88}$$

where

$$\bar{A}_{ij} \equiv \begin{cases} E_i & \text{for } i = j, \\ \sqrt{\gamma_i \gamma_j} A_{ij} & \text{for } i \neq j. \end{cases} \tag{2.89}$$

(2.85) becomes

$$\Gamma_\alpha = 1 \Big/ \sum_i \frac{1}{\gamma_i} q_{i\alpha}^2 = \vec{\bar{q}}_\alpha^T \bar{B} \vec{q}_\alpha, \tag{2.90}$$

where the $N \times N$ matrix $\bar{B}$ is defined as

$$\bar{B}_{ij} \equiv \sqrt{\gamma_i \gamma_j} B_{ij}, \tag{2.91}$$

and we have used (2.86), (2.87) and (2.64). $\bar{A}$, $\bar{B}$, and $\vec{q}_\alpha$'s are introduced for mathematical convenience in this chapter. We will discuss the physical meanings of these entities in Chapter 5.

For identical scatterers, i.e., $E_i = E_0$ and $\gamma_i = \gamma_0$ for all i, we can fix the value of Green's function at $k = k_0$, where $E_0 = \frac{1}{2}k_0^2$. We do not need

to explicitly take into account the quantum mechanical indistinguishability of identical scatterers, because scatterers are fixed at different positions in space. Previously defined matrices have simpler forms:

$$A_{ij} = \begin{cases} \cot\delta_0 = -\frac{E-E_0}{\gamma_0} & \text{for } i = j, \\ -\mathrm{Re}G_{ij} = A(x_{ij}) & \text{for } i \neq j, \end{cases} \tag{2.92}$$

$$\bar{A}_{ij} = \begin{cases} E_0 & \text{for } i = j, \\ \gamma_0 A_{ij} & \text{for } i \neq j, \end{cases} \tag{2.93}$$

and

$$\bar{B} = \gamma_0 B. \tag{2.94}$$

Furthermore,

$$\vec{\bar{q}}_\alpha = \vec{q'}_\alpha(E_\alpha), \tag{2.95}$$

and

$$\Gamma_\alpha = \gamma_0 \left(\vec{\bar{q}}_\alpha^T B \vec{\bar{q}}_\alpha \right). \tag{2.96}$$

2.4 Applications of Eigenchannel Expansion to Proximity Resonance

In this section, we study proximity resonance of N proximate scatterers using the concepts of eigenchannel expansion. Systems of N interacting resonances have been widely studied previously, e.g., [8, 9, 6]. However, our eigenchannel expansion approach gives new physical insights.

In this section, except for the general two-scatterer case, we only study *small samples* of identical s-wave point scatterers on a plane. In a "small sample", every pair of scatterers is proximate. Precisely, proximate means scatterers are placed within each other's effective radius at resonance. For identical s-wave point scatterers, proximate means $x_{ij} \equiv k_0 r_{ij} \lesssim 1$, or there is significant overlap between eigenchannels of scatterers: $\langle I_i | I_j \rangle \sim 1$. In contrast, in Chapter 6 we will study "large sample" cases, where for some pairs of scatterers $x_{ij} > 1$. Whether a sample is "small" or "large" is determined by the space spread of the sample, not by the number of scatterers.

Markov approximation is valid when, for the energy range of our interest,

$|\Delta G_{ij}| \ll |G_{ij}|$ for all i, j. For small samples, from (2.44),

$$\left|\frac{\partial G_{ij}}{\partial k}\right| = \left|\left(-\frac{1}{k^2 r_{ij}} + \frac{i}{k}\right) e^{ix_{ij}}\right| \approx \frac{1}{k^2 r_{ij}}, \tag{2.97}$$

and $|G_{ij}| \approx \frac{1}{k r_{ij}}$. Therefore, the validity condition for Markov approximation for small samples is: $\Delta k \ll k$ or

$$\Delta E \ll E \tag{2.98}$$

for the energy range of our interest.

Proximity resonance is a phenomenon of multiple scattering, which occurs when scatterers are proximate. A classical example is the case of weak, fixed frequency sound incident on two proximate, small identical air bubbles in water [10, 11, 12]. Quantum proximity resonances have been previously studied in [13, 14, 15, 5].

2.4.1 Two-scatterer Case

In this subsection, we consider the simplest case of multiple scattering — two identical scatterers separated by distance d. Now both matrices A and B are symmetric and have equal diagonal elements, so they commute. Therefore,

at each energy, the two eigenchannels are always

$$\vec{q'}_1 = \frac{1}{\sqrt{2}} \begin{pmatrix} 1 \\ \\ 1 \end{pmatrix} \text{ and } \vec{q'}_2 = \frac{1}{\sqrt{2}} \begin{pmatrix} 1 \\ \\ -1 \end{pmatrix}. \tag{2.99}$$

The amplitudes of scattered waves from each scatterer are perfectly in and out of phase with equal strength. The positions and widths of resonance peaks are determined by (2.88) and (2.96):

$$E_{1,2} = E_0 \pm \gamma_0 A(k_0 d), \tag{2.100}$$

$$\Gamma_{1,2} = \gamma_0 [1 \pm B(k_0 d)]. \tag{2.101}$$

For $k_0 d \ll 1$, the symmetric channel 1 becomes "s-like" and gives a broad peak, the antisymmetric channel 2 becomes "p-like" and gives a sharp peak. Both peaks are shifted from the peak of single scatterer. Fig. 2.4 shows an example of total cross section and phase angles as a function of energy for two proximate scatterers. Fig. 2.5 illustrates the two eigenchannels. Each eigenchannel α is illustrated by $\vec{q'}_\alpha$ and equivalently $Y_\alpha(\hat{\boldsymbol{r}})$. Each $\vec{q'}_\alpha$ is shown by colored dots centered at $\boldsymbol{r}_i$'s. For each dot, its color is determined by the sign of $q'_{i\alpha}$, and its radius is proportional to $|q'_{i\alpha}|$. Each $Y_\alpha(\hat{\boldsymbol{r}})$ is shown by plotting $|Y_\alpha(\hat{\boldsymbol{r}})|^2$ as a function of $\hat{\boldsymbol{r}}$. This eigenchannel illustration method is

used throughout this thesis. In the limit of $d \to 0$, $Y_1(\hat{\boldsymbol{r}})$ rigorously becomes an s-wave, and $Y_2(\hat{\boldsymbol{r}})$ a p-wave.

2.4.2 Three-scatterer Case

The three-scatterer case turns out to have a richer phenomenology. We consider three identical scatterers positioned proximately on a straight line separated by equal distance: $\boldsymbol{r}_1 = (-d, 0, 0), \boldsymbol{r}_2 = (0, 0, 0), \boldsymbol{r}_3 = (d, 0, 0)$. The difference to the two-scatterer case is that the relative amplitudes in each $\vec{q'}_\alpha$ are now energy dependent. Nonetheless, upon reflection about yz plane, there are always two symmetric channels 1, 3, and one antisymmetric channel 2. Fig. 2.6 shows an example of total cross section and phase angles as a function of energy for three scatterers. The eigenchannels at offresonant low energies are

$$\vec{q'}_1 = \begin{pmatrix} 0.576 \\ 0.580 \\ 0.576 \end{pmatrix}, \vec{q'}_2 = \begin{pmatrix} 0.707 \\ 0 \\ -0.707 \end{pmatrix}, \text{and } \vec{q'}_3 = \begin{pmatrix} 0.410 \\ -0.815 \\ 0.410 \end{pmatrix}. \quad (2.102)$$

Fig. 2.7 illustrates these eigenchannels. We see that channel 1 is s-like, 2 p-like, and 3 d-like. Indeed at offresonant low energies $Y_1(\hat{\boldsymbol{r}})$, $Y_2(\hat{\boldsymbol{r}})$, and $Y_3(\hat{\boldsymbol{r}})$ converge to s-, p-, and d-waves when $d \to 0$. At offresonant high energies,

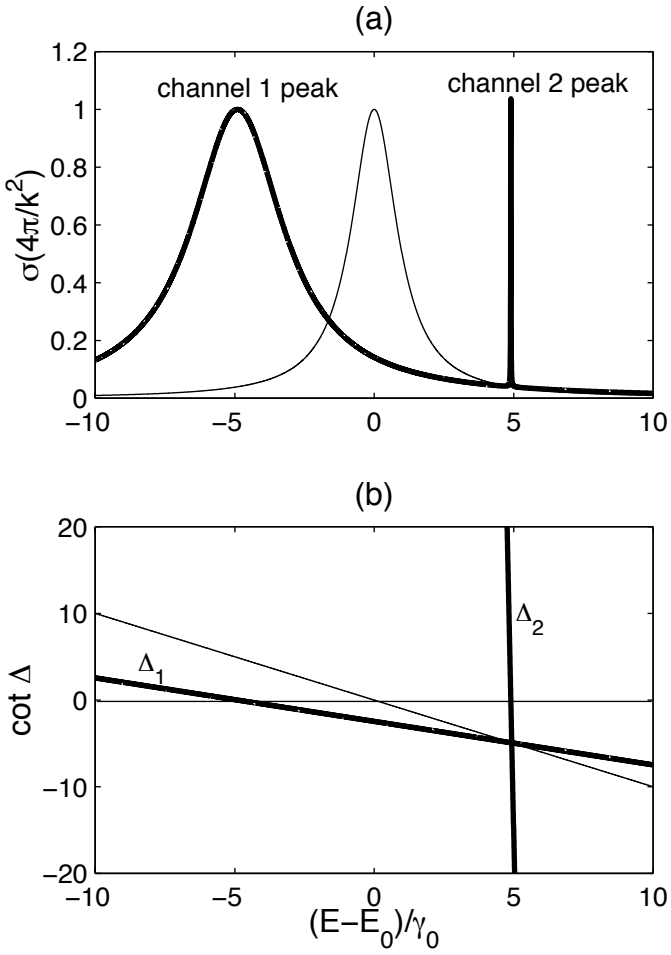

Figure 2.4: (a) Total cross section and (b) cotangent of phase angles as a function of energy for two identical scatterers separated by distance d, where $k_0 d = 0.2$ (wide lines). For comparison, total cross section and cotangent of phase angle of a single scatterer are also shown (narrow lines).

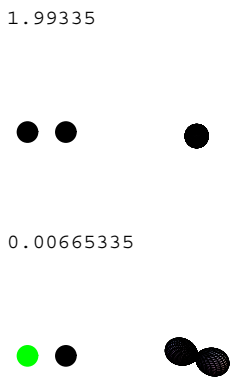

Figure 2.5: Eigenchannels for two scatterers, specified in Fig. 2.4. For each eigenchannel α, Γ_α/γ_0, $\vec{q'}_\alpha$, and $Y_\alpha(\hat{\boldsymbol{r}})$ are shown.

eigenchannels are still d-, p-, and s-like, with channel 1 and 3 switching place. Channel 1 gives most of the broad peak, and the other two channels give two sharp peaks.

Around $E = E_0 + 5.7\gamma_0$, $\cot\Delta_1$ and $\cot\Delta_3$ undergo an avoided crossing (Fig. 2.6(b)). Tracking channels 1 and 3 around the avoided crossing region, we find channel 1 is s-like and channel 3 is d-like before the crossing (below the crossing energy), yet channel 1 becomes d-like and channel 3 becomes s-like after the crossing. In contrast, $\cot\Delta_2$ rigorously crosses $\cot\Delta_1$ and $\cot\Delta_3$, because channel 2 has a different symmetry than channels 1 and 3. Indeed, for a general system without symmetry, there is always avoided crossing whenever two phase angles tend to cross (cf. Fig. 2.9(b)). The channel 3 peak exhibits an unsymmetric Fano lineshape [16, 17], deviated from the usual Lorentzian shape (Fig. 2.6(a)). The dip around $E \sim E_0 + 5.7\gamma_0$ before the peak arises from the avoided crossing between $\cot\Delta_1$ and $\cot\Delta_3$ near $\cot\Delta = 0$.

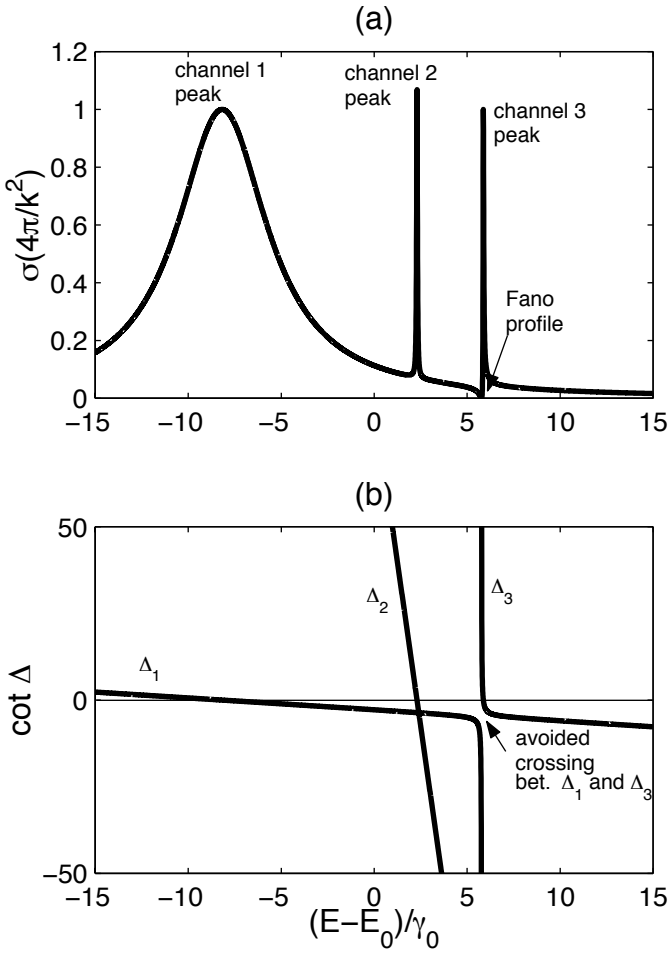

Figure 2.6: (a) Total cross section and (b) cotangent of phase angles as a function of energy for three proximate identical scatterers placed on a straight line separated by equal distance d: $\boldsymbol{r}_1 = (-d, 0, 0)$, $\boldsymbol{r}_2 = (0, 0, 0)$,and $\boldsymbol{r}_3 = (d, 0, 0)$, where $k_0 d = 0.2$.

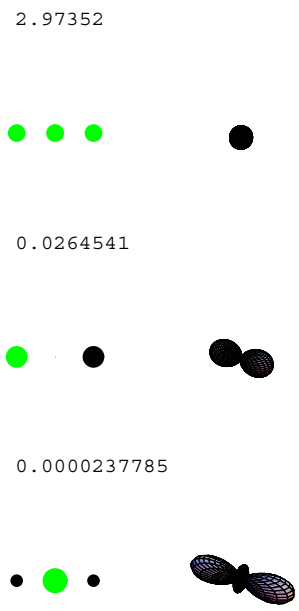

Figure 2.7: Eigenchannels at offresonant energies for three scatterers, specified in Fig. 2.6. In subsection 2.4.3, we will show they are actually offresonant eigenchannels. For each offresonant eigenchannel α, $\tilde{\Gamma}_\alpha/\gamma_0$, $\vec{\tilde{q}'}_\alpha$, and $\tilde{Y}_\alpha(\hat{\boldsymbol{r}})$ are shown. See subsection 2.4.3 for the definition of offresonant eigenchannel and meaning of symbols.

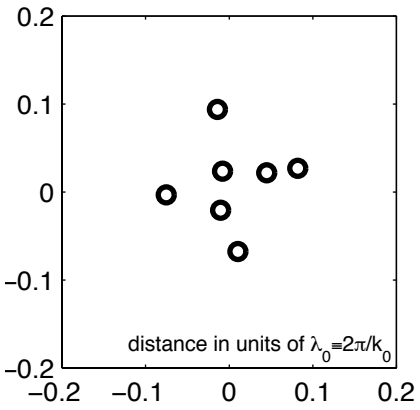

Figure 2.8: A typical small sample of 7 scatterers. The positions of the 7 identical scatterers proximately and randomly placed on a plane are shown.

2.4.3 Role of Imaginary Part of Green's Function

We are now going to discuss general cases of small samples of identical s-wave point scatterers. Fig. 2.8 shows a typical small sample of 7 identical scatterers proximately and randomly placed on a plane. Fig. 2.9 shows the total cross section and phase angles as a function of energy for the system of 7 scatterers.

At far offresonant energies (both low and high), $\cot\Delta$'s are linear in E. This can be explained by the eigensystem problem (2.60). From (2.92), we know when $|E - E_0|/\gamma_0 \gg |A_{ij}|$, i.e., off-diagonal elements of A are much

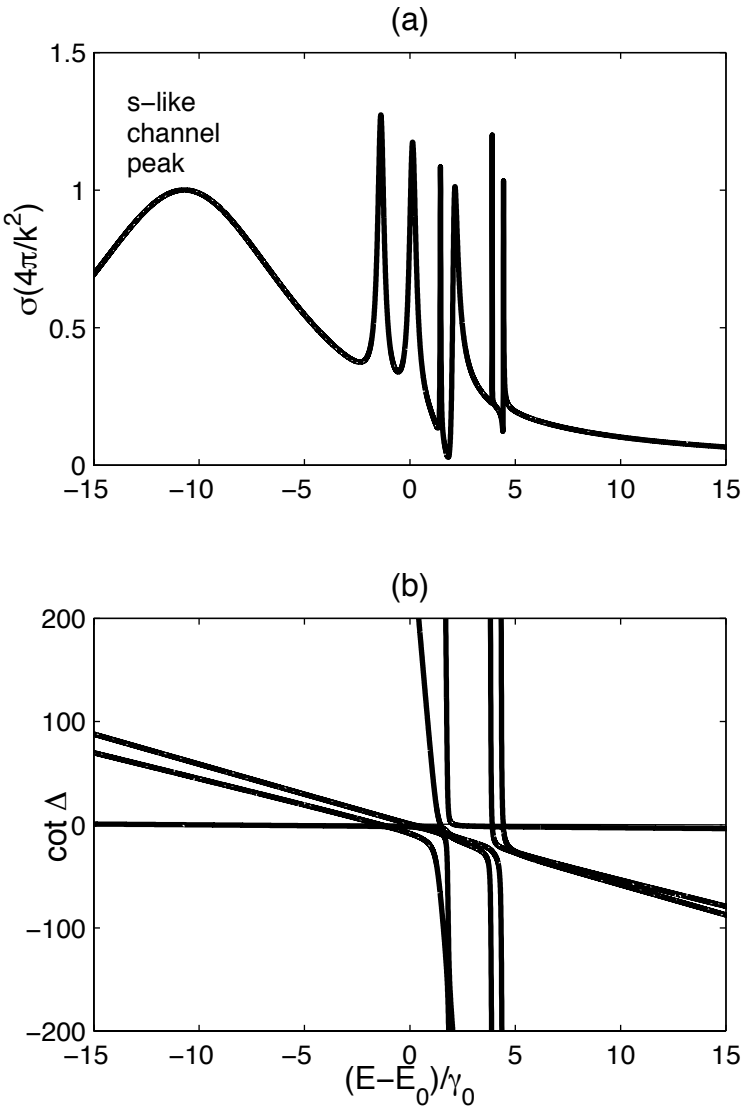

Figure 2.9: (a) Total cross section and (b) cotangent of phase angles as a function of energy for 7 identical scatterers, specified in Fig. 2.8.

smaller than diagonal elements and can be neglected, A is approximately proportional to unit matrix. Then from (2.60), $\vec{q}_\alpha$'s are approximately eigenvectors of B^{-1}, or B. Suppose $\tilde{\Gamma}_\alpha/\gamma_0$'s and $\vec{\tilde{q}}_\alpha$'s are eigenvalues and eigenvectors of B:

$$B\vec{\tilde{q}}_\alpha \equiv \frac{\tilde{\Gamma}_\alpha}{\gamma_0}\vec{\tilde{q}}_\alpha. \tag{2.103}$$

$\vec{\tilde{q}}_\alpha$'s are called offresonant eigenchannels, their orthonormal relation is the same as in (2.64). We also introduce $\vec{\tilde{q}'}_\alpha$'s, same as $\vec{\tilde{q}}_\alpha$ but with a different normalization. The normalization of $\vec{\tilde{q}'}_\alpha$'s is the same as in (2.65). The asymptotic offresonant eigenchannels are

$$\tilde{Y}_\alpha(\hat{\boldsymbol{r}}) \equiv \sum_i \tilde{q}_{i\alpha} y_i(\hat{\boldsymbol{r}}). \tag{2.104}$$

$\tilde{\Gamma}_\alpha$'s are called offresonant widths because from (2.60) and (2.103),

$$\cot\Delta = -\frac{E-E_0}{\gamma_0}\frac{\gamma_0}{\tilde{\Gamma}_\alpha}, \tag{2.105}$$

and thus

$$\tilde{\Gamma}_\alpha = -1 \Big/ \left(\frac{\partial \cot\Delta_\alpha(E)}{\partial E}\right) \quad \text{for } |E-E_0|/\gamma_0 \gg |A_{ij}|. \tag{2.106}$$

Offresonant eigenchannels are determined by the geometric configuration of scatterers only.

Here is a good place to refresh the definitions of $\vec{q}_\alpha$, $\vec{q'}_\alpha$, $\vec{\tilde{q}}_\alpha$, $\vec{\tilde{q}}_\alpha$, $\vec{\tilde{q}'}_\alpha$, and their interrelationship. For a system of N s-wave point scatterers of any kinds, at each energy E, there will always be N eigenchannels $\vec{q}_\alpha(E)$'s (or $\vec{q'}_\alpha(E)$'s, differ by normalization only), determined by (2.60). The orthogonal relation of $\vec{q}_\alpha$'s is $\vec{q}_\alpha^T(E)B\vec{q}_\beta(E) = 0$ ((2.64), and in this paragraph $\alpha \neq \beta$). If each scatterer is has one Breit-Wigner type resonance ((2.35)), each eigenchannel $\vec{q}_\alpha$ has one resonance at energy E_α. Internal state $\vec{\tilde{q}}_\alpha$ is related to eigenchannel at its resonance energy $\vec{q}_\alpha(E_\alpha)$ by (2.86). E_α's and $\vec{\tilde{q}}_\alpha$'s can be determined by (2.88). The orthogonal relation of $\vec{\tilde{q}}_\alpha$'s is $\vec{\tilde{q}}_\alpha^T\vec{\tilde{q}}_\alpha = 0$ because of (2.88). For identical scatterers, $\vec{\tilde{q}}_\alpha$ is simply $\vec{q'}_\alpha(E_\alpha)$ ((2.95)). For identical scatterers, offresonant eigenchannel $\vec{\tilde{q}}_\alpha$ (or $\vec{\tilde{q}'}_\alpha$, differ by normalization only) is related to eigenchannel at offresonant energies by

$$\vec{q}_\alpha(E) \to \vec{\tilde{q}}_\alpha \text{ or } \vec{q'}_\alpha(E) \to \vec{\tilde{q}'}_\alpha \text{ for } |E - E_0|/\gamma_0 \gg |A_{ij}|. \tag{2.107}$$

$\vec{\tilde{q}}_\alpha$'s are determined by (2.103), and their orthogonal relation is both $\vec{\tilde{q}}_\alpha^T B\vec{\tilde{q}}_\beta = 0$ and $\vec{\tilde{q}}_\alpha^T\vec{\tilde{q}}_\beta = 0$.

Fig. 2.10 illustrates the offresonant eigenchannels for the 7 scatterers. It is surprising to find that these offresonant eigenchannels are still s-, p-, d-, $\cdots$ like, even though the configuration of scatterers has no symmetry at

all. When $k_0 r_{ij} \lesssim 1$, we can solve the eigensystem problem of (2.103) by expanding the matrix elements of B into even powers of $k_0 r_{ij}$ or x_{ij}. From (2.49) and (2.50),

$$B_{ij} = 1 - \frac{1}{6} x_{ij}^2 + \frac{1}{120} x_{ij}^4 - \cdots = B_{ij}^{(0)} + B_{ij}^{(1)} + B_{ij}^{(2)} + \cdots . \tag{2.108}$$

Accordingly, offresonant eigenchannels and widths can be written as

$$\vec{q'}_\alpha = \vec{q'}_\alpha^{(0)} + \vec{q'}_\alpha^{(1)} + \vec{q'}_\alpha^{(2)} + \cdots , \tag{2.109}$$

and

$$\tilde{\Gamma}_\alpha = \tilde{\Gamma}_\alpha^{(0)} + \tilde{\Gamma}_\alpha^{(1)} + \tilde{\Gamma}_\alpha^{(2)} + \cdots . \tag{2.110}$$

Then solving the eigensystem problem of (2.103) is like multipole expansion.

Keeping only the 0th order of x_{ij} in B, we get only one offresonant channel, say $\vec{q}_1$, with non-0 offresonant width:

$$\vec{q'}_1^{(0)} = \frac{1}{\sqrt{N}} (1, 1, \cdots, 1)^T . \tag{2.111}$$

This is the s-like offresonant channel, whose offresonant width

$$\tilde{\Gamma}_1^{(0)} = N \gamma_0 . \tag{2.112}$$

For scatterers on a plane, adding the 2nd order of x_{ij} ($B_{ij}^{(1)}$) into account, we further get two p-like offresonant channels, whose offresonant widths to

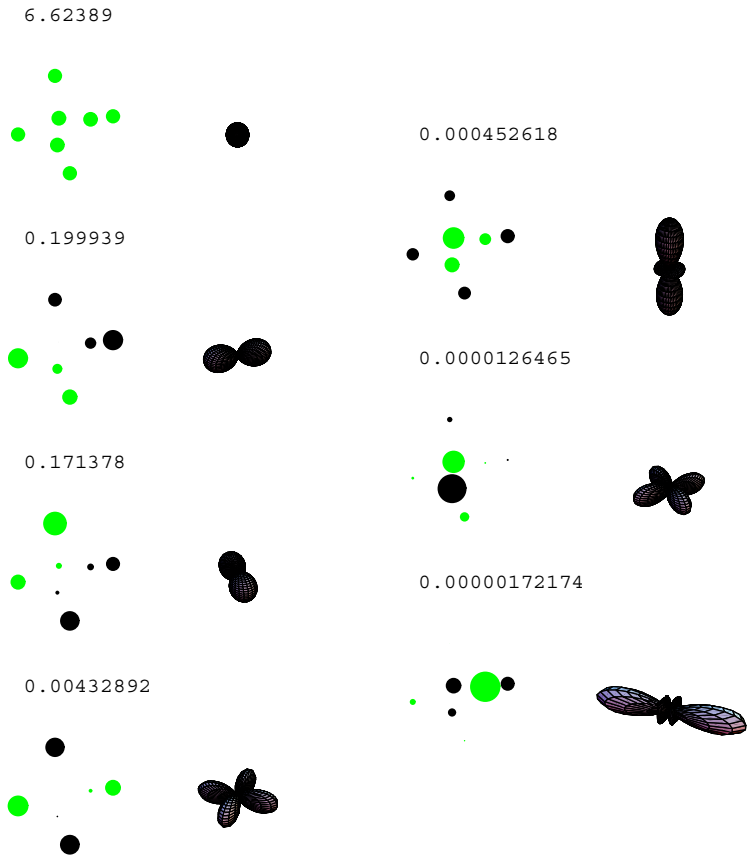

Figure 2.10: Offresonant eigenchannels for the 7 scatterers, specified in Fig. 2.9. For each offresonant channel α, $\tilde{\Gamma}_\alpha/\gamma_0$, $\vec{\tilde{q}}'_\alpha$, and $\tilde{Y}_\alpha(\hat{\boldsymbol{r}})$ are shown.

lowest order $\propto x_{ij}^2\gamma_0$. In general, adding the $2l$th order ($B_{ij}^{(l)}$) into account, we further get $(l+1)$ offresonant channels that look like 2^l-poles — lth order angular momentum eigenstates, and their offresonant widths to lowest order $\propto x_{ij}^{2l}\gamma_0$. This power expansion process can go on until we get all channels. The low order offresonant channels are not sensitive to the expansion coefficients in (2.108).

2.4.4 Role of Real Part of Green's Function

Now we put real part of Green's function, A_{ij}, back into consideration. First of all from (2.88), resonance energies E_α's are shifted from E_0. Nonetheless, the average of all E_α's is

$$\frac{1}{N}\sum_\alpha E_\alpha = \frac{1}{N}\mathrm{Tr}\bar{A} = E_0. \tag{2.113}$$

In the orthonormal offresonant eigenchannel $\vec{\tilde{q}}_\alpha$ basis, $B^{-1}A$ in (2.60) is simply replaced by $\tilde{A}$, where

$$\tilde{A}_{\alpha\beta} = \vec{\tilde{q}}_\alpha^T B B^{-1} A \vec{\tilde{q}}_\beta = \vec{\tilde{q}}_\alpha^T A \vec{\tilde{q}}_\beta. \tag{2.114}$$

In the orthonormal $\tilde{Y}_\alpha(\hat{\boldsymbol{r}})$ basis, the representation of asymptotic T-matrix is simply

$$(\tilde{A} - i1)^{-1}. \tag{2.115}$$

Except for a few highly symmetric cases, matrices A and B do not commute, i.e., offdiagonal elements of $\tilde{A}$ are non-0. Therefore, each eigenchannel at its resonance is a mix of offresonant eigenchannels:

$$\vec{\tilde{q}}_\alpha = \vec{q'}_\alpha(E_\alpha) = \sum_\beta c_{\alpha\beta}\vec{\tilde{q}'}_\beta. \tag{2.116}$$

The width is redistributed:

$$\Gamma_\alpha = \sum_\beta |c_{\alpha\beta}|^2 \tilde{\Gamma}_\beta, \tag{2.117}$$

but the total of all widths is constant:

$$\sum_\alpha \Gamma_\alpha = \mathrm{Tr}\bar{B} = N\gamma_0. \tag{2.118}$$

Numerical evidences show that the off-diagonal elements of $\tilde{A}$ can be considered as small, i.e., $|c_{\alpha\beta}|^2 \ll 1$ for $\alpha \neq \beta$. Eigenchannels at their respective resonance peaks mostly retain the s-, p-, d-, $\cdots$ like symmetry properties of their offresonant counter parts. The s-like channel (2.111) gives a broad peak, while the higher order channels give sharp peaks.

Expanding A_{ij} into powers of x_{ij}:

$$A_{ij} = -\frac{1}{x_{ij}} + \cdots, \tag{2.119}$$

we see the leading term $\propto \frac{1}{x_{ij}}$ and is negative. Therefore, the s-like eigenchannel's peak, E_1, is shifted lower in energy. To estimate the shift of E_1, we

neglect the offdiagonal elements of $\tilde{A}$, or equivalently, offdiagonal elements in the representation of $\bar{A}$ in $\vec{\tilde{q}}'_\alpha$ basis, and keep only the leading terms in expansion (2.108) and (2.119). From (2.88), (2.111), and (2.119), we have

$$E_1 \approx E_0 - (N-1)\left\langle \frac{1}{x} \right\rangle \gamma_0, \tag{2.120}$$

where

$$\left\langle \frac{1}{x} \right\rangle \equiv \sum_{i<j} \frac{1}{x_{ij}} \Big/ \left[\frac{N(N-1)}{2} \right] \tag{2.121}$$

is the average of $\frac{1}{x_{ij}}$. The higher order eigenchannels' peaks are at energies higher than E_1. Because for the s-like channel, all amplitudes are in phase and almost equal in strength, its peak has the largest shift and width among all resonance peaks. From the shift and width of s-like channel peak (2.120) and (2.112), we estimate that all resonances occur within the energy range

$$E_0 \pm \left[(N-1)\left\langle \frac{1}{x} \right\rangle + N \right] \gamma_0. \tag{2.122}$$

This should be the energy range of our interest. Therefore, for small samples of scatterers, the validity condition for Markov approximation, (2.98), becomes

$$N\left\langle \frac{1}{x} \right\rangle \gamma_0 \ll E_0, \tag{2.123}$$

where we have used the fact that $\left\langle \frac{1}{x} \right\rangle > 1$.

The mixing of offresonant eigenchannels also causes avoided crossings between phase angles. When the avoided crossing between two phase angles is near $\cot \Delta = 0$, i.e., near the two corresponding resonances, the resonance peaks have Fano-like unsymmetric shapes, deviating from Lorentzian shapes. In total cross section picture, overlapping of two resonance peaks causes the interference between the two resonances. In Chapter 5, we will further discuss the physical reason for the unsymmetric lineshape. It is because internal states are coupled to *two* offresonant eigenchannels, and there is interference between couplings.

2.5 Summary

We have shown that for a system of N s-wave point scatterers of any kinds, the T-matrix of the system is of rank N. Using eigenchannels of single scatterers as basis, the T-matrix can be represented analytically. Free space Green's function between the ith and jth scatterers is the projection of the outgoing part of the jth scatterer's eigenchannel onto the i scatterer's eigenchannel. At each energy, the N eigenchannels and their corresponding eigen-phase angles of the system are obtained by diagonalizing the T-matrix. The total

cross section is a sum of contributions from each eigenchannel. Position and width of each resonance peak are determined by where $\cot\Delta = 0$ and how fast $\cot\Delta$ changes as a function of energy. If each scatterer has one Breit-Wigner type resonance, each eigenchannel of the system gives one resonance. Positions and peaks of resonances are determined by matrices related to the real and imaginary parts of Green's function, respectively.

We have studied the small sample cases of proximate identical scatterers. The imaginary part of Green's function gives multipole-expansion-like offresonant eigenchannels and their corresponding offresonant widths. The real part of Green's function causes the shifts of resonance peaks. The s-like channel has a broad peak shifted lower in energy. The remaining $N-1$ resonances are sharp and are at energies higher than the s-like channel peak. Except for a few highly symmetric cases, real and imaginary parts of Green's function do not commute, which causes the slight mixing of offresonant eigenchannels at resonances. The mixing redistributes resonance widths, and gives rise to avoided crossing of phase angles. Avoided crossing between two phase angles near $\cot\Delta = 0$ causes the shapes of resonance peaks to be Fano-like unsymmetric.

Chapter 3

Superradiance: Evolution of Atoms

In the past few years, there have been significant breakthroughs in the cooling and trapping of atoms (e.g. [18, 19, 20]). Even in dilute atomic clusters, typical distances between neighboring atoms can be much smaller than the wavelength of a photon in resonance with a particular atomic transition, i.e., neighboring atoms are proximate. Atoms inside a single well of optical lattices with high filling factors satisfy this condition (see, e.g., [21]). Atoms in these clusters interact coherently with the radiation field. The coherent interaction between atoms and field are studied extensively, both experimen-

tally and theoretically. At currently achieved low temperatures, it is also not unreasonable to theoretically treat the atoms as fixed in space during the interaction.

In this chapter and next, we discuss a particular phenomenon of coherent interaction between atoms and field, namely "superradiance". Superradiance is the collective spontaneous emission of a group of atoms (or molecules). Superradiance was first discussed in a seminal paper by Dicke [22]. [23] is an excellent, and strangely as it seems, up to now the most comprehensive review on this subject. "Spontaneous" means initially the radiation field is in vacuum state. "Collective" means the atoms interact coherently with the field. Recently, collective behavior of two atoms has been observed in experiments [24, 25]. Theoretical studies of collective effects have been abundant for decades (e.g., [26, 27, 28, 29, 30, 31]). A large portion of the contents in this chapter and next do not go much beyond known literature by other authors. These contents provide useful background information, and are necessary to establish context for our new results in these two and later chapters.

In this chapter, we introduce the point two-level atom model, derive the master equation for the evolution of atoms while the radiation field is considered as a reservoir, and discuss the implications of the master equation.

3.1 Hamiltonian for Two-level Atoms in Radiation Field

3.1.1 Quantum Electrodynamics in Coulomb Gauge

We start from the general Hamiltonian for a number of charged particles in radiation field, based on quantum electrodynamics (QED) in Coulomb gauge. The results are standard and can be found in, e.g., [32].

In Coulomb gauge, the divergence of vector field is set to zero:

$$\nabla \cdot \boldsymbol{A}(\boldsymbol{r}) = 0, \tag{3.1}$$

i.e., the longitudinal component of the vector potential is zero:

$$\boldsymbol{A}_{\parallel}(\boldsymbol{r}) = 0. \tag{3.2}$$

Consequently, the scalar potential is the same as electrostatic potential with particles fixed at their *instantaneous* positions:

$$U(\boldsymbol{r}) = \frac{1}{4\pi\varepsilon_0} \sum_{\alpha} \frac{q_\alpha}{|\boldsymbol{r} - \boldsymbol{r}_\alpha|}, \tag{3.3}$$

where α is index for particles. The longitudinal component of the electric

field is also the same as static electric field:

$$\boldsymbol{E}_{\parallel}(\boldsymbol{r}) = \frac{1}{4\pi\varepsilon_0}\sum_{\alpha}\frac{q_\alpha(\boldsymbol{r}-\boldsymbol{r}_\alpha)}{|\boldsymbol{r}-\boldsymbol{r}_\alpha|^3}. \tag{3.4}$$

We use ν to denote the index of classical radiation wave modes in a large volume of L^3, and use ω_ν, $\boldsymbol{k}_\nu$ and $\boldsymbol{\epsilon}_\nu$ (assumed to be real) to denote the angular frequency, wave vector and polarization of mode ν. The transverse component of the vector potential is quantized as

$$\boldsymbol{A}_\perp(\boldsymbol{r}) = \boldsymbol{A}(\boldsymbol{r}) = \sum_{\nu}\mathcal{A}_{\omega_\nu}(a_\nu\boldsymbol{\epsilon}_\nu e^{i\boldsymbol{k}_\nu\cdot\boldsymbol{r}} + a_\nu^+\boldsymbol{\epsilon}_\nu e^{-i\boldsymbol{k}_\nu\cdot\boldsymbol{r}}), \tag{3.5}$$

where a_ν and a_ν^+ are field annihilation and creation operators, and $\mathcal{A}_{\omega_\nu} = [1/(2\varepsilon_0\omega_\nu L^3)]^{1/2}$ is a normalization constant. Thus, the transverse component of the electric field is:

$$\boldsymbol{E}_\perp(\boldsymbol{r}) = \sum_{\nu} i\omega_\nu\mathcal{A}_{\omega_\nu}(a_\nu\boldsymbol{\epsilon}_\nu e^{i\boldsymbol{k}_\nu\cdot\boldsymbol{r}} - a_\nu^+\boldsymbol{\epsilon}_\nu e^{-i\boldsymbol{k}_\nu\cdot\boldsymbol{r}}). \tag{3.6}$$

Sometimes it is useful to separate the a_ν and a_ν^+ components of $\boldsymbol{E}_\perp$, denoted as $\boldsymbol{E}^-$ and $\boldsymbol{E}^+$:

$$\boldsymbol{E}^-(\boldsymbol{r}) = \sum_{\nu} i\omega_\nu\mathcal{A}_{\omega_\nu}a_\nu\boldsymbol{\epsilon}_\nu e^{i\boldsymbol{k}_\nu\cdot\boldsymbol{r}}, \tag{3.7}$$

and $\boldsymbol{E}^+(\boldsymbol{r}) = [\boldsymbol{E}^-(\boldsymbol{r})]^+$. In the limit of $L^3 \to \infty$, we can replace the sum over all modes by an integral:

$$\sum_{\nu} = \sum_{\boldsymbol{k}_\nu}\sum_{\boldsymbol{\epsilon}_\nu} \to \frac{L^3}{(2\pi)^3}\int d\boldsymbol{k}\sum_{\boldsymbol{\epsilon}}. \tag{3.8}$$

The total Hamiltonian H is composed of three parts:

$$H = H_A + H_R + H_{AR}. \tag{3.9}$$

The particle part H_A depends on particle variables only:

$$H_A = \sum_\alpha \frac{\boldsymbol{p}_\alpha^2}{2m_\alpha} + V_c. \tag{3.10}$$

The first term on the right-hand side is kinetic energy. The second term V_c comes from coupling between particles and longitudinal field, and equals to electrostatic interaction based on the instantaneous positions of particles:

$$V_c = \frac{1}{4\pi\varepsilon_0} \sum_{\alpha<\beta} \frac{q_\alpha q_\beta}{|\boldsymbol{r}_\alpha - \boldsymbol{r}_\beta|}. \tag{3.11}$$

The field part H_R depends on field variables only:

$$H_R = \sum_\nu \omega_\nu a_\nu^+ a_\nu, \tag{3.12}$$

where we have neglected zero-point energies. The coupling part H_{AR}, coupling between particles and transverse field, depends on both particle and field variables:

$$H_{AR} = -\sum_\alpha \frac{q_\alpha}{m_\alpha} \boldsymbol{A}(\boldsymbol{r}_\alpha) \cdot \boldsymbol{p}_\alpha + \sum_\alpha \frac{q_\alpha^2}{2m_\alpha} \boldsymbol{A}(\boldsymbol{r}_\alpha)^2. \tag{3.13}$$

In most cases (except for very strong field), the second term involving $\boldsymbol{A}^2$ can be neglected.

The fact that the interaction between particles in V_c is instantaneous does not cause action-at-distance effects, because V_c is actually canceled by some terms from H_{AR}. The remaining terms from H_{AR} are fully retarded. This will be exemplified in subsection 3.2.5 for our case of identical two-level atoms in radiation field.

3.1.2 Point Two-level Atom Model

In many basic processes of interactions between a single atom and the radiation field, such as elementary emission and absorption, only two electronic levels are relevant. A very simplified model of atom, the point two-level atom model, can capture the essential physics of these processes [33].

A two-level atom i consists of a single electron e_i plus an "atomic core", which we assume to be infinitely heavy and fixed at $\boldsymbol{r}_i$. The particle part of the Hamiltonian H_{A_i} has two eigenstates — ground state $|g_i\rangle$ and the excited state $|e_i\rangle$, whose energy difference is ω_i. Therefore,

$$H_{A_i} = \omega_i \sigma_i^+ \sigma_i, \tag{3.14}$$

where $\sigma_i \equiv |g_i\rangle\langle e_i|$ and $\sigma_i^+ \equiv |e_i\rangle\langle g_i|$ are atom lowering and raising operators.

The dipole transition moment $\boldsymbol{d}_i$ (assumed to be real) between the two

states is defined as $\boldsymbol{d}_i \equiv \langle g_i|q_e(\boldsymbol{r}_{e_i} - \boldsymbol{r}_i)|e_i\rangle$. If there is no permanent dipole moment for both states, from commutation relations between $\boldsymbol{r}_{e_i}$ and H_{A_i}, we get

$$\frac{q_e}{m_e}\boldsymbol{p}_{e_i} = -i\omega_i \boldsymbol{d}_i(\sigma_i - \sigma_i^+). \tag{3.15}$$

If the spread of the wave function of the atom is small compared to the wavelengths of photons it is coupled to, we can assume the atom is infinitely small — existing at one point only. In this point two-level atom model, from (3.13), the coupling part depends on field variables at $\boldsymbol{r}_i$ only. Together with (3.15), the coupling part H_{A_iR} (after neglecting the $\boldsymbol{A}^2$ terms) is

$$H_{A_iR} = \sum_\nu i\omega_i \mathcal{A}_{\omega_\nu}(\boldsymbol{\epsilon}_\nu \cdot \boldsymbol{d}_i)(a_\nu e^{i\boldsymbol{k}_\nu\cdot\boldsymbol{r}_i} + a_\nu^+ e^{-i\boldsymbol{k}_\nu\cdot\boldsymbol{r}_i})(\sigma_i - \sigma_i^+). \tag{3.16}$$

Usually this simplification is referred to as dipole approximation.

3.1.3 The Hamiltonian

Now we are ready to write down the Hamiltonian for a group of two-level atoms in the field. The particle part H_A can be written as

$$H_A = H_{A0} + H_{DD}. \tag{3.17}$$

H_{A0} is a sum of particle parts of individual atoms:

$$H_{A0} = \sum_i \hbar\omega_i \sigma_i^+ \sigma_i, \tag{3.18}$$

H_{DD}, the dipole-dipole interaction, takes into account electrostatic interactions between electrons and atomic cores from *different* atoms:

$$H_{DD} = \sum_{i<j} \mathcal{D}_{ij}^0 (\sigma_i + \sigma_i^+)(\sigma_j + \sigma_j^+). \tag{3.19}$$

$\mathcal{D}_{ij}^0$ is the same as electrostatic interaction between two classical dipoles $\boldsymbol{d}_i$ and $\boldsymbol{d}_j$:

$$\mathcal{D}_{ij}^0 = \frac{1}{4\pi\varepsilon_0}\frac{1}{r_{ij}^3}[(\boldsymbol{d}_i \cdot \boldsymbol{d}_j) - 3(\hat{\boldsymbol{r}}_{ij} \cdot \boldsymbol{d}_i)(\hat{\boldsymbol{r}}_{ij} \cdot \boldsymbol{d}_j)], \tag{3.20}$$

where $\boldsymbol{r}_{ij} \equiv \boldsymbol{r}_i - \boldsymbol{r}_j$. (3.20) is accurate for point two-level atoms. The coupling part H_{AR} is a sum of coupling parts of individual atoms:

$$H_{AR} = \sum_\nu \sum_i i\omega_i \mathcal{A}_{\omega_\nu} (\boldsymbol{\epsilon}_\nu \cdot \boldsymbol{d}_i)(a_\nu e^{i\boldsymbol{k}_\nu \cdot \boldsymbol{r}_i} + a_\nu^+ e^{-i\boldsymbol{k}_\nu \cdot \boldsymbol{r}_i})(\sigma_i - \sigma_i^+). \tag{3.21}$$

Adding pieces together, we finally get the total Hamiltonian:

$$H = H_{A0} + H_R + H_{DD} + H_{AR}. \tag{3.22}$$

Expressions for each term are given by (3.18), (3.12), (3.19), and (3.21).

3.2 Derivation of Master Equation for Atoms

In this section, we derive the master equation for the evolution of atomic variables under (3.22). The derivation can be found in [34, 35, 36, 37], here we follow [37]. To track atomic variables while leaving out field variables, we use density matrix. Define the atomic density matrix ρ as

$$\rho \equiv \mathrm{Tr}_R \rho_{A+R}, \tag{3.23}$$

where ρ_{A+R} is the density matrix for atomic plus field variables, and Tr_R means trace over field variables. From (3.22), the evolution of ρ_{A+R} is given by

$$\dot{\rho}_{A+R} = -i[H, \rho_{A+R}] = -i\mathcal{L}\rho_{A+R}, \tag{3.24}$$

where the Liouville operator is defined as $\mathcal{L}\cdots \equiv [H, \cdots]$. Liouville operator acts on density matrices and gives matrices of the same dimension. The projection operator, to be introduced in subsection 3.2.1, has the same property. The formal solution to (3.24) is $\rho_{A+R}(t) = e^{-i\mathcal{L}t}\rho_{A+R}(0)$.

3.2.1 Projection Operator

Define the projection operator $\mathcal{P}$ as:

$$\mathcal{P}\cdots \equiv O_R \otimes \mathrm{Tr}_R \cdots, \tag{3.25}$$

where O_R is the density matrix for vacuum field. In fact, $\mathcal{P}\rho_{A+R} = O_R \otimes \rho$ contains information of atomic variables only.

We assume at $t = 0$, the field is in vacuum state and uncorrelated to the atoms, i.e., $\rho_{A+R}(0) = O_R \otimes \rho(0)$. The Laplace transform of (3.24) gives

$$z\hat{\rho}_{A+R}(z) - \rho_{A+R}(0) = -i\mathcal{L}\hat{\rho}_{A+R}(z). \tag{3.26}$$

Multiplying (3.26) by $\mathcal{P}$ and $(1-\mathcal{P})$ on the left, we get two equations for $\mathcal{P}\hat{\rho}_{A+R}(z)$ and $(1-\mathcal{P})\hat{\rho}_{A+R}(z)$:

$$z\mathcal{P}\hat{\rho}_{A+R}(z) - \rho_{A+R}(0) = -i\mathcal{P}\mathcal{L}\mathcal{P}\hat{\rho}_{A+R}(z) - i\mathcal{P}\mathcal{L}(1-\mathcal{P})\hat{\rho}_{A+R}(z), \tag{3.27}$$

$$z(1-\mathcal{P})\hat{\rho}_{A+R}(z) = -i(1-\mathcal{P})\mathcal{L}\mathcal{P}\hat{\rho}_{A+R}(z) - i(1-\mathcal{P})\mathcal{L}(1-\mathcal{P})\hat{\rho}_{A+R}(z). \tag{3.28}$$

Using (3.28) to eliminate $(1-\mathcal{P})\hat{\rho}_{A+R}$, and using the fact that $\mathcal{P}^2 = \mathcal{P}$ and $(1-\mathcal{P})^2 = 1-\mathcal{P}$, from (3.27), we get an expression for $\mathcal{P}\hat{\rho}_{A+R}(z)$ only:

$$\begin{aligned} &z\mathcal{P}\hat{\rho}_{A+R}(z) - \rho_{A+R}(0) = -i\mathcal{P}\mathcal{L}\mathcal{P}\hat{\rho}_{A+R}(z) \\ &-\mathcal{P}\mathcal{L}(1-\mathcal{P})\frac{1}{z + i(1-\mathcal{P})\mathcal{L}(1-\mathcal{P})}(1-\mathcal{P})\mathcal{L}\mathcal{P}\hat{\rho}_{A+R}(z). \end{aligned} \tag{3.29}$$

Reverse Laplace transform gives an integro-differential equation for $\mathcal{P}\rho_{A+R}(t)$:

$$\frac{\partial}{\partial t}\mathcal{P}\rho_{A+R}(t) = -i\mathcal{P}\mathcal{L}\mathcal{P}\rho_{A+R}(t)$$
$$-\mathcal{P}\mathcal{L}(1-\mathcal{P})\int_0^t d\tau e^{-i(1-\mathcal{P})\mathcal{L}(1-\mathcal{P})\tau}(1-\mathcal{P})\mathcal{L}\mathcal{P}\rho_{A+R}(t-\tau). \quad (3.30)$$

Decompose $\mathcal{L}$ into separate parts according to (3.22): $\mathcal{L} = \mathcal{L}_{A0} + \mathcal{L}_R + \mathcal{L}_{DD} + \mathcal{L}_{AR}$. Because some parts of $\mathcal{L}$ involve atomic or field variables only, some parts of $\mathcal{L}$ with $\mathcal{P}$ or $(1-\mathcal{P})$ on both sides are 0. In fact, $\mathcal{P}\mathcal{L}\mathcal{P} = (\mathcal{L}_{A0}+\mathcal{L}_{DD})\mathcal{P}$, $\mathcal{P}\mathcal{L}(1-\mathcal{P}) = \mathcal{P}\mathcal{L}_{AR}(1-\mathcal{P})$, and $(1-\mathcal{P})\mathcal{L}\mathcal{P} = (1-\mathcal{P})\mathcal{L}_{AR}\mathcal{P}$. (3.30) can thus be simplified to:

$$\frac{\partial}{\partial t}\mathcal{P}\rho_{A+R}(t) = -i(\mathcal{L}_{A0} + \mathcal{L}_{DD})\mathcal{P}\rho_{A+R}(t)$$
$$-\mathcal{P}\mathcal{L}_{AR}\int_0^t d\tau e^{-i(1-\mathcal{P})\mathcal{L}(1-\mathcal{P})\tau}\mathcal{L}_{AR}\mathcal{P}\rho_{A+R}(t-\tau). \quad (3.31)$$

No approximation has been made so far.

3.2.2 Born Approximation

From the original Hamiltonian (3.22), we see that H_{A0} and H_R are easy to solve, while H_{DD} and H_{AR} are difficult. We now replace $\mathcal{L}$ in the exponential of (3.31) by $\mathcal{L}_{A0} + \mathcal{L}_R$, dropping out $\mathcal{L}_{DD}$ and $\mathcal{L}_{AR}$:

$$\frac{\partial}{\partial t}\mathcal{P}\rho_{A+R}(t) = -i(\mathcal{L}_{A0} + \mathcal{L}_{DD})\mathcal{P}\rho_{A+R}(t)$$

$$-\mathcal{P}\mathcal{L}_{AR}\int_0^t d\tau e^{-i(1-\mathcal{P})(\mathcal{L}_{A0}+\mathcal{L}_R)(1-\mathcal{P})\tau}\mathcal{L}_{AR}\mathcal{P}\rho_{A+R}(t-\tau). \quad (3.32)$$

This is the (first order) Born approximation — keeping only the lowest order of $\mathcal{L}_{DD}$ and $\mathcal{L}_{AR}$. Born approximation is valid when H_{DD}, $H_{AR} \ll H_{A0}$, i.e., H_{DD} and H_{AR} can be considered as perturbation. Let γ_A be the rate of change of atomic variables under the influence of $H_{DD}+H_{AR}$, then Born approximation is valid when

$$\gamma_A \ll \omega_i. \quad (3.33)$$

We now move into interaction picture, where $\rho^I_{\cdots}(t) \equiv e^{i(\mathcal{L}_{A0}+\mathcal{L}_R)t}\rho_{\cdots}(t)$ and $\mathcal{L}^I_{\cdots}(t) \equiv e^{i(\mathcal{L}_{A0}+\mathcal{L}_R)t}\mathcal{L}_{\cdots}e^{-i(\mathcal{L}_{A0}+\mathcal{L}_R)t}$.

$$\frac{\partial}{\partial t}\mathcal{P}\rho^I_{A+R}(t) = -i\mathcal{L}^I_{DD}\mathcal{P}\rho^I_{A+R}(t) - \int_0^t d\tau \mathcal{P}\mathcal{L}^I_{AR}(t)\mathcal{L}^I_{AR}(t-\tau)\mathcal{P}\rho^I_{A+R}(t-\tau). \quad (3.34)$$

Explicitly, $\mathcal{L}^I_{AR}(t)\cdots = [H^I_{AR}(t), \cdots]$. In interaction picture, the operators σ_i, σ_i^+, a_ν, and a_ν^+ become $\sigma_i e^{-i\omega_i t}$, $\sigma_i^+ e^{i\omega_i t}$, $a_\nu e^{-i\omega_\nu t}$, and $a_\nu^+ e^{i\omega_\nu t}$. Therefore,

$$H^I_{AR}(t) = \sum_\nu \sum_i \mathcal{A}^I_i(t) \otimes \mathcal{R}^I_{\nu i}(t), \quad (3.35)$$

where $\mathcal{A}^I_i(t) \equiv i(\sigma_i e^{-i\omega_i t} - \sigma_i^+ e^{i\omega_i t})$ and $\mathcal{R}^I_{\nu i}(t) \equiv \omega_i \mathcal{A}_{\omega_\nu}(\boldsymbol{\epsilon}_\nu \cdot \boldsymbol{d}_i)[a_\nu e^{i(\boldsymbol{k}_\nu \cdot \boldsymbol{r}_i - \omega_\nu t)} + a_\nu^+ e^{-i(\boldsymbol{k}_\nu \cdot \boldsymbol{r}_i - \omega_\nu t)}]$.

Expanding $\mathcal{P}\mathcal{L}^I_{AR}(t)\mathcal{L}^I_{AR}(t-\tau)\mathcal{P}\rho^I_{A+R}(t-\tau)$ out explicitly, we get

$$\mathcal{P}\mathcal{L}^I_{AR}(t)\mathcal{L}^I_{AR}(t-\tau)\mathcal{P}\rho^I_{A+R}(t-\tau) = O_R \otimes \sum_\nu \sum_{i,j} \omega_i\omega_j \mathcal{A}^2_{\omega_\nu}(\boldsymbol{\epsilon}_\nu\cdot\boldsymbol{d}_i)(\boldsymbol{\epsilon}_\nu\cdot\boldsymbol{d}_j)$$
$$\times\{e^{i[\boldsymbol{k}_\nu\cdot(\boldsymbol{r}_i-\boldsymbol{r}_j)-\omega_\nu\tau]}[\mathcal{A}^I_i(t),\mathcal{A}^I_j(t-\tau)\rho^I_{A+R}(t-\tau)]$$
$$+e^{-i[\boldsymbol{k}_\nu\cdot(\boldsymbol{r}_i-\boldsymbol{r}_j)-\omega_\nu\tau]}[\rho^I_{A+R}(t-\tau)\mathcal{A}^I_j(t-\tau),\mathcal{A}^I_i(t)]\}, \tag{3.36}$$

where we have used

$$\mathrm{Tr}_R[\mathcal{R}^I_{\nu i}(t)\mathcal{R}^I_{\nu' j}(t-\tau)O_R] = \mathrm{Tr}_R[\mathcal{R}^I_{\nu' j}(t-\tau)O_R\mathcal{R}^I_{\nu i}(t)]$$
$$= \delta_{\nu\nu'}\omega_i\omega_j\mathcal{A}^2_{\omega_\nu}(\boldsymbol{\epsilon}_\nu\cdot\boldsymbol{d}_i)(\boldsymbol{\epsilon}_\nu\cdot\boldsymbol{d}_j)e^{i[\boldsymbol{k}_\nu\cdot(\boldsymbol{r}_i-\boldsymbol{r}_j)-\omega_\nu\tau]} \tag{3.37}$$

and

$$\mathrm{Tr}_R[\mathcal{R}^I_{\nu i}(t)O_R\mathcal{R}^I_{\nu' j}(t-\tau)] = \mathrm{Tr}_R[O_R\mathcal{R}^I_{\nu' j}(t-\tau)\mathcal{R}^I_{\nu i}(t)] = (3.37)^*. \tag{3.38}$$

To expand the commutators in (3.36) out, we make the rotating-wave approximation (RWA, or secular approximation) — neglecting terms containing $\sigma^+_i\sigma^+_j$ or $\sigma_i\sigma_j$. In interaction picture, these terms vary with angular frequency $\omega_i+\omega_j$. For RWA to be valid, $\omega_i+\omega_j$ must be much larger than the change rate of atomic variables due to $H^I_{DD}+H^I_{AR}$, i.e., γ_A. Therefore, RWA is compatible with Born approximation (3.33). After RWA, (3.34) becomes

$$\frac{\partial}{\partial t}\rho^I(t) = -i\mathcal{L}^I_{DD}(t)\rho^I(t) - \int_0^t d\tau \sum_\nu \sum_{i,j} \omega_i\omega_j \mathcal{A}^2_{\omega_\nu}(\boldsymbol{\epsilon}_\nu\cdot\boldsymbol{d}_i)(\boldsymbol{\epsilon}_\nu\cdot\boldsymbol{d}_j)$$

$$\times\{e^{i[\boldsymbol{k}_\nu\cdot(\boldsymbol{r}_i-\boldsymbol{r}_j)-\omega_\nu\tau]}(e^{i\omega_j\tau}e^{i\omega_{ij}t}[\sigma_i^+,\sigma_j\rho^I(t-\tau)]$$

$$+e^{-i\omega_j\tau}e^{-i\omega_{ij}t}[\sigma_i,\sigma_j^+\rho^I(t-\tau)])+\text{H.c.}\}, \tag{3.39}$$

where $\omega_{ij}\equiv\omega_i-\omega_j$.

3.2.3 Integration over $\hat{\boldsymbol{k}}$ and $\boldsymbol{\epsilon}$

Define B_{ij} as:

$$\int d\hat{\boldsymbol{k}}\sum_{\boldsymbol{\epsilon}}(\boldsymbol{\epsilon}\cdot\hat{\boldsymbol{d}}_i)(\boldsymbol{\epsilon}\cdot\hat{\boldsymbol{d}}_j)e^{i\boldsymbol{k}\cdot(\boldsymbol{r}_i-\boldsymbol{r}_j)}\equiv\frac{8\pi}{3}B_{ij}(k). \tag{3.40}$$

The normalization factor $\frac{8\pi}{3}$ ensures $B_{ii}=1$. Here we deliberately use the same symbol B_{ij} (and A_{ij} later in this chapter) as in Chapter 2, because there is correspondence between them, as will be shown in Chapter 5. B_{ij} is related to 0th and 2nd order spherical Bessel functions:

$$B_{ij}(k)\equiv B_1(kr_{ij})(\hat{\boldsymbol{d}}_i\cdot\hat{\boldsymbol{d}}_j)+B_2(kr_{ij})(\hat{\boldsymbol{r}}_{ij}\cdot\hat{\boldsymbol{d}}_i)(\hat{\boldsymbol{r}}_{ij}\cdot\hat{\boldsymbol{d}}_j), \tag{3.41}$$

where

$$B_1(x)\equiv j_0(x)-\frac{1}{2}j_2(x)=\frac{3}{2}\left(-\frac{\sin x}{x^3}+\frac{\cos x}{x^2}+\frac{\sin x}{x}\right) \tag{3.42}$$

and

$$B_2(x)\equiv\frac{3}{2}j_2(x)=\frac{3}{2}\left(3\frac{\sin x}{x^3}-3\frac{\cos x}{x^2}-\frac{\sin x}{x}\right). \tag{3.43}$$

Functions B_1 and B_2 are shown in Fig. 3.1. Replacing $\sum_\nu$ by an integral ((3.8)) in (3.39), we get

$$\frac{\partial}{\partial t}\rho^I(t) = -i\mathcal{L}^I_{DD}(t)\rho^I(t) - \int_0^t d\tau \int_0^\infty \omega d\omega \frac{1}{4\pi\varepsilon_0}\frac{2}{3\pi}\sum_{i,j} B_{ij}(\omega)\omega_i\omega_j d_i d_j$$
$$\times\{(e^{-i(\omega-\omega_j)\tau}e^{i\omega_{ij}t}[\sigma_i^+, \sigma_j\rho^I(t-\tau)] + e^{-i(\omega+\omega_j)\tau}e^{-i\omega_{ij}t}[\sigma_i, \sigma_j^+\rho^I(t-\tau)])$$
$$+\text{H.c.}\}, \tag{3.44}$$

where $\omega = k$.

3.2.4 Markov Approximation

(3.44) is still an integro-differential equation for $\rho^I(t)$. The terms in the integral of (3.44) are

$$\int_0^t d\tau \int_0^\infty d\omega\omega B_{ij}(\omega)e^{\pm i(\omega\pm\omega_j)\tau}\rho^I(t-\tau). \tag{3.45}$$

Due to the factor $e^{\pm i(\omega\pm\omega_j)\tau}$, after integration over ω, contribution to the integral over τ comes only from τ not much greater than a memory time τ_c. $\tau_c \sim 1/\Delta\omega$, where $\Delta\omega$ is the minimal range of ω around ω_i where $\omega B_{ij}(\omega)$ varies significantly. The range of $\Delta\omega$ where ω varies significantly is $\sim \omega_i$. The range of $\Delta\omega$ where $B_{ij}(\omega)$ varies significantly is $\sim 1/r_{ij}$, because the range of Δx where $j_0(x)$ and $j_2(x)$ vary significantly is ~ 1 ((3.41), (3.42), and (3.43),

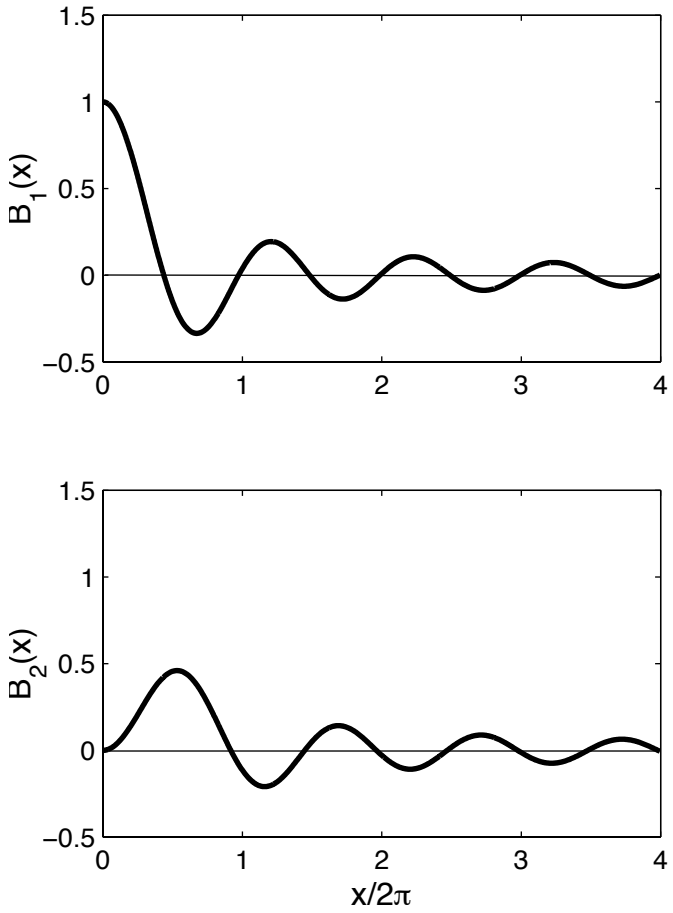

Figure 3.1: Functions $B_1(x)$ and $B_2(x)$. In subsection 3.2.6, we will show B_{ij} is actually the imaginary part of the generalized dipole-dipole interaction.

Fig. 3.1). Therefore, $\Delta\omega \sim \min(\omega_i, 1/r_{ij})$. If $t \gg \tau_c \sim \max(1/\omega_i, r_{ij})$, we can replace the upper limit of the integral for τ by ∞. Note r_{ij} is the time needed for radiation wave to travel from the ith atom to the jth. If ρ^I does not vary much during τ_c, i.e., $\gamma_A \tau_c \ll 1$ or equivalently

$$\gamma_A \ll \omega_i \text{ and } \gamma_A \ll \frac{1}{\max(r_{ij})}, \tag{3.46}$$

we can simply replace $\rho^I(t-\tau)$ by $\rho^I(t)$. This is the Markov approximation, valid when τ_c is short. After Markov approximation, (3.45) becomes

$$\int_0^\infty d\tau \int_0^\infty d\omega \omega B_{ij}(\omega) e^{\pm i(\omega \pm \omega_j)\tau} \rho^I(t). \tag{3.47}$$

Markov approximation is equivalent to taking the limit of $z \to 0^+$ in the denominator of (3.29).

Since

$$\int_0^\infty e^{\pm i(\omega \pm \omega_j)\tau} d\tau = \pi\delta(\omega \pm \omega_j) \pm i\frac{1}{\omega \pm \omega_j}, \tag{3.48}$$

(3.44) is simplified to an ordinary differential equation:

$$\begin{aligned}
\dot{\rho^I}(t) &= -i\mathcal{L}^I_{DD}(t)\rho^I(t) - \sum_{i,j} \gamma_{ij} B_{ij}(\omega_i)\{e^{-i\omega_{ij}t}[\sigma_j^+, \sigma_i \rho^I(t)] + \text{H.c.}\} \\
&+ i\sum_{i,j} \frac{\sqrt{\gamma_i\gamma_j}}{\pi\sqrt{\omega_i\omega_j}} \int_0^\infty d\omega \frac{\omega B_{ij}(\omega)}{\omega - \omega_i}\{ie^{-i\omega_{ij}t}[\sigma_j^+, \sigma_i\rho^I(t)] + \text{H.c.}\} \\
&+ i\sum_{i,j} \frac{\sqrt{\gamma_i\gamma_j}}{\pi\sqrt{\omega_i\omega_j}} \int_0^\infty d\omega \frac{\omega B_{ij}(\omega)}{\omega + \omega_i}\{ie^{i\omega_{ij}t}[\sigma_j, \sigma_i^+\rho^I(t)] + \text{H.c.}\},
\end{aligned} \tag{3.49}$$

where

$$\gamma_i \equiv \frac{1}{4\pi\varepsilon_0} d_i^2 \omega_i^3 \frac{2}{3} \tag{3.50}$$

is the half decay rate of spontaneous emission from the excited state to the ground state for a single atom i in vacuum field.

3.2.5 Lamb Shift

We proceed further for the case of identical atoms only: $\omega_i = \omega_0$, $d_i = d_0$, and $\gamma_i = \gamma_0$ for all i. Again here we do not need to explicitly take into account the quantum mechanical indistinguishability of identical atoms, because they are fixed at different positions in space. We will come back to nonidentical atoms in Chapter 5.

Rearranging terms in (3.49), we get

$$\begin{aligned}
\dot{\rho^I} &= -i\mathcal{L}^I_{DD}\rho^I - \sum_{i,j} \gamma_0 B_{ij} \{[\sigma_i^+ \sigma_j, \rho^I] - 2\sigma_i \rho^I \sigma_j^+\} \\
&\quad + i \sum_{i \neq j} \frac{\gamma_0}{2\pi\omega_0} \left\{ \int_{-\infty}^{\infty} \omega B_{ij}(\omega) \left(\frac{1}{\omega - \omega_0} + \frac{1}{\omega + \omega_0} \right) d\omega \right\} [\sigma_i^+ \sigma_j, \rho^I] \\
&\quad + i \sum_{i} \frac{\gamma_0}{2\pi\omega_0} \left\{ \int_{-\infty}^{\infty} \omega \left(\frac{1}{\omega - \omega_0} + \frac{1}{\omega + \omega_0} \right) d\omega \right\} [\sigma_i^+ \sigma_i, \rho^I],
\end{aligned} \tag{3.51}$$

where $B_{ij} \equiv B_{ij}(\omega_0)$.

Consider the $\sum_i$ term in (3.51) first. Define

$$\delta_0 \equiv -\frac{\gamma_0}{2\pi\omega_0}\int_{-\infty}^{\infty}\omega\left(\frac{1}{\omega-\omega_0}+\frac{1}{\omega+\omega_0}\right)d\omega. \tag{3.52}$$

From the commutator $[\sigma_i^+\sigma_i, \rho^I]$, we see this δ_0 is the correction to energy difference between the excited state and the ground state of a single atom due to coupling to the transverse field. This is the Lamb shift of a single atom. Unfortunately, the integral in (3.52) diverges, which means Lamb shift is infinite in our model. This can be fixed by, e.g., introducing a cut-off frequency in the integral in (3.52). Advanced treatment of Lamb shift requires renormalization, which is beyond the scope of this thesis.

The $\sum_{i\neq j}$ term in (3.51) gives the energy shift due to different atoms coupling to the same transverse field, or the "collective Lamb shift". However, this time the integral is finite and can be done analytically by residue method. In fact,

$$\frac{1}{2\pi\omega_0}\int_{-\infty}^{\infty}\omega j_0(kr_{ij})\left(\frac{1}{\omega-\omega_0}+\frac{1}{\omega+\omega_0}\right)d\omega = \frac{\cos x_{ij}}{x_{ij}}, \tag{3.53}$$

where $\boldsymbol{x}_{ij} \equiv k_0(\boldsymbol{r}_i - \boldsymbol{r}_j)$, $k_0 = \omega_0$, and

$$\begin{aligned}&\frac{1}{2\pi\omega_0}\int_{-\infty}^{\infty}\omega j_2(kr_{ij})\left(\frac{1}{\omega-\omega_0}+\frac{1}{\omega+\omega_0}\right)d\omega\\ &= -3\frac{1}{x_{ij}^3}+\left(3\frac{\cos x_{ij}}{x_{ij}^3}+3\frac{\sin x_{ij}}{x_{ij}^2}-\frac{\cos x_{ij}}{x_{ij}}\right).\end{aligned} \tag{3.54}$$

In (3.54), the first term on the right-hand side comes from the pole at $\omega = 0$. After we make another RWA for H_{DD}:

$$H_{DD} = \sum_{i \neq j} \mathcal{D}^0_{ij} \sigma_i^+ \sigma_j, \tag{3.55}$$

this term eventually gives a term in (3.51) that cancels the term $-i\mathcal{L}^I_{DD}\rho^I$! Ditto at the end of subsection 3.1.1, we show here that some terms from H_{AR} (different atoms coupling to the same transverse field, contribution mainly from coupling to near-zero-frequency field modes) exactly cancel H_{DD} (electrostatic interactions V_c between electrons and atomic cores from different atoms).

After integration, (3.51) becomes:

$$\begin{aligned} \dot{\rho}^I &= -i \sum_i \delta_0 [\sigma_i^+ \sigma_i, \rho^I] - i \sum_{i \neq j} \gamma_0 A_{ij} [\sigma_i^+ \sigma_j, \rho^I] \\ &\quad - \sum_{i,j} \gamma_0 B_{ij} (\sigma_i^+ \sigma_j \rho^I + \rho^I \sigma_i^+ \sigma_j - 2\sigma_i \rho^I \sigma_j^+), \end{aligned} \tag{3.56}$$

where

$$A_{ij}(\omega) \equiv A_1(kr_{ij})(\hat{\boldsymbol{d}}_i \cdot \hat{\boldsymbol{d}}_j) + A_2(kr_{ij})(\hat{\boldsymbol{r}}_{ij} \cdot \hat{\boldsymbol{d}}_i)(\hat{\boldsymbol{r}}_{ij} \cdot \hat{\boldsymbol{d}}_j), \tag{3.57}$$

with

$$A_1(x) \equiv \frac{3}{2} \left(\frac{\cos x}{x^3} + \frac{\sin x}{x^2} - \frac{\cos x}{x} \right), \tag{3.58}$$

$$A_2(x) \equiv \frac{3}{2}\left(-3\frac{\cos x}{x^3} - 3\frac{\sin x}{x^2} + \frac{\cos x}{x}\right), \tag{3.59}$$

and $A_{ij} \equiv A_{ij}(\omega_0)$. $\gamma_0 A_{ij}$ is the collective Lamb shift. Functions A_1 and A_2 are shown in Fig. 3.2.

Coming back to noninteraction picture, (3.56) becomes

$$\begin{aligned}\dot{\rho} &= -i\sum_i(\omega_0+\delta_0)[\sigma_i^+\sigma_i,\rho] - i\sum_{i\neq j}\gamma_0 A_{ij}[\sigma_i^+\sigma_j,\rho] \\ &\quad -\sum_{i,j}\gamma_0 B_{ij}(\sigma_i^+\sigma_j\rho + \rho\sigma_i^+\sigma_j - 2\sigma_i\rho\sigma_j^+).\end{aligned} \tag{3.60}$$

3.2.6 Effective Hamiltonian and Generalized Dipole-dipole Interaction

We can incorporate the single atom Lamb shift δ_0 into ω_0 by defining the new ω_0 to be the original $\omega_0 + \delta_0$. We introduce the effective Hamiltonian $\bar{H}$ as

$$\bar{H} \equiv \sum_i(\omega_0 - i\gamma_0)\sigma_i^+\sigma_i + \sum_{i\neq j}\mathcal{D}_{ij}\sigma_i^+\sigma_j, \tag{3.61}$$

where

$$\begin{aligned}\mathcal{D}_{ij} &\equiv \gamma_0(A_{ij} - iB_{ij}) = \gamma_0\frac{3}{2}\left\{\left(\frac{1}{x_{ij}^3} - \frac{i}{x_{ij}^2} - \frac{1}{x_{ij}}\right)(\hat{\boldsymbol{d}}_i\cdot\hat{\boldsymbol{d}}_j)\right. \\ &\quad \left.+\left(-3\frac{1}{x_{ij}^3} + 3\frac{i}{x_{ij}^2} + \frac{1}{x_{ij}}\right)(\hat{\boldsymbol{x}}_{ij}\cdot\hat{\boldsymbol{d}}_i)(\hat{\boldsymbol{x}}_{ij}\cdot\hat{\boldsymbol{d}}_j)\right\}e^{ix_{ij}}.\end{aligned} \tag{3.62}$$

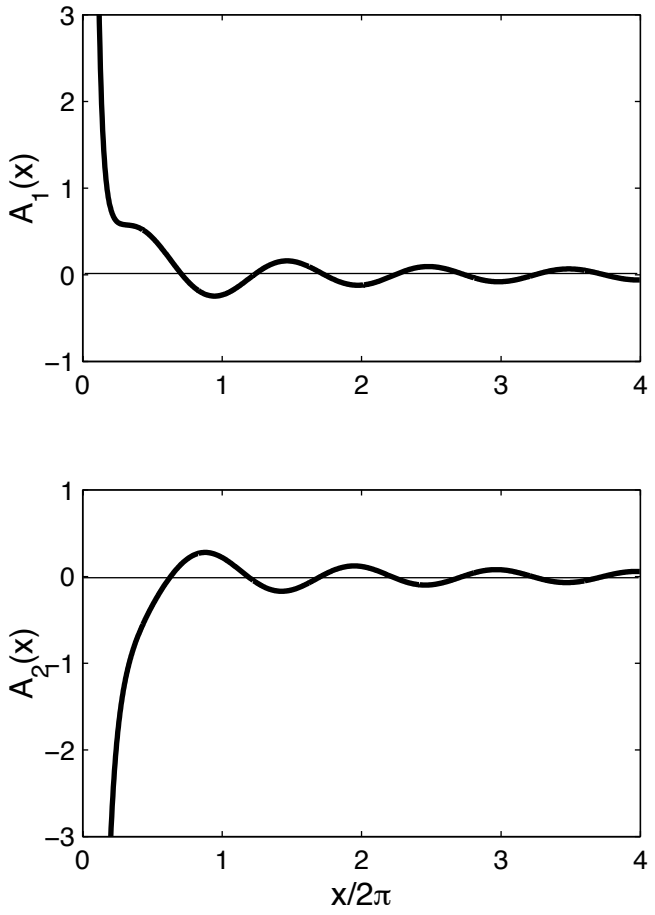

Figure 3.2: Collective Lamb shift: functions $A_1(x)$ and $A_2(x)$. In subsection 3.2.6, we will show A_{ij} is actually the real part of the generalized dipole-dipole interaction.

As we have pointed out in previous subsection, the single atoms Lamb shift δ_0 diverges in our model and the advanced treatment of it requires renormalization. However, the collective Lamb shift between different atoms, $\gamma_0 A_{ij}$'s, are finite in our model and are kept. They are not affected by renormalization, e.g., they are not affected by the introduction of a large cut-off frequency in the integral in $\sum_{i \neq j}$ term of (3.51).

$\mathcal{D}_{ij}$ is the generalized dipole-dipole interaction between two atoms. $\gamma_0 A_{ij}$ and $\gamma_0 B_{ij}$ are its real and imaginary parts. It comes from the electrostatic interactions between two atoms, H_{DD}, *plus* terms from H_{AR} due to two atoms coupling to the same transverse radiation field. The generalized dipole-dipole interaction $\mathcal{D}_{ij}$ is fully retarded ($e^{ix_{ij}}$ factor). It equals to the interaction between two classical dipoles $\boldsymbol{d}_i$ and $\boldsymbol{d}_j$ oscillating with angular frequency ω_0 [38]. $\mathcal{D}_{ij}$ is similar to D^0_{ij}. In fact,

$$\mathrm{Re}\mathcal{D}_{ij} = \gamma_0 A_{ij} \to \mathcal{D}^0_{ij} \text{ as } \omega_0 \to 0. \tag{3.63}$$

With the definition of the effective Hamiltonian $\bar{H}$ (3.61), (3.60) can be written as

$$\dot{\rho} = -i(\bar{H}\rho - \rho\bar{H}^+) + \sum_{i,j} 2\gamma_0 B_{ij} \sigma_i \rho \sigma_j^+ . \tag{3.64}$$

This the the final form of the master equation for the evolution of atomic

variables we are looking for.

3.3 Discussion of Master Equation

3.3.1 Manifolds

We group atomic states into manifolds according to the number of atoms in excited state. The mth manifold $\mathcal{E}_m$ consists of all states where there are m excited atoms, i.e., all degenerate eigenstates of H_{A0} whose corresponding eigenvalue is $m\omega_0$. Suppose there are N identical atoms in total, the number of states in $\mathcal{E}_m$ $(m = 0, 1, \cdots, N)$ is

$$\begin{pmatrix} N \\ m \end{pmatrix} = \frac{N!}{m!(N-m)!}. \tag{3.65}$$

The master equation (3.64) has two terms on the right-hand side. The first term means the evolution of atomic variables under the influence of the effective dissipative Hamiltonian $\bar{H}$. Dissipation is the result of spontaneous emission. From (3.61), we see $\bar{H}$ is block diagonal, i.e., it only connects states within the same manifold. $\bar{H}$ can be written as

$$\bar{H} = \bar{H}_0 \oplus \bar{H}_1 \oplus \cdots \oplus \bar{H}_N, \tag{3.66}$$

where $\bar{H}_m$ is the effective Hamiltonian within $\mathcal{E}_m$. The second term on the right-hand side of (3.64) means population increase in a manifold $\mathcal{E}_m$ due to spontaneous emission from one manifold above $\mathcal{E}_{m+1}$. Since B_{ij} is the dissipative (imaginary) part of $\bar{H}$, population increase from this term exactly offsets the dissipation from the first term. Therefore, (3.64) conserves the total population $\mathrm{Tr}\rho$.

If initially ρ is block diagonal, i.e., there is no correlation between states in different manifolds, ρ remains block diagonal. Let us look at what happens to each manifold. There is no population transfer to the highest initially occupied manifold. The evolution within this manifold is entirely governed by $\bar{H}$. For all lower manifolds, the evolution of each manifold is governed by $\bar{H}$ plus population transfer from one manifold above.

If real and imaginary parts of the effective Hamiltonian $\bar{H}$ commute, eigenstates of $\bar{H}$ form a complete *orthogonal* basis. In this basis, if initially all offdiagonal elements of ρ (correlation between states) are 0 (even within the same manifold), they will remain 0. Therefore, the evolution of atoms is completely determined by energy levels of the eigenstates (related to real part of $\bar{H}$), and the coupling between states differ by one manifold through spontaneous emission (related to imaginary part of $\bar{H}$). All examples later in

this section have commutative real and imaginary parts of $\bar{H}$. This is always true for two atoms (subsection 3.3.3). It is also true for highly symmetric cases, or after certain approximations (subsection 3.3.2). For a general non-symmetric system of atoms, real and imaginary parts of $\bar{H}$ do not commute. We will further discuss its consequences in later chapters.

3.3.2 Dicke Model of Superradiance and Beyond

A trivial case for master equation (3.64) is when all atoms are far apart, i.e., $r_{ij} \to \infty$. A_{ij} and $B_{ij} \to 0$ for $i \neq j$, so each atom decays independently as if there were no other atoms around.

In [22], Dicke proposes a simple model which captures the collective effects of atoms, and lays the foundation of superradiance. The Dicke model assumes all atoms are very proximate to each other, with all dipoles parallel to each other, but neglects the collective Lamb shift. In our context here, it is equivalent to say the model assumes $A_{ij} = 0$ and $B_{ij} = 1$ for all i, j. This is physically unjustifiable, since

$$|A_{ij}| \gg 1 \text{ for } |x_{ij}| \ll 1. \tag{3.67}$$

In Dicke model, real and imaginary parts of $\bar{H}$ commute. Furthermore, as

will be shown immediately, very few states are coupled through spontaneous emission.

Each two-level atom can be mapped to a spin $\frac{1}{2}$ particle, e.g., by mapping the excited state to spin up state, and the ground state to spin down state. A group of two-level atoms is then mapped to a group of spin $\frac{1}{2}$ particles. We use $|J, M\rangle$ to denote collective state(s) of particles whose total spin is J, and whose projection of total spin along z axis is M. Each manifold consists of states with the same M — all states within $\mathcal{E}_m$ have $M = m - \frac{N}{2}$. In Dicke model ensures, only states with the same J are connected through spontaneous emission. Fig. 3.3 shows the spontaneous emission diagram for Dicke model.

Within each manifold, the most "symmetric" state is the state with maximum possible J, i.e., $J = \frac{N}{2}$. State $|\frac{N}{2}, m - \frac{N}{2}\rangle$ corresponds to the linear combination with equal coefficient of all possibilities of m atoms in excited state out of a total of N. The spontaneous emission half rate from $|\frac{N}{2}, m-\frac{N}{2}\rangle$ to $|\frac{N}{2}, m - 1 - \frac{N}{2}\rangle$ is easy to get:

$$\gamma_{\mathcal{E}_m \to \mathcal{E}_{m-1}} = \gamma_0 m(N - m + 1). \tag{3.68}$$

γ_0 is the single atom spontaneous emission half rate. m is the number of

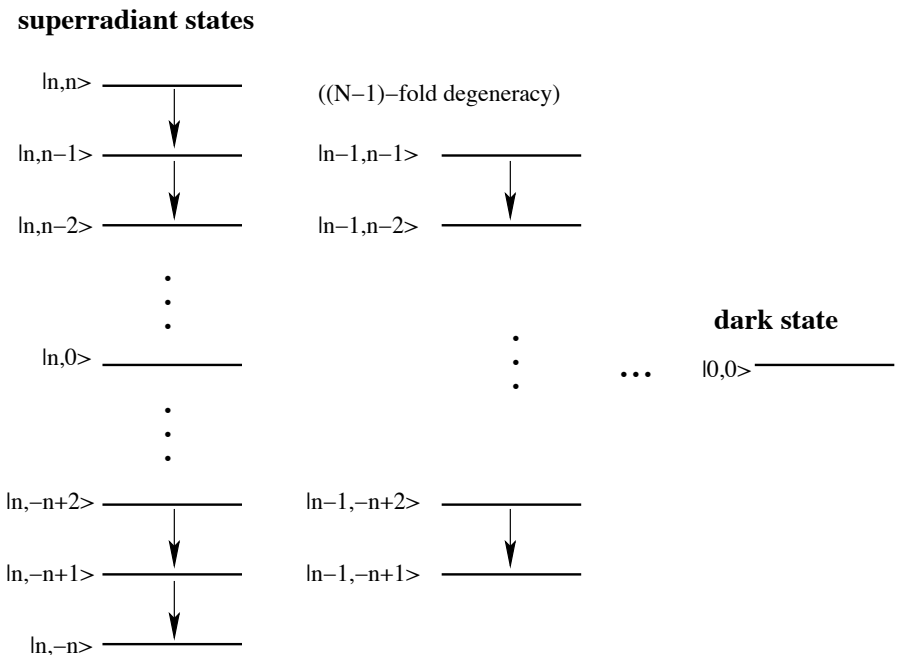

Figure 3.3: Spontaneous emission diagram for a group of N atoms (N even) in Dicke model of superradiance. Each collective state is labeled by $|J, M\rangle$ ($n = \frac{N}{2}$). The energy level of each state is shown. Each arrow denotes coupling between two states through spontaneous emission.

excited atoms in initial state, and $N-m+1$ is the number of ground atoms in *final* state. Dicke refers to $J=\frac{N}{2}$ states as "superradiant" states. Each superradiant state has the largest spontaneous emission rate within each manifold. If N is even, the most "antisymmetric" state is the $|0,0\rangle$ state. It is a "dark state" since it is not connected to any other state through radiation field.

Within the first excited manifold $\mathcal{E}_1$, the superradiant state is

$$|S\rangle = \frac{1}{\sqrt{N}} \sum_i |e_i\rangle. \tag{3.69}$$

$|e_i\rangle$ is the state where atom i is in excited state and all other atoms are in ground states. Its spontaneous emission rate is N times as large as a single atom. All other states have $J=\frac{N}{2}-1$ and are metastable states. They do not decay and are "subradiant" states.

For some highly symmetric configurations of atoms, we can put A_{ij} back into account without losing the high symmetry of Dicke model — any permutation of atoms does not change the configuration. An example is atoms parallelly and equally placed on a ring, with each dipole perpendicular to the ring plane (Fig. 3.4). In these cases, still only states with the same J are coupled through spontaneous emission (because $B_{ij}=1$), but the energy

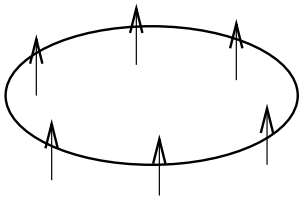

Figure 3.4: Arrangement of atomic dipoles on a ring such that any permutation of atoms does not change the configuration.

levels of states are shifted due to collective Lamb shift.

To get some physical intuition, we consider A_{ij}'s between nearest neighbors only. A_{ij} is positive when atoms are proximate ((3.57), Fig. 3.2). Take the superradiant states of the ring configuration of Fig. 3.4 for example. The energy shift of each state is proportional to the average number of nearest-neighbor pairs with one in excited state and one in ground state. Therefore, there is no shift for the highest ($m = N$) and lowest ($m = 0$) manifold. All other states' energies are shifted upward, with maximum shift at $m \approx \frac{N}{2}$. Further detailed study (e.g., [39]) shows that if initially all atoms are in excited states, the frequency of emitted photons will gradually increase as atoms cascade down through superradiant states. Initially the photons are red shifted relative to the single atom emission, and finally they are blue

shifted. Fig. 3.5 shows the cascading from the highest manifold, without and with nearest neighbor A_{ij}'s taken into account.

3.3.3 Two-atom Case

In this subsection, we solve the master equation (3.64) for two atoms in detail.

$$\bar{H} = \begin{pmatrix} 2\omega_0 - i2\gamma_0 & & & \\ & \omega_0 - i\gamma_0 & \gamma_0(A_{12} - iB_{12}) & \\ & \gamma_0(A_{12} - iB_{12}) & \omega_0 - i\gamma_0 & \\ & & & 0 \end{pmatrix}. \tag{3.70}$$

Real and imaginary parts of $\bar{H}$ commute. The two eigenstates of $\bar{H}$ within $\mathcal{E}_1$ are the symmetric superradiant state $|S\rangle = \frac{1}{\sqrt{2}}(|e_1\rangle + |e_2\rangle)$ and the antisymmetric subradiant state $|A\rangle = \frac{1}{\sqrt{2}}(|e_1\rangle - |e_2\rangle)$, whose corresponding eigenvalues are $\omega_0 + \gamma_0 A_{12} - i\gamma_0(1 + B_{12})$ and $\omega_0 - \gamma_0 A_{12} - i\gamma_0(1 - B_{12})$. The whole spontaneous emission diagram is shown in Fig. 3.6.

It is interesting to see what happens if initially atom 1 is in excited state and atom 2 is in ground state. This is the simplest case where real and imaginary parts of $\bar{H}$ commute, but there is initial correlation between eigenstates of $\bar{H}$ within the same manifold. Since the initial atomic state

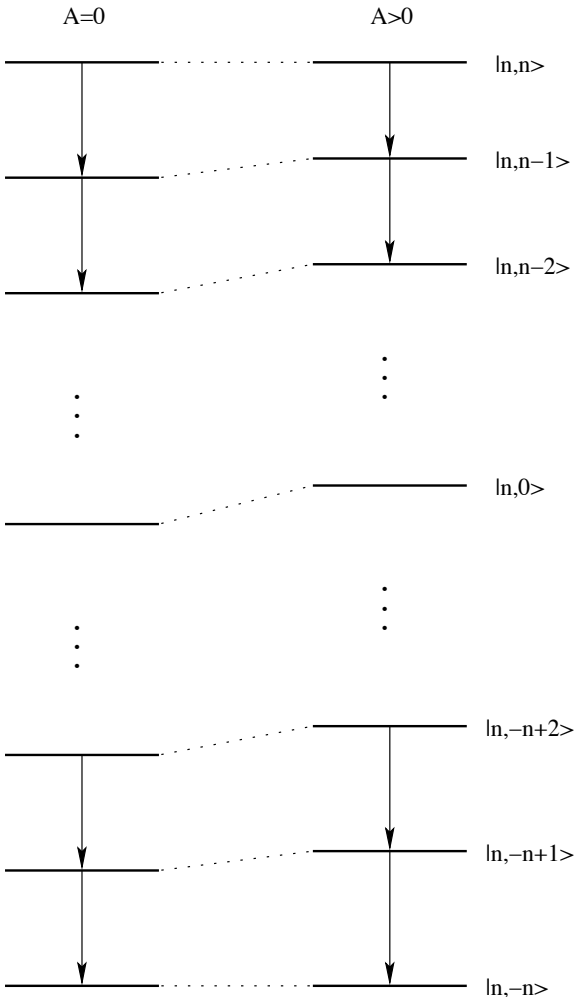

Figure 3.5: Spontaneous emission from the highest manifold through superradiant states for the ring configuration of Fig. 3.4, without and with nearest-neighbor A_{ij}'s taken into account. Energy levels are equally spaced if $A_{ij} = 0$. They are shifted as shown when $A_{ij} > 0$.

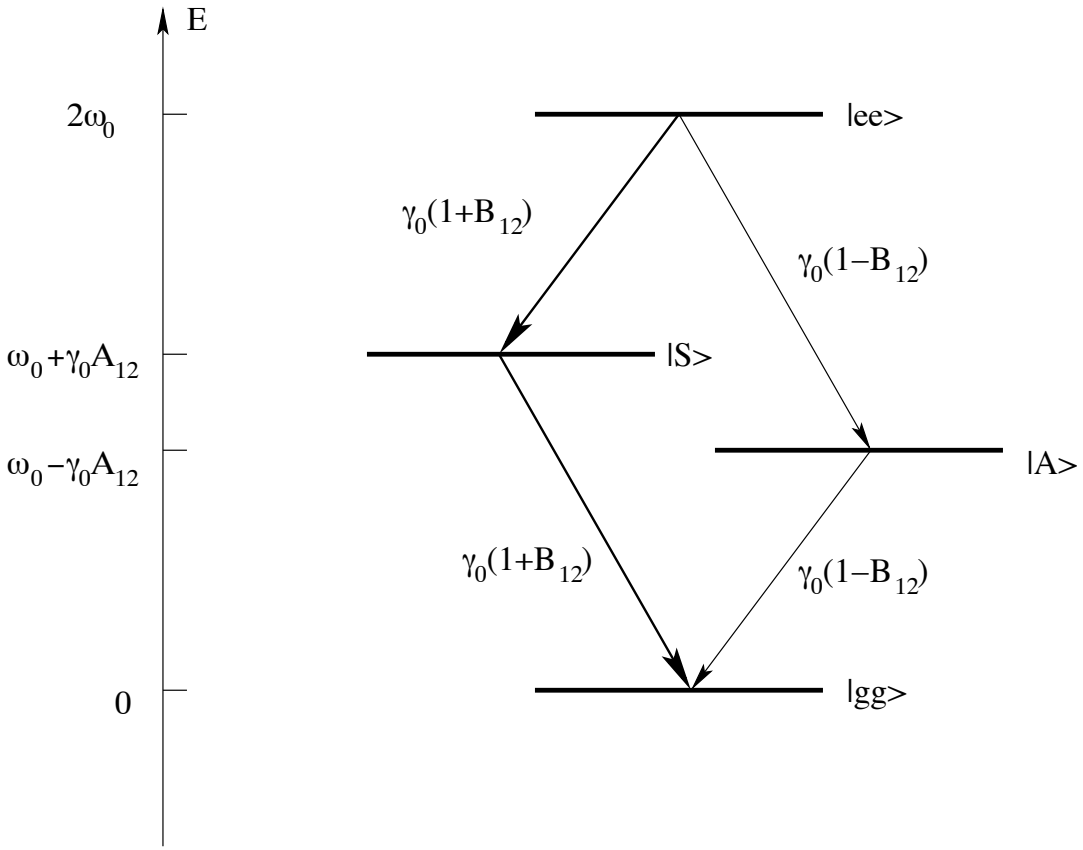

Figure 3.6: Spontaneous emission diagram for two atoms. Energy levels of states and spontaneous emission half rates between states are all shown.

$|a(0)\rangle = |e_1\rangle = \frac{1}{\sqrt{2}}(|S\rangle + |A\rangle)$, the evolution of atoms within $\mathcal{E}_1$ is

$$\begin{aligned} |a(t)\rangle &= \tfrac{1}{\sqrt{2}}\left(|S\rangle e^{-i[\omega_0+\gamma_0 A_{12}-i\gamma_0(1+B_{12})]t} + |A\rangle e^{-i[\omega_0-\gamma_0 A_{12}-i\gamma_0(1-B_{12})]t}\right) \\ &= |e_1\rangle e^{-i\omega_0 t}e^{-\gamma_0 t}\left(e^{-i\gamma_0 A_{12}t}e^{-\gamma_0 B_{12}t} + e^{i\gamma_0 A_{12}t}e^{\gamma_0 B_{12}t}\right)/2 \\ &\quad + |e_2\rangle e^{-i\omega_0 t}e^{-\gamma_0 t}\left(e^{-i\gamma_0 A_{12}t}e^{-\gamma_0 B_{12}t} - e^{i\gamma_0 A_{12}t}e^{\gamma_0 B_{12}t}\right)/2. \end{aligned} \tag{3.71}$$

The probability of finding atom 1 in excited state is

$$P_{|e_1\rangle}(t) = \frac{1}{4}e^{-2\gamma_0(1+B_{12})t} + \frac{1}{4}e^{-2\gamma_0(1-B_{12})t} + \frac{1}{2}\cos(2\gamma_0 A_{12}t)e^{-2\gamma_0 t}. \tag{3.72}$$

This is double decay plus damped Rabi oscillation. Similarly, the probability of finding atom 2 in excited state is

$$P_{|e_2\rangle}(t) = \frac{1}{4}e^{-2\gamma_0(1+B_{12})t} + \frac{1}{4}e^{-2\gamma_0(1-B_{12})t} - \frac{1}{2}\cos(2\gamma_0 A_{12}t)e^{-2\gamma_0 t}. \tag{3.73}$$

Fig. 3.7 shows the probability of finding atoms 1 and 2 in excited states as a function of time.

3.3.4 Gauge Transformation

This subsection quotes [37] directly. Let us look back at the Hamiltonian in Coulomb gauge, (3.22). The term H_{AR} has the form of (3.21) because it comes from the $\boldsymbol{A}\cdot\boldsymbol{p}$ term in (3.13). Part of this term eventually cancels the H_{DD} term.

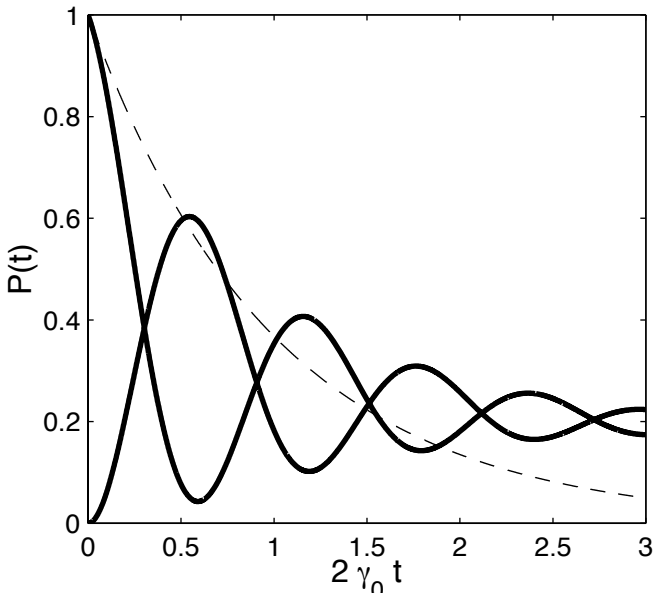

Figure 3.7: Probability of finding atom 1 and atom 2 in excited states as a function of time (solid lines). Two identical atoms are separated by distance $d = 0.1\lambda_0$ ($\lambda_0 \equiv 2\pi/k_0$), with their dipoles parallel to each other and perpendicular to the displacement between them, i.e., $\boldsymbol{d}_1 \| \boldsymbol{d}_2$ and $\boldsymbol{d}_1, \boldsymbol{d}_2 \perp \boldsymbol{x}_{12}$. Thus $A_{12} = 5.194$ and $B_{12} = 0.9227$. Initially atom 1 is in excited state and atom 2 in ground state. For comparison, the probability of finding the atom in excited state if there is only one atom and it is initially in excited state is also shown (dashed line).

Define the dipole operator of atom i as:

$$\boldsymbol{D}_i \equiv \boldsymbol{d}_i(\sigma_i + \sigma_i^+). \tag{3.74}$$

Under certain gauge transformation with some approximation, the Hamiltonian (3.22) is transformed to

$$H' = H_{A0} + H_R + H'_{AR}, \tag{3.75}$$

where the new coupling term

$$\begin{aligned} H'_{AR} &= -\sum_i \boldsymbol{D}_i \cdot \boldsymbol{E}_\perp(\boldsymbol{r}_i) \\ &= \sum_\nu \sum_i i\omega_\nu \mathcal{A}_{\omega_\nu}(\boldsymbol{\epsilon}_\nu \cdot \boldsymbol{d}_i)(-a_\nu e^{i\boldsymbol{k}_\nu \cdot \boldsymbol{r}_i} + a_\nu^+ e^{-i\boldsymbol{k}_\nu \cdot \boldsymbol{r}_i})(\sigma_i + \sigma_i^+). \end{aligned} \tag{3.76}$$

After RWA, the only difference to (3.21) is that the ω_i in (3.21) is replaced by ω_ν in (3.76). Note there is no H_{DD} term in (3.75)!

From the new Hamiltonian H', the master equation can be derived in a similar fashion. In place of (3.51), we have

$$\begin{aligned} \dot{\rho^I} &= -\sum_{i,j} \gamma_0 B_{ij} \{[\sigma_i^+ \sigma_j, \rho^I] - 2\sigma_i \rho^I \sigma_j^+\} \\ &\quad + i \sum_{i \neq j} \frac{\gamma_0}{2\pi\omega_0^3} \left\{ \int_{-\infty}^{\infty} \omega^3 B_{ij}(\omega) \left(\frac{1}{\omega - \omega_0} + \frac{1}{\omega + \omega_0} \right) d\omega \right\} [\sigma_i^+ \sigma_j, \rho^I] \\ &\quad + i \sum_i \frac{\gamma_0}{2\pi\omega_0^3} \left\{ \int_{-\infty}^{\infty} \omega^3 \left(\frac{1}{\omega - \omega_0} + \frac{1}{\omega + \omega_0} \right) d\omega \right\} [\sigma_i^+ \sigma_i, \rho^I]. \end{aligned} \tag{3.77}$$

The Lamb shift of individual atoms can be defined similarly:

$$\delta_0 \equiv -\frac{\gamma_0}{2\pi\omega_0^3}\int_{-\infty}^{\infty}\omega^3\left(\frac{1}{\omega-\omega_0}+\frac{1}{\omega+\omega_0}\right)d\omega, \tag{3.78}$$

and it still diverges. To evaluate the collective Lamb shift, in place of (3.54), we have

$$\frac{1}{2\pi\omega_0^3}\int_{-\infty}^{\infty}\omega^3 j_2(kr_{ij})\left(\frac{1}{\omega-\omega_0}+\frac{1}{\omega+\omega_0}\right)d\omega. \tag{3.79}$$

The integrand no longer has a pole at $\omega = 0$. This is consistent with the fact that H' does not include H_{DD}. The final form of the master equation is not affected by gauge transformation. However, as we will see in Chapter 4, the spectrum of spontaneous emission is slightly affected.

3.4 Summary

In this chapter, we have derived the Hamiltonian H for a group of point two-level atoms in radiation field. From H, the master equation (3.64) for the evolution of atomic variables initially in vacuum field is derived. In the derivation, we have applied Born approximation (perturbation), rotating-wave approximation and Markov approximation (short memory).

For identical atoms, the evolution of atoms can be thought of as under the influence of a dissipative effective Hamiltonian $\bar{H}$. Dissipation is the result of

spontaneous emission. States within the same manifold are connected by $\bar{H}$. States differ by one manifold are connected through spontaneous emission. $\bar{H}$ includes the lamb shift and decay of single atoms, as well as the generalized dipole-dipole interactions between atoms — $\mathcal{D}_{ij} = \gamma_0(A_{ij} - iB_{ij})$.

In two-atom or some highly symmetric cases, real and imaginary parts of $\bar{H}$ commute. It is then natural to use the complete orthogonal set of eigenstates of $\bar{H}$ as basis. The energy levels of eigenstates are determined by real part of $\bar{H}$. The couplings between states through spontaneous emission are determined by imaginary part of $\bar{H}$. Examples of these cases are discussed. In Dicke model of superradiance, we assume $B_{ij} = 1$ and $A_{ij} = 0$ for all i, j.

Chapter 4

Superradiance: Spontaneous Emission Spectrum

The master equation (3.64) gives the evolution of atomic variables while the radiation field is considered as a reservoir. In principle, the evolution of the field can be obtained from the evolution of atoms. In other words, we can first obtain the evolution of atoms without the knowledge of the field; once we know the evolution of atoms, we can then obtain the information of the field. As a continuation of Chapter 3, in this chapter, we introduce the resolvent method, and use the resolvent method to derive the spontaneous emission spectrum of two-level atoms in radiation field.

4.1 Resolvent Method

In this section, we introduce the resolvent method, which is very useful for a continuous Hamiltonian H that can be separated into a simple part H_0 and a difficult but small part V. The resolvent method is quite standard, here we follow the description in [32].

4.1.1 Projection Operator

We regroup the Hamiltonian H into two parts:

$$H = H_0 + V. \tag{4.1}$$

The easy part $H_0 = H_{A0} + H_R$. The difficult perturbation part V is $H_{DD} + H_{AR}$ or H'_{AR} depending on gauge.

A *projection operator* P projects a state into the subspace ("inner space") spanned by a set of orthonormal eigenstates of H_0 (unperturbed states). For example, we define P_m as the projection operator projecting onto atomic states within $\mathcal{E}_m$ and vacuum field state:

$$P_m \equiv \sum_{|a_m\rangle \in \mathcal{E}_m} |a_m; 0\rangle\langle a_m; 0|, \tag{4.2}$$

where $|a_m\rangle$ denotes a collective atomic state in $\mathcal{E}_m$ and $|0\rangle$ denotes the vacuum field state. The projection operator onto the complementary subspace ("outer space") is $Q = 1 - P$. It is easy to verify the basic properties of projection operators, such as $P^2 = P$, $Q^2 = Q$, and because inner space is spanned by eigenstates of H_0, $PH_0Q = QH_0P = 0$.

For a spontaneous emission process, if initially atoms are in $\mathcal{E}_m$, we can choose $P = P_m$ and $Q = Q_m \equiv 1 - P_m$. The initial state belongs to inner space and the final state belongs to outer space. The process is described by a matrix element of $Q_m U(T) P_m$, where time evolution operator $U(T) \equiv e^{-iHT}$. Later in this section, we will show $P_m H P_m = \bar{H}_m$ in a different context than in Chapter 3.

4.1.2 Resolvent and Level-shift Operator

The resolvent $G(z)$ of a Hamiltonian H is

$$G(z) \equiv \frac{1}{z - H}, \tag{4.3}$$

where z is a complex number. It comes from the Fourier transform of $U(T)$. Reverse Fourier transform gives

$$U(T) = \lim_{\eta \to 0^+} -\frac{1}{2\pi i} \int_{-\infty}^{\infty} dE e^{-iET} G(E + i\eta) \text{ for } T > 0. \tag{4.4}$$

With the introduction of resolvent, we can obtain $QU(T)P$ from the simpler $QG(z)P$.

We now proceed to get an algebraic expression for $QG(z)P$. From the definition of $G(z)$ (4.3),

$$(z - H)G(z) = 1. \tag{4.5}$$

Multiply (4.5) by P on the right, and by P or Q on the left, we get two equations for $PG(z)P$ and $QG(z)P$. Similar to procedures used in subsection 3.2.1, we can get the expressions for both $PG(z)P$ and $QG(z)P$. After applying the basic properties of projection operators, the two expressions are simplified to:

$$PG(z)P = \frac{P}{z - PH_0P - PR(z)P}, \tag{4.6}$$

and

$$QG(z)P = \frac{Q}{z - QHQ}V\frac{P}{z - PH_0P - PR(z)P}, \tag{4.7}$$

where the *level-shift operator*

$$R(z) \equiv V + V\frac{Q}{z - QHQ}V. \tag{4.8}$$

When $z = E + i\eta$, (4.8) becomes

$$R(E + i\eta) = V + V\frac{Q}{E - QHQ}V - i\pi VQ\delta(E - QHQ)QV, \tag{4.9}$$

because integration over $1/(E - QHQ + i\eta)$ gives a real principle value part and an imaginary delta function part.

Because we expect

$$P_m G(z) P_m = \frac{P_m}{z - \bar{H}_m}, \tag{4.10}$$

from (4.6) we naturally expect

$$P_m (H_0 + R(z)) P_m = \bar{H}_m. \tag{4.11}$$

Later in this section we will show this is indeed true for $z = E + i\eta$, after RWA to H and Born-Markov approximation to the level-shift operator $R(z)$.

4.1.3 Born Approximation

From (4.8), the level-shift operator can be expanded as

$$R(z) = V + V\frac{Q}{z - H_0}V + V\frac{Q}{z - H_0}V\frac{Q}{z - H_0}V + \cdots. \tag{4.12}$$

The (first order) Born approximation is to keep the first two terms only and neglect terms of higher orders of V in (4.12). Or, explicitly:

$$PR(z)P \approx PVP + PV\frac{Q}{z - H_0}VP. \tag{4.13}$$

The nature of the Born approximation when we choose $P = P_m$ is best understood in the gauge where $V = H'_{AR}$ and after RWA. In this gauge,

$P_m V P_m = 0$. After RWA, $P_m R(z) P_m$ includes all processes starting from and ending in states in inner space P_m, which involve the virtual emission and absorption of photons. The term $P_m V \frac{Q_m}{z - H_0} V P_m$ in (4.13) includes all processes shown in Fig. 4.1. Born approximation neglects other processes, some of which are shown in Fig. 4.2 for example.

Born approximation contains only virtual states in outer space Q that are coupled to states in inner space P through V only once. In other words, it contains virtual states that are only one step away from unperturbed states in P. This is the same Born approximation as in subsection 3.2.2. When $P = P_m$, it contains only virtual states with at most one photon. Indeed, (3.37) and (3.38) involve field states with at most one photon only.

If we include some atomic states within $\mathcal{E}_m$ in inner space P, we should include all states within $\mathcal{E}_m$ in P in order to apply the Born approximation appropriately. If we do not include all states within $\mathcal{E}_m$ in P, then for example, the process of Fig. 4.1(c) with $a, a'' \in P$ and $a' \notin P$ will not be included in Born approximation, but it is of the same order as the process of Fig. 4.1(c) with $a, a', a'' \in P$. On the other hand, processes in Fig. 4.2 are always of higher order than processes in Fig. 4.1 — they contain virtual states that are at least two steps away from states in P_m.

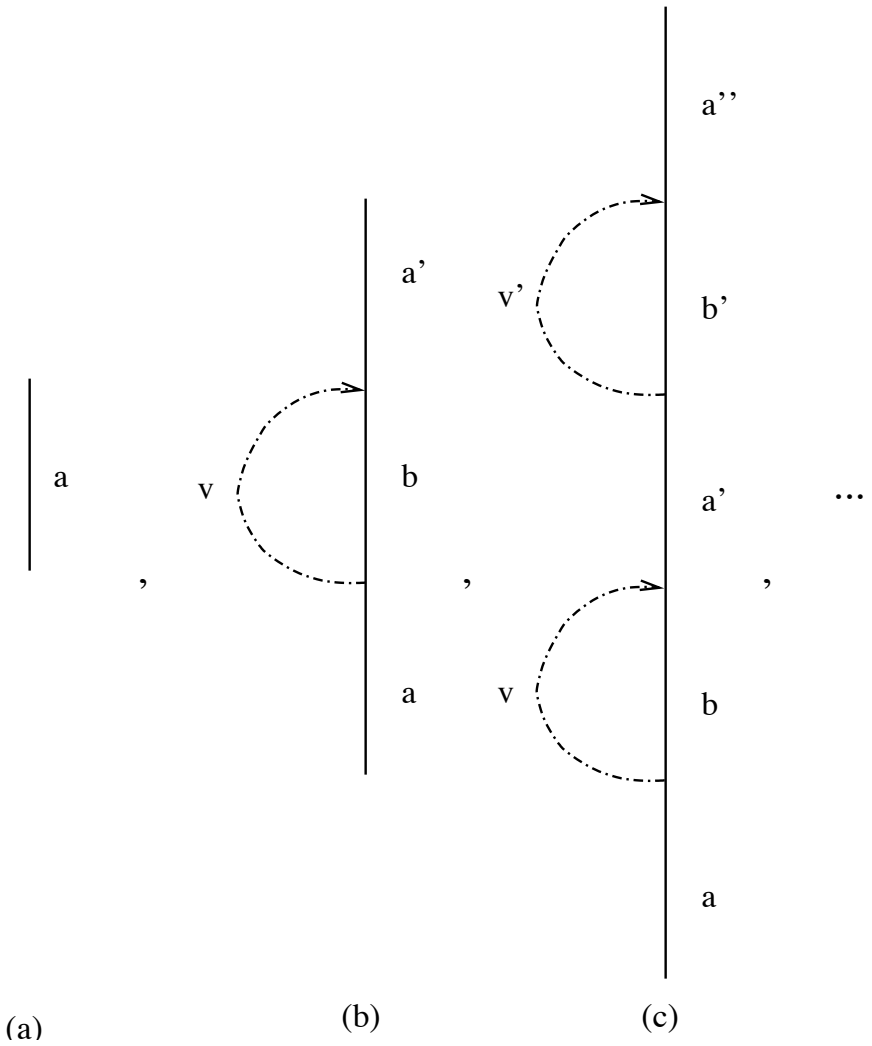

Figure 4.1: Processes included in Born approximation if $P = P_m$. Solid lines denote atomic states, $a, a', a'' \in \mathcal{E}_m$ and $b, b' \in \mathcal{E}_{m-1}$. Dashed lines denote photons. Time evolution is from bottom to top in each diagram. Each intersection of an atom line and a photon line means an interaction by V.

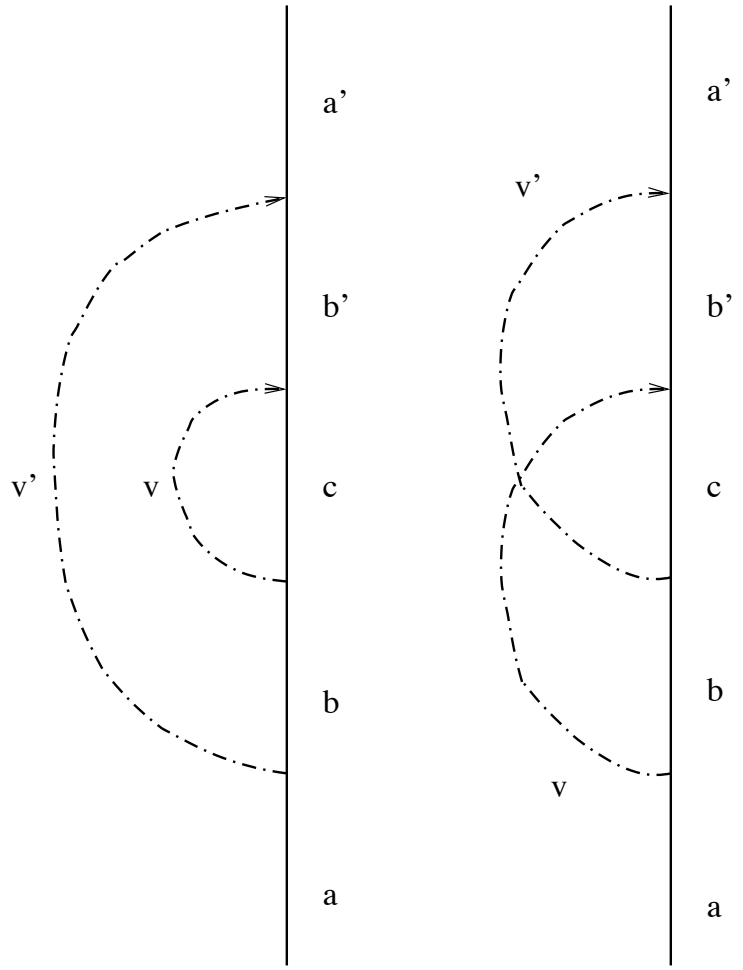

Figure 4.2: Sample processes not included in Born approximation. $a, a' \in \mathcal{E}_m$, $b, b' \in \mathcal{E}_{m-1}$ and $c \in \mathcal{E}_{m-2}$.

4.1.4 Markov Approximation

Both (4.6) and (4.7) contains the expression

$$\frac{P}{z - PH_0P - PR(z)P}. \tag{4.14}$$

We are interested in this expression when $z = E + i\eta$. (4.14) is large when E is near eigenvalues of PH_0P. Furthermore, this expression varies rapidly as a function of E near eigenvalues of PH_0P. Compared to the expression (4.14), $PR(z)P$ is approximately constant.

For $P = P_m$, eigenvalue of $P_mH_0P_m$ is $m\omega_0$ (in this subsection ω_0 does not include the single atom Lamb shift δ_0), so $P_mR(z)P_m \approx P_mR(m\omega_0 + i\eta)P_m$. As expected in subsection 4.1.2, we find

$$P_m(H_0 + R(m\omega_0 + i\eta))P_m = \bar{H}_m, \tag{4.15}$$

where we have used the Born approximation (4.13).

To study how $P_mR(E + i\eta)P_m$ varies near $E \approx m\omega_0$, we assume $E = (m-1)\omega_0 + \omega$. From (4.13), we have

$$P_m(H_0 + R(E + i\eta))P_m = \bar{H}_m(\omega), \tag{4.16}$$

where

$$\bar{H}_m(\omega) \equiv \sum_i [\omega_0 + \delta_0(\omega) - i\gamma_0(\omega)]\sigma_i^+\sigma_i + \sum_{i\neq j} \mathcal{D}_{ij}(\omega)\sigma_i^+\sigma_j \text{ (within } \mathcal{E}_m), \tag{4.17}$$

and

$$\mathcal{D}_{ij}(\omega) \equiv \gamma_0(\omega)[A_{ij}(\omega) - iB_{ij}(\omega)]. \tag{4.18}$$

Coupling through V to the field by a single atom gives $\delta_0(\omega) - i\gamma_0(\omega)$. $\delta_0(\omega)$ and $\gamma_0(\omega)$ are obtained by regarding (3.52) or (3.78) and (3.50) as definitions for $\delta_0(\omega_0)$ and $\gamma_0(\omega_0)$ (with γ_i, ω_i, and d_i in (3.50) replaced by γ_0, ω_0, and d_0). Coupling through V to the field by different atoms gives $\gamma_0(\omega)[A_{ij}(\omega) - iB_{ij}(\omega)]$ (see (3.57) and (3.41) for the definitions of $A_{ij}(\omega)$ and $B_{ij}(\omega)$).

The requirement that $P_m R(E + i\eta)P_m$ does not vary much for E around where (4.14) is large means the requirement that $\delta_0(\omega)$, $\gamma_0(\omega)$, $A_{ij}(\omega)$ and $B_{ij}(\omega)$ do not vary much for the frequency range of our interest, namely $\omega \sim \omega_0 \pm \gamma_A$. This is compatible with the condition for Markov (short memory) approximation (3.46) in subsection 3.2.4. The approximation that $PR(z)P$ is constant is Markov approximation in a different context. We will discuss the validity of Markov approximation for different cases when we encounter them later. As in Chapter 3, we can incorporate δ_0 into the new ω_0 after Markov approximation.

After Born-Markov approximation, we have

$$P_m G(E + i\eta)P_m = \frac{P_m}{E - \bar{H}_m}, \tag{4.19}$$

and

$$Q_m G(E+i\eta)P_m = \frac{Q_m}{E+i\eta-Q_m H Q_m} V \frac{P_m}{E-\bar{H}_m}. \tag{4.20}$$

4.2 Spectrum of Spontaneous Emission

According to the master equation (3.64), for any initial atomic state $|a_m\rangle$ in manifold $\mathcal{E}_m$ with $m > 0$, it will cascade down to atomic ground state $|0\rangle$ through spontaneous emissions. In other words, for any initial state $|a_m;0\rangle$, the final state is $|0;\nu_1\nu_2\cdots\nu_m\rangle$, where $|\nu\rangle$ denotes the existence of a photon in mode ν. In this section, we use the resolvent method to calculate $\langle 0;\nu_1\nu_2\cdots\nu_m|U(T\to\infty)|a_m;0\rangle$, and subsequently obtain the spectrum, or final distribution of photons.

4.2.1 Single-photon Process

(4.20) is directly applicable when the initial atomic state is within $\mathcal{E}_1$. When $m = 1$, Born approximation is unnecessary in deriving (4.19) and (4.20), because after RWA, processes shown in Fig. 4.2 are impossible.

The probability of eventually finding a photon $|\nu\rangle$ is $|\langle 0;\nu|U(T\to\infty)|a_1;0\rangle|^2$. $\langle 0;\nu|U(T\to\infty)|a_1;0\rangle$ can be obtained from $Q_1 G(E+i\eta)P_1$ by (4.4). Be-

cause we are assuming the final state is the unperturbed eigenstate of H_0, we are essentially making the approximation that $QHQ \approx QH_0Q$ in (4.20). From (4.20),

$$\langle 0;\nu|G(E+i\eta)|a_1;0\rangle = \frac{1}{E+i\eta-\omega_\nu}\langle 0;\nu|V\frac{1}{E-\bar{H}_1}|a_1;0\rangle. \tag{4.21}$$

The integration of (4.4) can be done by residue method. Poles of (4.21) in the bottom half of complex E plane are at $\omega_\nu - i\eta$ and eigenvalues of $\bar{H}_1$. $\bar{H}_1$ is dissipative, i.e., all its eigenvalues have finite negative imaginary parts. In the limit of $T \to \infty$, only the pole at $\omega_\nu - i\eta$ will contribute to the integral in (4.4) due to the factor of e^{-iET} in the integrand. Therefore,

$$\langle 0;\nu|U(T\to\infty)|a_1;0\rangle = e^{-i\omega_\nu T}\langle 0;\nu|V\frac{1}{\omega_\nu-\bar{H}_1}|a_1;0\rangle. \tag{4.22}$$

The spectral intensity I_ω satisfies

$$\int_0^\infty I_\omega d\omega = \sum_\nu |\langle 0;\nu|U(T\to\infty)|a_1;0\rangle|^2. \tag{4.23}$$

I_ω can be obtained by replacing the sum in (4.23) by an integral ((3.8)), and then equating the integrands. It can be written as

$$I_\omega = \langle a_1|c(\omega)I(\omega)|a_1\rangle, \tag{4.24}$$

where we have used

$$\int d\hat{\boldsymbol{k}} \sum_{\boldsymbol{\epsilon}} (V|0;\nu\rangle\langle 0;\nu|V) \;=\; \mathcal{A}^2_{\omega_\nu}\omega_\nu^2 d_0^2 \frac{8\pi}{3}\sum_{i,j} B_{ij}(\omega)\sigma_i^+\sigma_j$$

(within $\mathcal{E}_1$) for $V = H'_{AR}$. (4.25)

The coefficient $c(\omega) = \omega^3/\omega_0^3$. For $V = H_{DD} + H_{AR}$, ω_ν^2 in (4.25) is replaced by ω_0^2 and $c(\omega) = \omega/\omega_0$. As mentioned in subsection 3.3.4, the spontaneous emission spectrum is slightly different for the two gauges. Since we are interested in the spectrum where $\omega \sim \omega_0 \pm \gamma_A$ within the Markov approximation, we can assume $c(\omega) \approx 1$ and $B_{ij}(\omega) \approx B_{ij}$ for both gauges. $I(\omega)$ is a Hermitian operator acting on atomic states within $\mathcal{E}_1$:

$$I(\omega) \equiv \frac{1}{\pi} \frac{1}{\omega - \bar{H}_1^+} \bar{B}_1 \frac{1}{\omega - \bar{H}_1}, \tag{4.26}$$

where we define

$$\bar{B} \equiv \sum_i \gamma_0 \sigma_i^+ \sigma_i + \sum_{i \neq j} \gamma_0 B_{ij} \sigma_i^+ \sigma_j \tag{4.27}$$

as the imaginary part of $\bar{H}$, and $\bar{B}_1$ as imaginary part of $\bar{H}_1$. Similarly, we define

$$\bar{A} \equiv \sum_i \omega_0 \sigma_i^+ \sigma_i + \sum_{i \neq j} \gamma_0 A_{ij} \sigma_i^+ \sigma_j \tag{4.28}$$

as the real part of $\bar{H}$, and $\bar{A}_1$ as the real part of $\bar{H}_1$. After averaging over all possible initial conditions, i.e., $|a_1\rangle$'s,

$$I_\omega = \frac{1}{N} \mathrm{Tr} I(\omega). \tag{4.29}$$

4.2.2 Examples of Single-photon Cases

From (4.26), if real and imaginary parts of $\bar{H}_1$ commute: $[\bar{A}_1, \bar{B}_1] = 0$, we can easily work in the orthonormal basis of eigenstates of $\bar{H}_1$. Suppose $\omega_\alpha - i\Gamma_\alpha$'s and $|\bar{q}_\alpha\rangle$'s are eigenvalues and eigenstates of $\bar{H}_1$:

$$\bar{A}_1|\bar{q}_\alpha\rangle \equiv \omega_\alpha|\bar{q}_\alpha\rangle \ (\alpha = 1, 2, \cdots, N), \tag{4.30}$$

and

$$\bar{B}_1|\bar{q}_\alpha\rangle = \Gamma_\alpha|\bar{q}_\alpha\rangle. \tag{4.31}$$

From (4.26) and (4.29), we get

$$I_\omega = \frac{1}{N\pi} \sum_\alpha \frac{\Gamma_\alpha}{(\omega - \omega_\alpha)^2 + {\Gamma_\alpha}^2}. \tag{4.32}$$

The spontaneous emission spectrum is a sum of Lorentzians, with each eigenstate of $\bar{H}_1$ contributing one Lorentzian peak. The peak positions are determined by the real part of $\bar{H}_1$, shifted from ω_0 due to the real part of dipole-dipole interactions. The widths are determined by the imaginary part of $\bar{H}_1$, or the imaginary part of dipole-dipole interactions. The total area under the spectrum is 1, because there is exactly one photon in the final state. The area under each peak is the same, $\frac{1}{N}$, because we have assumed the probability of each initial state is the same.

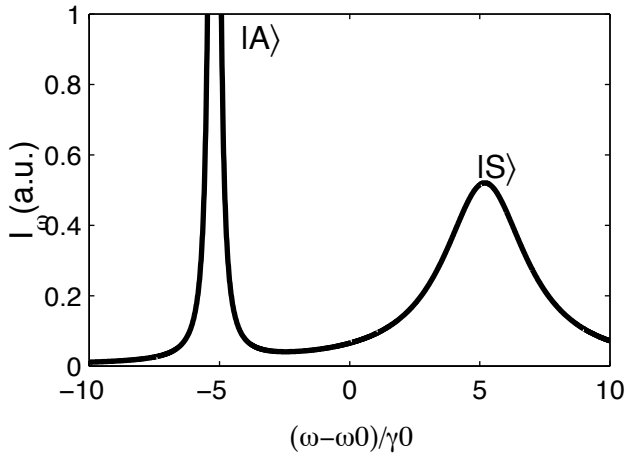

Figure 4.3: Spontaneous emission spectrum from the first excited manifold for two identical point two-level atoms separated by distance $d = 0.1\lambda_0$, with dipoles parallel to each other, and perpendicular to the displacement between them. The eigenstate of $\bar{H}_1$ responsible for each peak is labeled.

Fig. 4.3 shows an example of the spontaneous emission spectrum for two identical proximate atoms. The two eigenstates of $\bar{H}_1$ are just the superradiant state $|S\rangle$ and the subradiant state $|A\rangle$ defined in subsection 3.3.3.

If real and imaginary parts of $\bar{H}_1$ do not commute, we can still use (4.30) to find the position of spectral peaks. The width (4.31) is replaced by

$$\Gamma_\alpha \equiv \langle \bar{q}_\alpha | \bar{B}_1 | \bar{q}_\alpha \rangle. \tag{4.33}$$

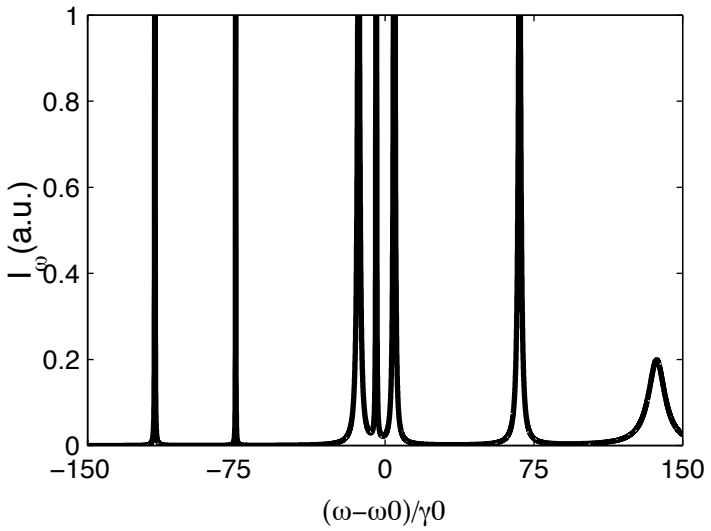

Figure 4.4: Spontaneous emission spectrum from the first excited manifold for 7 identical atoms proximately and randomly placed on a plane, with dipoles parallel to each other and perpendicular to the plane. The positions of the atoms are the same as the positions of scatterers in Fig. 2.8.

Because $[\bar{A}_1, \bar{B}_1] \neq 0$, there are *interferences* between overlapping spectral peaks. The lineshapes are deviated from Lorentzians. Fig. 4.4 shows an example of the spontaneous emission spectrum for seven identical proximate atoms randomly placed on a plane.

4.2.3 Multi-photon Process

If the initial state is within a manifold higher than $\mathcal{E}_1$, the cascading problem is much more complicated. We only outline the cascading problem briefly in this subsection. For example, if the initial state is $|a_2;0\rangle$, then the intermediate state after one photon has been emitted, $|a_1;\nu_2\rangle$, is unstable. The eventual final state $|0;\nu_1\nu_2\rangle$ has two photons. To study the cascading process of $|a_2;0\rangle \to |a_1;\nu_2\rangle \to |0;\nu_1\nu_2\rangle$, we use multiple projection operators: P_2, $P_1 = \sum_{|a_1\rangle\in\mathcal{E}_1} |a_1;\nu_2\rangle\langle a_1;\nu_2|$, and $Q = 1 - P_2 - P_1$. Using procedures similar to subsection 4.1.2,we can get

$$QG(z)P_2 = \frac{Q}{z - QHQ} VP_1G(z)P_1VP_2G(z)P_2. \tag{4.34}$$

From this, we can get an expression for $QG(E + i\eta)P_2$, and subsequently $\langle 0;\nu_1\nu_2|U(T \to \infty)|a_2;0\rangle$. Consistent with the Markov approximation, we assume the existence of the first emitted photon ν_2 does not affect the further evolution of the system (as opposed to virtually emitted photons). Furthermore, we cannot distinguish which of the final two photons ν_1 and ν_2 was emitted first, so we should equally consider the cascading process of

$|a_2;0\rangle \to |a_1;\nu_1\rangle \to |0;\nu_1\nu_2\rangle$. Thus we have

$$\langle 0;\nu_1\nu_2|G(E+i\eta)|a_2;0\rangle = \frac{1}{E+i\eta-\omega_{\nu_1}-\omega_{\nu_2}}$$
$$\times\left[\sum_{|a_1\rangle\in\mathcal{E}_1}\langle 0;\nu_1\nu_2|V\frac{1}{E-\bar{H}_1}|a_1;\nu_2\rangle\right.$$
$$\left.\times\langle a_1;\nu_2|V\frac{1}{E-\bar{H}_2}|a_2;0\rangle+\nu_1\leftrightarrow\nu_2\right], \tag{4.35}$$

where $\nu_1 \leftrightarrow \nu_2$ means exchange of ν_1 and ν_2. Therefore,

$$\langle 0;\nu_1\nu_2|U(T\to\infty)|a_2;0\rangle = \left[\sum_{|a_1\rangle\in\mathcal{E}_1}\langle 0;\nu_1\nu_2|V\frac{1}{\omega_{\nu_1}-\bar{H}_1}|a_1;\nu_2\rangle\right.$$
$$\left.\times\langle a_1;\nu_2|V\frac{1}{\omega_{\nu_1}+\omega_{\nu_2}-\bar{H}_2}|a_2;0\rangle+\nu_1\leftrightarrow\nu_2\right]e^{-i(\omega_{\nu_1}+\omega_{\nu_2})T}. \tag{4.36}$$

Note the two terms in brackets interfere with each other, so there are cross terms in $|\langle 0;\nu_1\nu_2|U(T\to\infty)|a_2;0\rangle|^2$.

4.3 Summary

In this chapter, we have provided the resolvent method to calculate the time evolution operator. Born and Markov approximations applied to the level-shift operator in this chapter are the same Born and Markov approximations in Chapter 3 in a different context.

We have studied in detail the spontaneous emission spectrum of a group of point two-level atoms initially in the first excited manifold. Eigenvalues of the real part of the effective Hamiltonian within the first excited manifold $\bar{H}_1$ determine the positions of spectral peaks. The imaginary part of $\bar{H}_1$ determines their widths. If real and imaginary parts of $\bar{H}$ do not commute, interferences between peaks cause the lineshapes to deviate from Lorentzians.

This chapter focuses on the *final* distribution of *photons*, while Chapter 3 focuses on the *time evolution* of *atoms*.

Chapter 5

Photon Scattering by Point Two-level Atoms in Ground State

This is the central chapter of this thesis.

The spontaneous emission spectra of two-level atoms from the first excited manifold shown in Chapter 4 (Figs. 4.3 and 4.4) are similar to the spectra (total cross section as a function of energy) of s-wave scatterers in Chapter 2 (Figs. 2.4 and 2.9). This is no coincidence. As will be shown in this chapter,

there is correspondence between particle scattering by a group of s-wave point scatterers and photon scattering by a group of point two-level atoms in ground state. The resonant scattering process of a photon by two-level atoms in ground state consists of two steps. First the atoms are excited to the first excited manifold by absorbing the incident photon. Then through spontaneous emission of a photon (the scattered photon), atoms decay back to ground state. Chapter 4 discusses the latter step.

The quantum theory of photon scattering by a group of atoms have been widely studied previously, e.g., in [40, 41, 42, 43]. In this chapter, we provide a multiple scattering point of view, similar to what is discussed in Chapter 2, for photon scattering by a group of atoms in ground state, taking all orders of multiple scattering effects into account.

In this chapter, we first formulate the photon scattering process using the effective Hamiltonian and resolvent method introduced in Chapters 3 and 4. We then provide a multiple scattering formulation for photon scattering by a group of point two-level atoms in ground state, and show it is equivalent to the effective Hamiltonian formulation. Thus we reveal its correspondence to particle scattering by a group of s-wave point scatterers. With the knowledge of correspondence, we provide an effective Hamiltonian view for particle

scattering by a group of scatterers.

In this chapter, we also study the applications of eigenchannel expansion introduced in Chapter 2 to proximity resonance of atoms, and its comparison to proximity resonance of scatterers.

5.1 Basic Photon Scattering Theory

5.1.1 T-matrix and Effective Hamiltonian

The basic quantum scattering theory introduced in subsection 2.1.1 can also be applied to the photon scattering problem. We follow the description in [32] in this subsection. For photon scattering by a group of point two-level atoms, the free space Hamiltonian is

$$H_0 = H_{A0} + H_R \tag{5.1}$$

and the potential V is coupling between atoms and the radiation field:

$$V = H_{DD} + H_{AR} \text{ or } H'_{AR} \tag{5.2}$$

depending on gauge. See subsections 3.1.3 and 3.3.4 for definition of terms. For photon scattering by atoms in ground state, the initial and final unper-

turbed states are $|0;\nu\rangle$ and $|0;\nu'\rangle$, both eigenstates of H_0. (Here $|0\rangle$ denotes atomic ground state.)

The definitions of the S-matrix and T-matrix, (2.5) and (2.7), are directly applicable. From the relationship between $U(T\to\infty)$ and the resolvent $G(z)$ (see (4.4) and arguments in subsection 4.2.1), we find that the T-matrix within the subspace of energy E, $\mathcal{T}_E$, is related to the resolvent by

$$\mathcal{T}_E = V + VG(E+i\eta)V. \tag{5.3}$$

For scattering by identical atoms in ground state, $\omega_\nu = \omega_{\nu'} = \omega$ so $E=\omega$. After rotating-wave approximation (RWA), $V|0;\nu\rangle \in P_1$, where inner space P_1 is spanned by eigenstates of H_0 included in the projection operator

$$P_1 \equiv \sum_{a_1\in\mathcal{E}_1} |a_1;0\rangle\langle a_1;0| \tag{5.4}$$

((4.2)), where a_1 denotes a collective atomic state within the first excited manifold $\mathcal{E}_1$. (Here $|0\rangle$ denotes vacuum field state.) From (4.19), we get the matrix element

$$\mathcal{T}_{\omega,\nu'\nu} \equiv \langle 0;\nu'|\mathcal{T}_\omega|0;\nu\rangle = \langle 0;\nu'|V\frac{P_1}{\omega-\bar{H}_1}V|0;\nu\rangle, \tag{5.5}$$

where $\bar{H}_1$ is the effective Hamiltonian (3.61) for a group of atoms within $\mathcal{E}_1$. As discussed in subsection 4.2.1, Born approximation is unnecessary for

evolution of atoms within $\mathcal{E}_1$.

The scattering process described by (5.5) is illustrated by the diagram in Fig. 5.1. From right to left, the two V's in (5.5) denote absorption of photon $|\nu\rangle$ and emission of photon $|\nu'\rangle$ respectively. The $P_1G(E+i\eta)P_1 = \frac{P_1}{\omega - \bar{H}_1}$ denotes the evolution of atoms within $\mathcal{E}_1$, including virtual emission and absorption of photons — it is the sum of all processes shown in Fig. 4.1.

5.1.2 Optical Theorem, Asymptotic T-matrix

The general equation (2.3), rewritten below, applies to photon scattering too.

$$|\psi\rangle = |\phi\rangle + |\phi_s\rangle, \tag{5.6}$$

where $|\phi\rangle$, $|\phi_s\rangle$ and $|\psi\rangle$ are the incident, scattered, and total wave.

In this subsection, we treat the radiation field semiclassically (see, e.g., [45, 46]). For our study of one-photon scattering by atoms in ground state, this treatment gives the same result as full quantum mechanical treatment to the field. The $\boldsymbol{E}^-(\boldsymbol{r})$ field for any field state $|\psi\rangle$ is defined as

$$\boldsymbol{E}^-_\psi(\boldsymbol{r}) \equiv \langle 0|\boldsymbol{E}^-(\boldsymbol{r})|\psi\rangle. \tag{5.7}$$

Besides a normalization factor, the $\boldsymbol{E}^-(\boldsymbol{r})$ field of the single photon in mode ν state, $|\nu\rangle \equiv a^+_\nu|0\rangle$, is a plane wave $\boldsymbol{\epsilon}_\nu e^{i\boldsymbol{k}_\nu\cdot\boldsymbol{r}}$. If the $\boldsymbol{E}^-(\boldsymbol{r})$ field of the incident

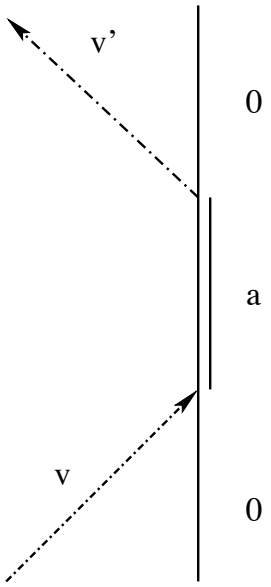

Figure 5.1: The process of photon scattering by two-level atoms in ground state, described by (5.5). Single solid lines denote atomic ground state. Dashed lines denote photons. Each intersection of an atom line and a photon line means an interaction by V. The double solid line denotes the evolution of atoms within $\mathcal{E}_1$, including virtual emission and absorption of photons. It is the sum of all processes shown in Fig. 4.1, with $a, a', a'', \cdots \in \mathcal{E}_1$ and $b, b', \cdots = 0$.

wave is a plane wave $\boldsymbol{\epsilon} e^{i\boldsymbol{k}\cdot\boldsymbol{r}}$, we write down the asymptotic $\boldsymbol{E}^{-}(\boldsymbol{r})$ field for (5.6) as:

$$\boldsymbol{E}^{-}_{\psi}(\boldsymbol{r}) \cong \boldsymbol{\epsilon} e^{i\boldsymbol{k}\cdot\boldsymbol{r}} + \boldsymbol{f}(\boldsymbol{k}, \boldsymbol{\epsilon}, \hat{\boldsymbol{r}}) \frac{e^{ikr}}{r} \text{ for } r \to \infty. \tag{5.8}$$

$\boldsymbol{f}(\boldsymbol{k}, \boldsymbol{\epsilon}, \hat{\boldsymbol{r}})$ is the *vector* scattering amplitude. It satisfies the optical theorem

$$\frac{4\pi}{k} \mathrm{Im}[\boldsymbol{\epsilon} \cdot \boldsymbol{f}(\boldsymbol{k}, \boldsymbol{\epsilon}, \hat{\boldsymbol{r}} = \hat{\boldsymbol{k}})] = \sigma(\boldsymbol{k}, \boldsymbol{\epsilon}), \tag{5.9}$$

where the total cross section

$$\sigma(\boldsymbol{k}, \boldsymbol{\epsilon}) \equiv \int |\boldsymbol{f}(\boldsymbol{k}, \boldsymbol{\epsilon}, \hat{\boldsymbol{r}})|^2 d\hat{\boldsymbol{r}}. \tag{5.10}$$

The resonant photon scattering spectrum, total cross section σ as a function of incident photon frequency ω, is also the absorption spectrum of the atoms. This is because for a photon to be resonantly scattered, it must be absorbed by the atoms first.

The asymptotic form of $\mathcal{T}_\omega$, T_ω, can be defined as an operator acting on functions of $(\hat{\boldsymbol{k}}, \boldsymbol{\epsilon})$:

$$T_\omega y(\hat{\boldsymbol{k}}, \boldsymbol{\epsilon}) \equiv \frac{3k}{8\pi} \int d\hat{\boldsymbol{k}}' \sum_{\boldsymbol{\epsilon}'} \boldsymbol{\epsilon} \cdot \boldsymbol{f}(k\hat{\boldsymbol{k}}', \boldsymbol{\epsilon}', \hat{\boldsymbol{k}}) y(\hat{\boldsymbol{k}}', \boldsymbol{\epsilon}'). \tag{5.11}$$

Eigenchannels are eigenstates of $\mathcal{T}_\omega$, and asymptotically, eigenfunctions of T_ω, whose eigenvalues are $\sin\Delta(\omega) e^{i\Delta(\omega)}$'s, where $\Delta(\omega)$'s are eigen-phase angles.

The discussion in this subsection is also applicable to scattering of *classical* radiation waves [38]. We only need to let $\boldsymbol{E}^-(\boldsymbol{r})$ to be understood as classical electric field.

5.2 Photon Scattering by a Single Point Two-level Atom in Ground State

5.2.1 Photon Scattering by a Single Point Two-level Atom in Ground State

For a single two-level atom placed at $\boldsymbol{r}_i$, with transition frequency ω_i (with Lamb shift incorporated), transition dipole $\boldsymbol{d}_i$, the effective Hamiltonian $\bar{H} = (\omega_i - i\gamma_i)\sigma_i^+\sigma_i$, where the half decay rate γ_i is defined as in (3.50). From (5.5), the T-matrix within the energy shell ω, $\mathcal{T}_i$, is

$$\mathcal{T}_{i,\nu'\nu} \propto \frac{\gamma_i}{\omega - \omega_i + i\gamma_i} e^{i(\boldsymbol{k}_\nu - \boldsymbol{k}_{\nu'})\cdot\boldsymbol{r}_i}, \tag{5.12}$$

The Markov (short memory) approximation assumes the Lamb shift and half decay rate γ_i are constant within the range of resonance $\omega \sim \omega_i \pm \gamma_i$. From (5.12), there is only one non-0 eigenvalue for the asymptotic T-matrix T_i,

which is

$$t_i = -\frac{\gamma_i}{\omega - \omega_i + i\gamma_i}, \tag{5.13}$$

and its corresponding eigenfunction is

$$y_i(\hat{\boldsymbol{k}}, \boldsymbol{\epsilon}) \equiv \frac{1}{\sqrt{\frac{8\pi}{3}}}(\boldsymbol{\epsilon} \cdot \hat{\boldsymbol{d}}_i)e^{-ik\hat{\boldsymbol{k}}\cdot\boldsymbol{r}_i}. \tag{5.14}$$

Therefore, a single atom is a single-channel scatterer for photons. From (5.14), the *eigenchannel* $|I_i\rangle$ of a single atom is

$$\langle\nu|I_i\rangle \propto \frac{1}{\sqrt{\frac{8\pi}{3}}}(\boldsymbol{\epsilon}_\nu \cdot \hat{\boldsymbol{d}}_i)e^{-i\boldsymbol{k}_\nu\cdot\boldsymbol{r}_i}. \tag{5.15}$$

$|I_i\rangle$ is the photon angular momentum eigenstate with $l = 1$ (with $\boldsymbol{r}_i$ as origin).

In the limit of a point atom, the wave matrix Ω_i can be written as

$$\Omega_i - 1 = t_i|O_i\rangle\langle I_i|, \tag{5.16}$$

where the scattered wave $|O_i\rangle$ is the outgoing part of $|I_i\rangle$. (5.16) is true everywhere except at $\boldsymbol{r} = \boldsymbol{r}_i$. The $\boldsymbol{E}^-(\boldsymbol{r})$ field of $|O_i\rangle$, $\boldsymbol{E}_i^-(\boldsymbol{r})$, is

$$\boldsymbol{E}_i^-(\boldsymbol{r}) \propto \left\{(\hat{\boldsymbol{x}} \times \hat{\boldsymbol{d}}_i) \times \hat{\boldsymbol{x}}\frac{1}{x} + [3\hat{\boldsymbol{x}}(\hat{\boldsymbol{x}} \cdot \hat{\boldsymbol{d}}_i) - \hat{\boldsymbol{d}}_i]\left(-\frac{i}{x^2} + \frac{1}{x^3}\right)\right\}e^{ix}, \tag{5.17}$$

where $\boldsymbol{x} \equiv k(\boldsymbol{r} - \boldsymbol{r}_i)$. It is the same as the radiation field of a classical oscillating dipole. $\boldsymbol{E}_i^-(\boldsymbol{r})$ diverges at $\boldsymbol{r}_i$, so it is impossible to get an expression

for $\langle\nu|O_i\rangle$. On the other hand, the $\boldsymbol{E}^-(\boldsymbol{r})$ field of $|I_i\rangle$ is $[\boldsymbol{E}_i^-(\boldsymbol{r})-\boldsymbol{E}_i^{-*}(\boldsymbol{r})]/2i$, which is finite at $\boldsymbol{r}_i$. $\langle\nu|I_i\rangle$ is given by (5.15).

There are two terms in the curly brackets of (5.17). The term involving $\frac{1}{x^2}$ and $\frac{1}{x^3}$ is the near field term, which does not survive in the asymptotic region $r \to \infty$. The term involving $\frac{1}{x}$ is the far field term, which survives in the asymptotic region and determines the scattering amplitude $\boldsymbol{f}(\boldsymbol{k}, \boldsymbol{\epsilon}, \hat{\boldsymbol{r}})$ in (5.8).

$$\boldsymbol{f}(\boldsymbol{k}, \boldsymbol{\epsilon}, \hat{\boldsymbol{r}}) = \alpha_i k^2 (\boldsymbol{\epsilon} \cdot \hat{\boldsymbol{d}}_i)(\hat{\boldsymbol{r}} \times \hat{\boldsymbol{d}}_i) \times \hat{\boldsymbol{r}} e^{-ik\hat{\boldsymbol{r}}\cdot\boldsymbol{r}_i}, \tag{5.18}$$

where the dynamical polarizability

$$\alpha_i \equiv \frac{3t_i}{2k^3}. \tag{5.19}$$

The the total cross section averaged over all possible directions $\hat{\boldsymbol{k}}$'s and polarizations $\boldsymbol{\epsilon}$'s of the incident photon, σ, is given by

$$\sigma = \frac{\pi}{2k^2} \sin^2 \delta_i, \tag{5.20}$$

where the eigen-phase angle δ_i satisfies

$$t_i = \sin \delta_i e^{i\delta_i}. \tag{5.21}$$

There is one resonance due to the excited state of the atom. The position of the peak is at $\omega = \omega_i$, and its half width is γ_i.

In this subsection, we have shown that a single point two-level atom in ground state is a single-channel point scatterer of photon. [44] is a recent review of point scatterer method in literature. The atom behaves like a classical point dipole which is polarizable only along $\hat{\boldsymbol{d}}_i$ direction with dynamical polarizability α_i [38].

5.2.2 Correspondence to Particle Scattering by a Single s-wave Point Scatterer

The discussion in the previous subsection is very similar to section 2.2. In this subsection, we point out the correspondence between particle scattering by a single s-wave point scatterer with one internal Breit-Wigner type resonance and photon scattering by a single point two-level atom in ground state.

For a particle, besides a normalization factor the plane wave $e^{i\boldsymbol{k}\cdot\boldsymbol{r}}$ is the momentum eigenstate $|\boldsymbol{k}\rangle$. From (2.29),

$$\langle \boldsymbol{k}|I_i\rangle \propto \frac{1}{\sqrt{4\pi}} e^{-i\boldsymbol{k}\cdot\boldsymbol{r}_i} \tag{5.22}$$

(compare with (5.15)). $|I_i\rangle$ is particle angular momentum eigenstate with $l = 0$. We assume the size of the s-wave scatterer or the two-level atom is small compared to the incident wavelength, so each is a single-channel scat-

terer ((2.28), (5.16)). In each case, the eigenchannel is angular momentum eigenstate with lowest possible l, and we can neglect the scattering of waves of higher l. In the limit of a point scatterer or atom, we can get the exact wave function everywhere except at $\boldsymbol{r}_i$. For particle scattering, because $G_i(\boldsymbol{r})$ diverges at $\boldsymbol{r}_i$, it is also impossible to get an expression for $\langle \boldsymbol{k}|O_i\rangle$. For both particle and photon scattering, the scattered wave is outside the Hilbert space $|\boldsymbol{k}\rangle$'s or $|\nu\rangle$'s span.

For particle scattering, a Breit-Wigner type resonance is due to a quasibound state in the potential well of the scatterer. A particle can be temporarily trapped inside the scatterer. On the other hand, with RWA, an atom in the excited state can be thought of as a photon temporarily "trapped" inside the atom, since the atom in ground state gets into excited state by absorbing the incident photon, and decays back to ground state by emitting a new photon. Therefore, the excited state of the atom gives resonance to scattering of photon, just as the quasibound state of the scatterer to scattering of particle. (2.35) and (5.13) have the same form.

The particle in the quasibound state corresponds to the atom in the excited state plus the radiation field in vacuum state. The particle in plane wave states (the continuum) corresponds to the atom in ground state plus

the field in one photon states. If we limit the Hilbert space of the particle to the internal state (the quasibound state inside the scatterer), we can write down its effective Hamiltonian as

$$\bar{H} = (E_i - i\gamma_i)\sigma_i^+\sigma_i, \tag{5.23}$$

the same as $\bar{H}$ for a two-level atom. σ_i and σ_i^+ should be understood as particle annihilation and creation operators. E_i is the energy level of the quasibound state plus "Lamb shift" — correction due to coupling to the continuum. γ_i is the half decay rate, again due to coupling to the continuum.

5.3 Photon Scattering by a Group of Point Two-level Atoms in Ground State

5.3.1 Multiple Scattering View and Green's Function

With the knowledge of correspondence between photon scattering by a single atom in ground state and particle scattering by a single scatterer, we now study the photon scattering by a group of point two-level atoms in ground state. We can use the same multiple scattering formulation as used for particle scattering by a group of s-wave point scatterers in subsection 2.3.1. Same

as (2.40) and (2.41), for any incident wave $|\phi\rangle$, which is a one-photon state, i.e., a linear combination of $|\nu\rangle$'s with $\omega_\nu = \omega$, the total wave is

$$|\psi\rangle = |\phi\rangle + \sum_i t_i |O_i\rangle\langle I_i|\psi_i\rangle, \tag{5.24}$$

and the effective incident wave for the ith atom is

$$|\psi_i\rangle = |\phi\rangle + \sum_{j\neq i} t_j |O_j\rangle\langle I_j|\psi_j\rangle. \tag{5.25}$$

For any incident wave $|\phi\rangle$, we have

$$\langle I_i|\phi\rangle \propto \hat{\boldsymbol{d}}_i \cdot \boldsymbol{E}^-_\phi(\boldsymbol{r}_i), \tag{5.26}$$

where $\boldsymbol{E}^-_\phi(\boldsymbol{r})$ is the $\boldsymbol{E}^-(\boldsymbol{r})$ field of $|\phi\rangle$. Therefore, the Green's matrix G is

$$G_{ij} = \begin{cases} 0 & \text{for } i = j, \\ \langle I_i|O_j\rangle \propto \hat{\boldsymbol{d}}_i \cdot \boldsymbol{E}^-_j(\boldsymbol{r}_i) & \text{for } i \neq j. \end{cases} \tag{5.27}$$

The proportionality constant can be fixed by

$$\lim_{\boldsymbol{r}_i \to \boldsymbol{r}_j} \mathrm{Im} G_{ij} = 1 \text{ for } \hat{\boldsymbol{d}}_i = \hat{\boldsymbol{d}}_j \text{ and } i \neq j. \tag{5.28}$$

From (5.17), (5.27) and (5.28), we get

$$\begin{aligned} G_{ij} &= \frac{3}{2}\left\{\left(-\frac{1}{x_{ij}^3} + \frac{i}{x_{ij}^2} + \frac{1}{x_{ij}}\right)(\hat{\boldsymbol{d}}_i \cdot \hat{\boldsymbol{d}}_j)\right. \\ &\quad \left. + \left(3\frac{1}{x_{ij}^3} - 3\frac{i}{x_{ij}^2} - \frac{1}{x_{ij}}\right)(\hat{\boldsymbol{x}}_{ij} \cdot \hat{\boldsymbol{d}}_i)(\hat{\boldsymbol{x}}_{ij} \cdot \hat{\boldsymbol{d}}_j)\right\} e^{ix_{ij}} \\ &= -A_{ij}(\omega) + iB_{ij}(\omega) \text{ (for } i \neq j), \end{aligned} \tag{5.29}$$

where $\boldsymbol{x}_{ij} \equiv k(\boldsymbol{r}_i - \boldsymbol{r}_j)$, and $A_{ij}(\omega)$ and $B_{ij}(\omega)$ are the same as introduced in Chapter 3 ((3.57) and (3.41)). The overlap between eigenchannels of single atoms

$$\langle I_i | I_j \rangle = \int d\hat{\boldsymbol{k}} \sum_{\boldsymbol{\epsilon}} y_i^*(\hat{\boldsymbol{k}}, \boldsymbol{\epsilon}) y_j(\hat{\boldsymbol{k}}, \boldsymbol{\epsilon}) = B_{ij}(\omega) \tag{5.30}$$

(see (3.40) and (3.41)).

Same as (2.42) and (2.43), we define the vector for incident wave $\vec{\phi}$ as $\phi_i = \langle I_i | \phi \rangle$, and the vector for effective incident waves $\vec{\psi}$ as $\psi_i = \langle I_i | \phi \rangle$. Then same as (2.46), we have

$$\vec{\psi} = (1 - GT)^{-1} \vec{\phi}. \tag{5.31}$$

From (5.24), the scattered wave

$$|\phi_s\rangle = \sum_i t_i \psi_i |O_i\rangle. \tag{5.32}$$

From (5.32), the near field terms of $|O_i\rangle$'s in (5.17) do not survive eventually in the scattering amplitude $\boldsymbol{f}(\boldsymbol{k}, \boldsymbol{\epsilon}, \hat{\boldsymbol{r}})$, but they are included in the Green's matrix G. The near field term is especially important for the Green's function between proximate atoms.

For multiple scattering of a classical radiation wave by a group of point dipoles, with the ith dipole positioned at $\boldsymbol{r}_i$ and polarizable only along $\hat{\boldsymbol{d}}_i$

with dynamical polarizability α_i, if the electric field of the incident wave is the same as $\boldsymbol{E}^-_{\phi}(\boldsymbol{r})$, then the electric field of the scattered wave is the same as $\boldsymbol{E}^-_{\phi_s}(\boldsymbol{r})$. The multiple scattering of classical radiation waves has been studied previously in [47, 5].

5.3.2 Equivalence between Multiple Scattering View and Effective Hamiltonian View

For a group of identical atoms, under Markov approximation we neglect the frequency dependence of the Green's function by choosing $G_{ij} = G_{ij}(\omega_0)$. We will discuss the validity of Markov approximation for different cases later. Then the multiple scattering formulation discussed in the previous subsection is equivalent to the formulation in subsection 5.1.1 for the T-matrix (5.5) involving the effective Hamiltonian for a group of identical atoms. To see this, we point out that from (3.62) and (5.29),

$$\mathcal{D}_{ij} = -\gamma_0 G_{ij}! \tag{5.33}$$

The generalized dipole-dipole interaction between atoms i and j is proportional to the projection of the outgoing part of the eigenchannel of atom j onto the eigenchannel of atom i.

On reflection, this is hardly unexpected. In multiple scattering view, the Green's matrix element G_{ij} means a photon scattered by atom i can be scattered again by atom j, or a photon temporarily trapped in atom i can be temporarily trapped again in atom j after emission by atom i. In effective Hamiltonian view, the generalized dipole-dipole interaction $\mathcal{D}_{ij}$ is due to atoms i and j coupling to the same continuum (one-photon field states) — a photon (virtually) emitted by atom i can be reabsorbed by atom j (see discussion in subsection 4.1.3). These two views are equivalent.

As shown in (3.62) or (5.33), the generalized dipole-dipole interaction between atoms, $\mathcal{D}_{ij}$, is dependent on γ_0, the half decay rate of a single atom. Recall from Chapter 3 that δ_0 (the Lamb shift) and γ_0 originate from a single atom i coupling to the continuum. In this chapter, we have learned the coupling is only to the eigenchannel $|I_i\rangle$ component of the continuum. $\mathcal{D}_{ij}$'s originate from different atoms coupling to the same continuum. When neighboring atoms are proximate, i.e., within each other's effective radius: $x_{ij} \equiv k_0 r_{ij} \lesssim 1$, or equivalently, there is significant overlap between the eigenchannels of neighboring atoms: $B_{ij} \not\ll 1$, $\mathcal{D}_{ij}$ is comparable to δ_0 and γ_0. In this case, the atoms interact with the continuum collectively. Heuristically, when atoms are proximate, you cannot distinguish from which atom a photon

is emitted.

In Chapter 3, we did not proceed further to derive the effective Hamiltonian for a group of nonidentical atoms. In the previous subsection, however, we already have the multiple scattering formulation for photon scattering by a group of nonidentical atoms in ground state. From its equivalence to the effective Hamiltonian formulation, we know that the effective Hamiltonian for a group of nonidentical point two-level atoms within the first excited manifold, $\bar{H}_1$, is

$$\bar{H}_1 \equiv \sum_i (\omega_i - i\gamma_i)\sigma_i^+\sigma_i + \sum_{i\neq j} \mathcal{D}_{ij}\sigma_i^+\sigma_j \text{ (within } \mathcal{E}_1), \tag{5.34}$$

where $\mathcal{D}_{ij}$ is replaced by

$$\mathcal{D}_{ij} = -\sqrt{\gamma_i\gamma_j}G_{ij} = \sqrt{\gamma_i\gamma_j}A_{ij} - i\sqrt{\gamma_i\gamma_j}B_{ij}. \tag{5.35}$$

This formulation is useful only when ω_i's are close to each other, so Markov approximation can still be applicable, i.e., we can still assume Lamb shifts, γ_i's and G_{ij}'s are constants within the frequency range of our interest.

5.3.3 Correspondence to Particle Scattering by a Group of s-wave Point Scatterers

Correspondingly, we can also give an effective Hamiltonian for a single particle (within the "first excited manifold") inside a group of s-wave point scatterers. The approximation that E_i's (Lamb shifts), γ_i's and Green's matrix elements are constants independent of energy (see subsection 2.3.6) is the Markov approximation. After Markov approximation, we can write

$$\bar{H}_1 \equiv \sum_i (\omega_i - i\gamma_i)\sigma_i^+\sigma_i + \sum_{i\neq j} \mathcal{M}_{ij}\sigma_i^+\sigma_j. \tag{5.36}$$

The "generalized monopole-monopole interaction" $\mathcal{M}_{ij}$ is

$$\mathcal{M}_{ij} = -\sqrt{\gamma_i\gamma_j}G_{ij} = \sqrt{\gamma_i\gamma_j}A_{ij} - i\sqrt{\gamma_i\gamma_j}B_{ij}, \tag{5.37}$$

where A_{ij} and B_{ij} $(i \neq j)$ are defined as in (2.61) and (2.49). $\mathcal{M}_{ij}$ is due to different quasibound states coupling to the same continuum.

We only study the case where there is only one incident particle, just as we only study the case where there is only one incident photon. We use $|e_i\rangle$ to denote the quasibound state of the particle inside the ith scatterer. In $|e_i\rangle$ basis, representation of the effective Hamiltonian (5.36) within the first excited manifold (including all states which have one particle inside the

scatterers) is just

$$\bar{H}_1 = \bar{A} - i\bar{B}, \tag{5.38}$$

where matrices $\bar{A}$ and $\bar{B}$ are given by (2.89) and (2.91). The internal state $\vec{\bar{q}}_\alpha$ introduced in subsection 2.3.6 is actually a collective quasibound state — a state quasibound in a group of scatterers.

$$|\bar{q}_\alpha\rangle = \sum_i \bar{q}_{i\alpha}|e_i\rangle. \tag{5.39}$$

We will further discuss the collective quasibound state in subsection 5.3.5.

For one-photon scattering by atoms in ground state, we only need the effective Hamiltonian within $\mathcal{E}_1$, $\bar{H}_1$. We can call the real and imaginary parts of $\bar{H}_1$, $\bar{A}_1$ and $\bar{B}_1$ introduced in subsection 4.2.1, directly as $\bar{A}$ and $\bar{B}$. For photon scattering, $|e_i\rangle$ means the state in which atom i is in the excited state and all other atoms are in ground states. Representation of $\bar{A}$ and $\bar{B}$ in $|e_i\rangle$ basis corresponds to matrices $\bar{A}$ and $\bar{B}$ introduced in Chapter 2 for particle scattering. The state $|\bar{q}_\alpha\rangle$ introduced in subsection 4.2.2 is a collective excited state of atoms within $\mathcal{E}_1$, corresponding to the collective quasibound state of a single particle inside scatters (5.39). For photon scattering, in $|e_i\rangle$ basis, the form of the equations corresponding to (5.38), (2.89) and (2.91) is the same.

For multi-particle states inside identical scatterers, similar to (3.61), we can write an effective Hamiltonian for any manifold:

$$\bar{H} = \sum_i (\omega_0 - i\gamma_0)\sigma_i^+\sigma_i + \sum_{i\neq j} \mathcal{M}_{ij}\sigma_i^+\sigma_j. \tag{5.40}$$

For (5.40) to be valid, some restrictions are necessary. Each scatterer i can only have two states: the unoccupied state $|g_i\rangle$ and occupied by a single particle state (quasibound state for particle) $|e_i\rangle$. In other words, two particles cannot occupy the same scatterer, just as a two-level atom cannot be excited twice. Particles must be identical. There must be no direct interactions between particles. The quantum mechanical indistinguishability of particles must be taken into account explicitly, just as in subsection 4.2.3, where the indistinguishability of photons were taken into account explicitly. The full discussion of multi-particle and multi-photon processes are beyond the scope of this thesis.

5.3.4 Eigenchannels and T-matrix

We come back to photon scattering by a group of atoms in ground state in this subsection. With the full knowledge of correspondence between particle scattering and photon scattering, the contents of subsections 2.3.2—2.3.5 can

be easily adapted. Here we briefly restate some important results from these subsections for photon scattering by a group of atoms in ground state.

Matrices A and B are defined as

$$A_{ij} \equiv \begin{cases} t_i^{-1} + i = \cot\delta_i & \text{for } i = j, \\ -\mathrm{Re}G_{ij} & \text{for } i \neq j, \end{cases} \tag{5.41}$$

and

$$B_{ij} \equiv \langle I_i | I_j \rangle = \int d\hat{\boldsymbol{k}} \sum_{\boldsymbol{\epsilon}} y_i^*(\hat{\boldsymbol{k}}, \boldsymbol{\epsilon}) y_j(\hat{\boldsymbol{k}}, \boldsymbol{\epsilon}) = \begin{cases} 1 & \text{for } i = j, \\ \mathrm{Im}G_{ij} = B(x_{ij}) & \text{for } i \neq j. \end{cases} \tag{5.42}$$

The T-matrix is of rank N, and $BT(1 - GT)^{-1}B$ is representation of the asymptotic T-matrix in the nonorthogonal $y_i(\hat{\boldsymbol{k}}, \boldsymbol{\epsilon})$ basis. At each frequency of incident photon, eigenchannels $\vec{q}_\alpha$'s or $|I_\alpha\rangle$'s or asymptotically $Y_\alpha(\hat{\boldsymbol{k}}, \boldsymbol{\epsilon})$'s, and eigen-phase angles Δ_α's can be obtained by solving the eigensystem problem

$$B^{-1}A\vec{q}_\alpha = \cot\Delta_\alpha \vec{q}_\alpha, \tag{5.43}$$

and

$$|I_\alpha\rangle \equiv \sum_i q_{i\alpha}|I_i\rangle,\ Y_\alpha(\hat{\boldsymbol{k}}, \boldsymbol{\epsilon}) \equiv \sum_i q_{i\alpha} y_i(\hat{\boldsymbol{k}}, \boldsymbol{\epsilon}). \tag{5.44}$$

In place of (2.77), the total cross section

$$\sigma = \frac{\pi}{2k^2} \sum_{\alpha} \sin^2 \Delta_\alpha, \tag{5.45}$$

and the optical theorem for photon scattering (5.9) is also satisfied.

The photon angular momentum eigenstates (with $\boldsymbol{r}_i$ as origin), just as $|\nu\rangle$'s, form a complete set for one-photon field states. Except for one of the three $l = 1$ states, $|I_i\rangle$, all other eigenstates have $\hat{\boldsymbol{d}}_i \cdot \boldsymbol{E}^-(\boldsymbol{r}_i) = 0$. In place of (2.42), we have

$$\phi_i \propto \hat{\boldsymbol{d}}_i \cdot \boldsymbol{E}^-_\phi(\boldsymbol{r}_i). \tag{5.46}$$

For all the infinitely degenerate incident waves (one-photon states) with the same frequency, we can have a basis in which all but N waves with $\hat{\boldsymbol{d}}_i \cdot \boldsymbol{E}^-(\boldsymbol{r}_i) = 0$ for each i. The system only scatters the N waves with non-0 $\hat{\boldsymbol{d}}_i \cdot \boldsymbol{E}^-(\boldsymbol{r}_i)$'s and does not scatter the rest at all. Therefore, the rank of the T-matrix is N.

5.3.5 Resonances and Effective Hamiltonian

With the introduction of $\bar{H}_1$ for both particle inside scatterers and atoms, the meaning of the discussions in subsection 2.3.6 is clear. For both particle and photon scattering, the real part of $\bar{H}_1$, $\bar{A}$, determines the position of each

resonance E_α (or ω_α) (in the sense of (2.80)) and its corresponding internal state $|\bar{q}_\alpha\rangle$:

$$\bar{A}|\bar{q}_\alpha\rangle = E_\alpha|\bar{q}_\alpha\rangle \tag{5.47}$$

(see (2.88) and (4.30)). The imaginary part of $\bar{H}_1$, $\bar{B}$, determines the half width of the resonance (in the sense of (2.81)):

$$\Gamma_\alpha = \langle\bar{q}_\alpha|\bar{B}|\bar{q}_\alpha\rangle \tag{5.48}$$

(see (2.90) and (4.33)). The internal state $|\bar{q}_\alpha\rangle$ is related to the eigenchannel at resonance $\vec{q}_\alpha(E_\alpha)$ by (2.86), or

$$|q_{i\alpha}(E_\alpha)|^2 \propto \gamma_i|\bar{q}_{i\alpha}|^2. \tag{5.49}$$

The strength of the scattered wave from scatterer (atom) i, $|q_{i\alpha}|^2$, is proportional to the probability of finding the particle inside scatterer i (atom i in the excited state), $|\bar{q}_{i\alpha}|^2$, times the half decay rate of the quasibound state of scatterer i (the excited state of atom i), γ_i.

Except for a few highly symmetric cases, real and imaginary parts of $\bar{H}_1$, $\bar{A}$ and $\bar{B}$ do not commute (or equivalently matrices A and B do not commute). If we diagonalize the real part $\bar{A}$, we get the position of resonance peaks and internal states $|\bar{q}_\alpha\rangle$'s, as shown in previous paragraph. The

imaginary part $\bar{B}$ is not diagonal in $|\bar{q}_\alpha\rangle$ basis. Diagonal elements give the half widths of resonances, and offdiagonal elements give interferences between resonances. When there is overlap between two resonance peaks, i.e., $|E_\alpha - E_\beta| \lesssim \Gamma_\alpha + \Gamma_\beta$, interference between them causes the resonance peaks to be unsymmetric, deviating from Lorentzians.

For identical scatterers (atoms), diagonalization of the imaginary part $\bar{B}$ (or matrix B) gives offresonant eigenchannel $\vec{\tilde{q}'}_\alpha$'s and their offresonant half width $\tilde{\Gamma}_\alpha$'s. In $\vec{\tilde{q}'}_\alpha$ (or $\vec{\tilde{q}}_\alpha$) basis, the real part $\bar{A}$ (or matrix A) is not diagonal. $\bar{A}$ (or A) gives the positions of resonance peaks. Offdiagonal elements cause the mixing of offresonant channels, and thus the interferences between peaks.

The evolution of a particle inside scatterers (atomic variables within $\mathcal{E}_1$) is governed by $\bar{H}_1$. Each resonance corresponds to an eigenvalue of $\bar{H}_1$ or a pole of T-matrix on complex E plane. Again, when $[\bar{A}, \bar{B}] \neq 0$, interference between resonances comes from the nonorthogonality between eigenstates of $\bar{H}_1$.

5.4 Proximity Resonance of Atoms

In this section, we study the proximity resonance of N atoms using the concept of eigenchannel expansion. The Green's function or generalized dipole-dipole interaction between two point two-level atoms depends on not only the distance between them, but also the orientation of their transition dipoles. If all atoms are on a plane with each dipole perpendicular to the plane, then it depends on the distance between the atoms only: $A_{ij} = A_1(x_{ij})$ and $B_{ij} = B_1(x_{ij})$. In subsections 5.4.1–5.4.3, we consider identical proximate point two-level atoms in this situation only. This is directly comparable to the case of identical proximate scatterers on a plane, discussed in section 2.4.

We only study small samples of atoms in this section, where each pair of atoms is proximate: $x_{ij} \lesssim 1$ for all i, j. We will study large samples in Chapter 6. The Markov approximation is valid when, for the frequency range of our interest, $|\Delta G_{ij}| \ll |G_{ij}|$ for all i, j. For small samples of two-level atoms on a plane with each dipole perpendicular to the plane,

$$\left|\frac{\partial G_{ij}}{\partial k}\right| \approx \frac{9}{2}\frac{1}{k^4 r_{ij}^3} \tag{5.50}$$

and $|G_{ij}| \approx \frac{3}{2}\frac{1}{(kr_{ij})^3}$. Therefore, the validity condition for Markov approxi-

mation is: $|\Delta k| \ll k$ or

$$\Delta\omega \ll \omega \tag{5.51}$$

for the frequency range of our interest (compare with (2.98)).

5.4.1 Two-atom Case

Fig. 5.2 shows the total cross section and cotangent of phase angles as a function of incident photon frequency for two identical proximate atoms. As mentioned in subsection 5.1.2, the resonant scattering spectrum is also the absorption spectrum. Real and imaginary parts of $\bar{H}_1$ commute in two-atom case. The two eigenchannels $\vec{q'}_\alpha$'s are the as in (2.99), frequency independent. On resonance, their corresponding internal states are just $|S\rangle = \frac{1}{\sqrt{2}}(|e_1\rangle + |e_2\rangle)$ and $|A\rangle = \frac{1}{\sqrt{2}}(|e_1\rangle - |e_2\rangle)$ introduced in subsection 3.3.3. Fig. 5.3 illustrates these two eigenchannels. The method of illustration of eigenchannels is the same as in Chapter 2. $\vec{q'}_\alpha$ is illustrated by colored dots centered at $\boldsymbol{r}_i$'s. For each dot, its color is determined by the sign of $q'_{i\alpha}$, and its radius is proportional to $|q'_{i\alpha}|$. $Y_\alpha(\hat{\boldsymbol{k}}, \boldsymbol{\epsilon})$ is illustrated by plotting $\sum_{\boldsymbol{\epsilon}} |Y_\alpha(\hat{\boldsymbol{k}}, \boldsymbol{\epsilon})|^2$ as a function of $\hat{\boldsymbol{k}}$. Not surprisingly, the symmetric channel 1 is "dipole-like" and gives a broad peak, the antisymmetric channel 2 is "quadrupole-like" and

gives a sharp peak.

The configuration of atoms is the same as in Fig. 4.3. Indeed, the positions and widths of peaks are the same for both the absorption and the spontaneous emission spectrum. However, the heights of the peaks are different. In the emission spectrum, the area under each peak is the same ((4.32)). In the absorption spectrum, the maximum contribution from each eigenchannel is the same, namely $\frac{\pi}{2k^2}$ ((5.45)), thus the area under channel 1 peak is much larger than the area under channel 2 peak. In calculating the emission spectrum, we assume the initial state is equally likely in $|S\rangle$ and $|A\rangle$. The absorption spectrum tells us that the atoms are more easily to be excited into $|S\rangle$ state from ground state than into $|A\rangle$ state.

In contrast to the two-scatterer case discussed in subsection 2.4.1 (see Fig. 2.4), the symmetric channel peak is shifted upwards in frequency and the antisymmetric channel peak is shifted downwards compared to single-atom resonance. This is because for photon scattering by atoms, the expansion of A_{ij} is

$$A_{ij} = \frac{3}{2}\frac{1}{x_{ij}^3} - \cdots. \tag{5.52}$$

The leading term is positive (compare with (2.119)).

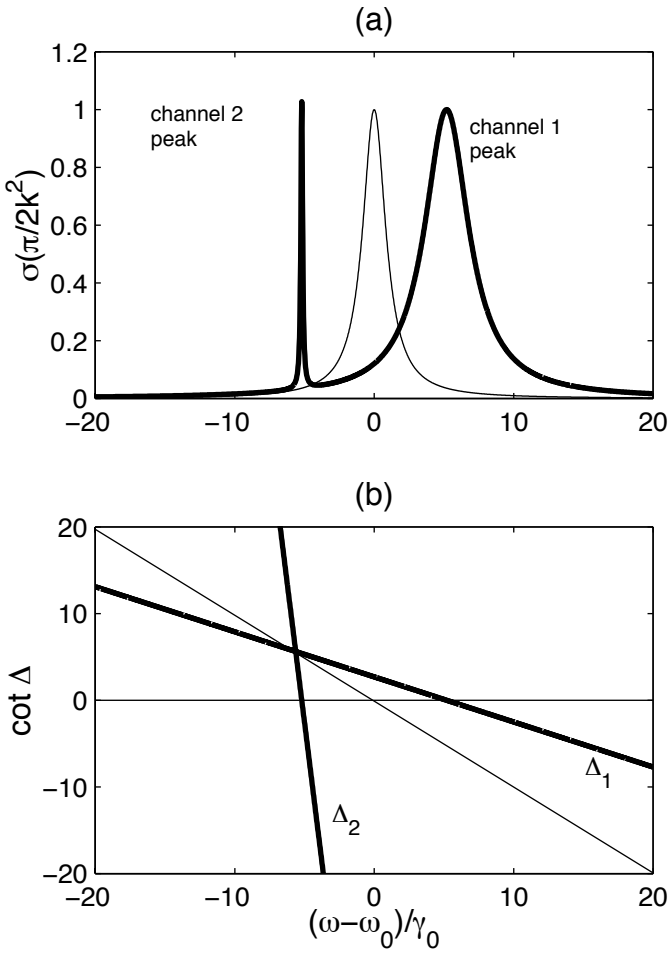

Figure 5.2: (a) total cross section and (b) cotangent of phase angles as a function of incident photon frequency for two atoms separated by distance $d = 0.1\lambda_0$ (wide lines). The configuration of atoms is the same as in Fig. 4.3. For comparison, total cross section and cotangent of phase angle of a single atom are also shown (narrow lines).

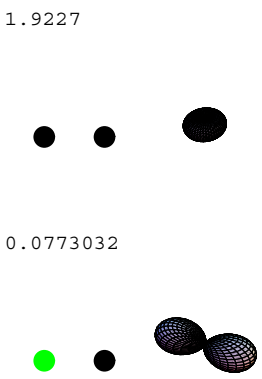

Figure 5.3: Eigenchannels for two atoms, specified in Fig. 5.2. For each eigenchannel α, Γ_α/γ_0, $\vec{q'}_\alpha$, and $Y_\alpha(\hat{\boldsymbol{k}}, \boldsymbol{\epsilon})$ are shown.

5.4.2 Three-atom Case

Fig. 5.4 shows the total cross section and cotangent of phase angles as a function of incident photon frequency for three identical proximate atoms on a line (compare with Fig. 2.6). Fig. 5.5 illustrates the offresonant eigenchannels of the three atoms (compare with Fig. 2.7). Similar to the discussion in subsection 2.4.2, the offresonant eigenchannels are dipole-, quadrupole-, and octapole-like. The dipole-like channel gives a broad peak shifted in frequency. The remaining two channels give two sharp peaks at frequencies lower than the broad peak. We will discuss the general features of the offresonant eigenchannels and the absorption spectrum of small samples in next subsection.

As discussed in Chapter 2 and in subsection 5.3.5, the unsymmetric Fano lineshape of channel 3 peak (Fig. 5.4(a)) can be explained by the avoided crossing between $\cot\Delta_1$ and $\cot\Delta_3$ near $\cot\Delta = 0$ (Fig. 5.4(b)), or equivalently, by the interference between two resonance peaks — channels 1 and 3 peaks — because the real and imaginary parts of $\bar{H}_1$ do not commute. Here we elaborate on the interference between two resonances, applicable to both photon and particle scattering. The decay of the internal state $|\bar{q}_\alpha\rangle$ is due

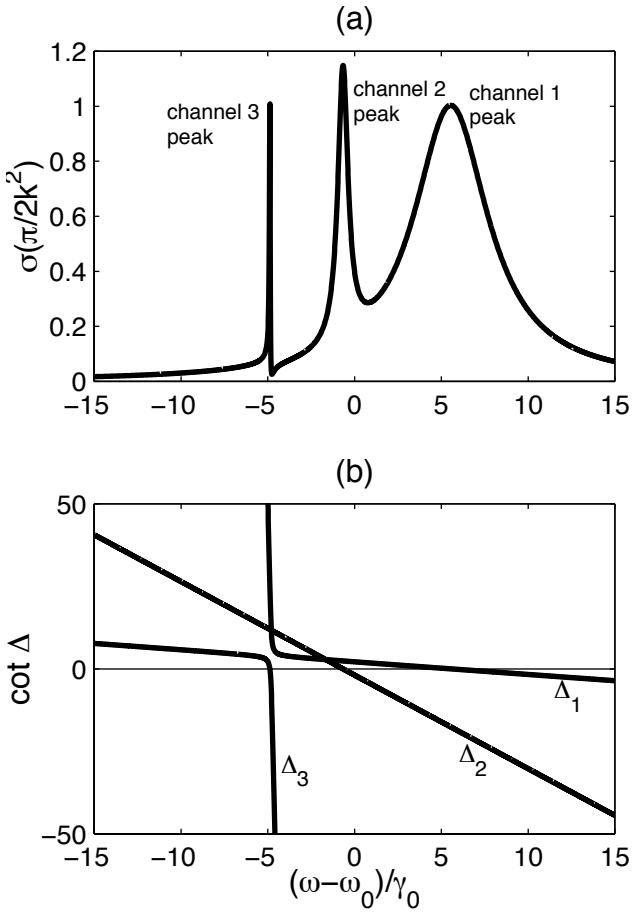

Figure 5.4: (a) total cross section and (b) cotangent of phase angles as a function of incident photon frequency for three identical proximate atoms on a straight line with neighboring atoms separated by equal distance d, where $k_0 d = 0.7$.

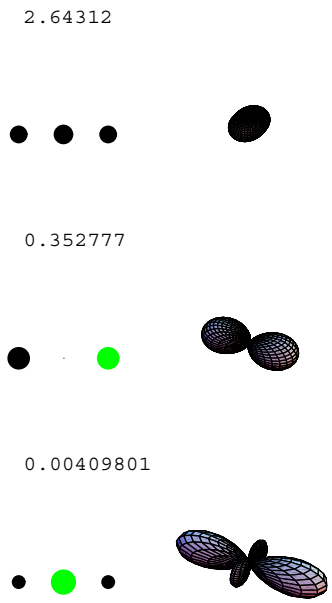

Figure 5.5: Offresonant eigenchannels for three atoms, specified in Fig. 5.4. For each eigenchannel α, $\tilde{\Gamma}_\alpha/\gamma_0$, $\vec{\tilde{q}'}_\alpha$, and $\tilde{Y}_\alpha(\hat{\boldsymbol{k}}, \boldsymbol{\epsilon})$ are shown.

to its coupling to the continuum — eigenchannel $\vec{q}_\alpha(\omega_\alpha)$ or $|I_\alpha(\omega_\alpha)\rangle$. Two different internal states are orthogonal to each other:

$$\vec{\bar{q}}_\alpha^T \vec{\bar{q}}_\beta = 0 \text{ or } \langle \bar{q}_\alpha | \bar{q}_\beta \rangle = 0. \tag{5.53}$$

Yet there is overlap between the continua they are coupled to, or there is overlap between their corresponding eigenchannels *at their respective resonant frequencies (energies)*:

$$\langle I_\alpha(\omega_\alpha) | I_\beta(\omega_\beta) \rangle = \vec{q}_\alpha^T(\omega_\alpha) B \vec{q}_\beta(\omega_\beta) \neq 0, \tag{5.54}$$

when $[\bar{A}, \bar{B}] \neq 0$ (or $[A, B] \neq 0$). In other words, the two internal states are decaying into the same continuum. The interference between decay of two internal states causes their resonance peaks deviating from Lorentzians.

5.4.3 General Cases

Fig. 5.6 shows the total cross section and cotangent of phase angles as a function of incident photon frequency for 7 identical atoms proximately and randomly placed on a plane, with each dipole perpendicular to the plane. The configuration of atoms is the same as atoms in Fig. 4.4, and scatterers in Fig. 2.9.

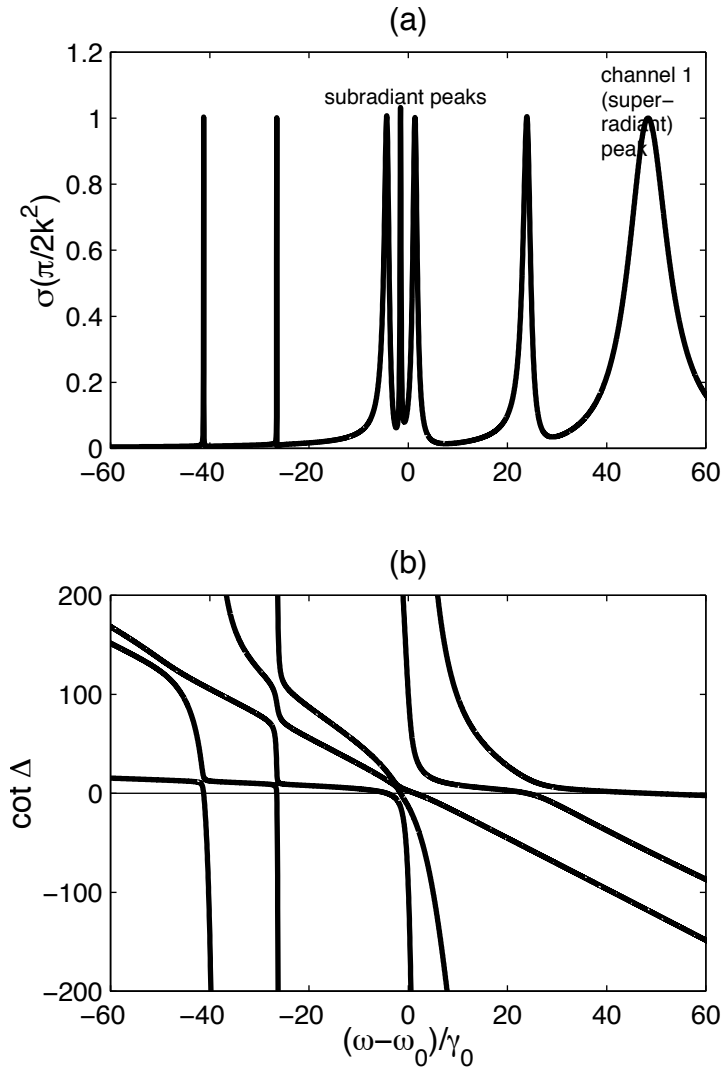

Figure 5.6: (a) Total cross section and (b) cotangent of phase angles as a function of incident photon frequency for 7 identical proximate atoms. The configuration of atoms is specified in Fig. 4.4. The positions of the atoms are shown in Fig. 2.8.

Fig. 5.7 illustrates the offresonant eigenchannels for the 7 atoms. As discussed in subsection 2.4.3, offresonant eigenchannels are obtained by diagonalization of B. For proximate atoms in small samples, the eigensystem of B can be solved by expanding the matrix elements of B into even powers of x_{ij}. For photon scattering by atoms, we have

$$B_{ij} = 1 - \frac{1}{5}x_{ij}^2 + \frac{3}{280}x_{ij}^4 - \cdots = B_{ij}^{(0)} + B_{ij}^{(1)} + B_{ij}^{(2)} + \cdots \tag{5.55}$$

(compare with (2.108)). If we keep only the lowest (0th) order of x_{ij} in B, namely $B_{ij} = 1$, we get the dipole-like offresonant channel

$$\vec{q'}_1^{(0)} = \frac{1}{\sqrt{N}}(1, 1, \cdots, 1)^T, \tag{5.56}$$

whose offresonant width $\tilde{\Gamma}_1^{(0)} = N\gamma_0$. Note this is the same as Dicke model, which assumes $B_{ij} = 1$ and $A_{ij} = 0$. Adding the $2l$th order of x_{ij} ($B_{ij}^{(l)}$) into account, we further get $(l+1)$ offresonant eigenchannels that look like $2^{(l+1)}$-poles — $(l+1)$th order photon angular momentum eigenstates. Their offresonant widths to lowest order $\propto x_{ij}^{2l}\gamma_0$.

For a general nonsymmetric system, $[A, B] \neq 0$. As discussed in subsection 2.4.4, the real part causes the shift of resonance peaks and mixing of offresonant eigenchannels. The broad dipole-like channel peak is shifted upwards in frequency. Furthermore, the magnitude of the shift is more than

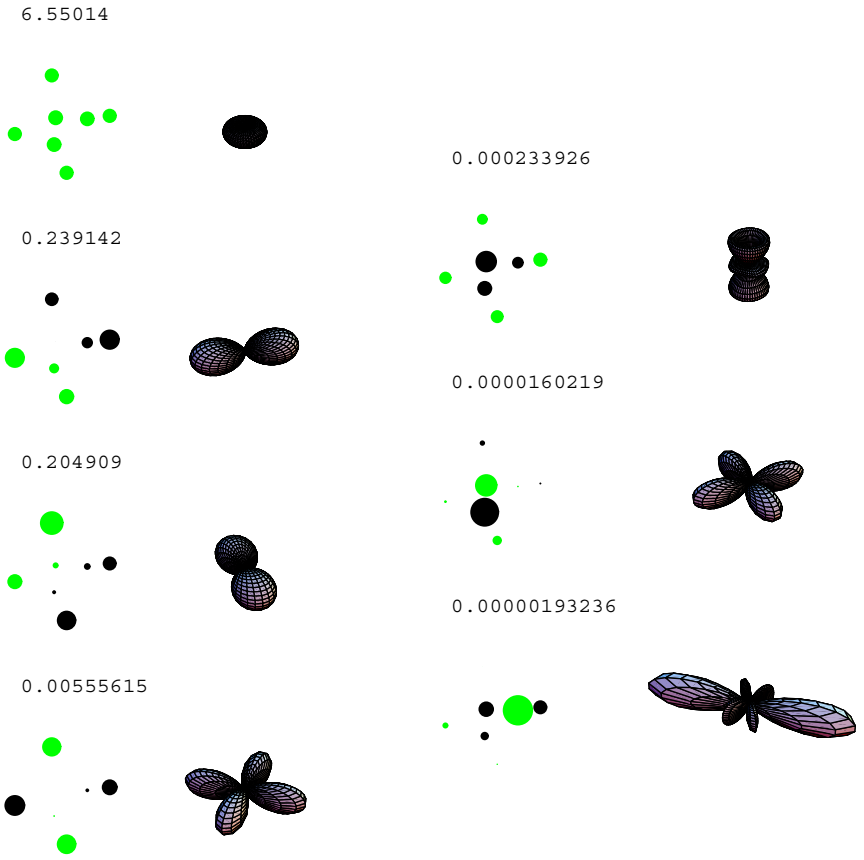

Figure 5.7: Offresonant eigenchannels for seven atoms, specified in Fig. 5.6. For each channel α, $\tilde{\Gamma}_\alpha/\gamma_0$, $\vec{\tilde{q}'}_\alpha$, and $\tilde{Y}_\alpha(\hat{\boldsymbol{k}}, \boldsymbol{\epsilon})$ are shown (compare with Fig. 2.10).

the s-like channel peak in particle scattering case. This is because for photon scattering, the leading term of $A_{ij} \propto \frac{1}{x_{ij}^3}$ ((5.52)), as opposed to $\frac{1}{x_{ij}}$ for particle scattering ((2.119)). The higher order channels give sharp proximity resonance peaks at frequencies lower than the broad peak.

Numerical evidence shows that there is also more mixing of offresonant channels for photon scattering than for particle scattering. Typically for the same configuration of atoms and scatterers, $|c_{\alpha\beta}|$ (defined as in (2.116), for $\alpha \neq \beta$) for photon scattering by atoms is larger than particle scattering by scatterers. Again, this is because A_{ij} is more sensitive to the distance between atoms than to scatterers, so A and B are "more noncommutating" for photon scattering than for particle scattering.

For both particle and photon scattering by small samples, the internal state corresponding to the broad resonance peak is the closest thing to the superradiant state within $\mathcal{E}_1$ in Dicke's original model (see subsection 3.3.2). The s-like or dipole-like offresonant eigenchannel is the superradiant channel. The internal states corresponding to sharp peaks are subradiant states. The higher order offresonant eigenchannels are subradiant channels.

Similar to the discussion in subsection 2.4.4, if we neglect the offdiagonal elements of A (or $\bar{A}$) in offresonant eigenchannel basis, and keep only the

leading terms in expansion (5.55) and (5.52), the position of the superradiant channel peak is

$$\omega_1 \approx \omega_0 + \frac{3}{2}(N-1)\left\langle \frac{1}{x^3} \right\rangle \gamma_0, \tag{5.57}$$

where

$$\left\langle \frac{1}{x^3} \right\rangle \equiv \sum_{i<j} \frac{1}{x_{ij}^3} \Bigg/ \left[\frac{N(N-1)}{2} \right]. \tag{5.58}$$

The superradiant channel peak has the largest shift and width among all peaks, so we estimate that all resonances occur within the frequency range

$$\omega_0 \pm \left[\frac{3}{2}(N-1)\left\langle \frac{1}{x^3} \right\rangle + N \right] \gamma_0. \tag{5.59}$$

Therefore, the validity condition for Markov approximation, (5.51), is

$$N\left\langle \frac{1}{x^3} \right\rangle \gamma_0 \ll \omega_0 \tag{5.60}$$

for small samples of two-level atoms on a plane, with each dipole perpendicular to the plane. This is more stringent than for particle scattering ((2.123)), because $\left\langle \frac{1}{x^3} \right\rangle > \left\langle \frac{1}{x} \right\rangle$ for small samples.

5.4.4 Spherically Symmetric Atom

Each s-wave point scatterer is spherically symmetric. For identical proximate scatterers not confined to a plane, there are 1 s-like, 3 p-like, $\cdots$, $(2l+1)$

2^l-pole-like, $\cdots$ offresonant eigenchannels. However, a point two-level atom is not spherically symmetric, because there exists a special direction — the orientation of the transition dipole.

To draw better parallelism to particle scattering by scatterers not confined to a plane, we modify the two-level atom model to introduce a model of spherically symmetric atom. In this model, each atom i has one ground state $|g_i\rangle$ and three degenerate excited states $|e_{ix}\rangle$, $|e_{iy}\rangle$ and $|e_{iz}\rangle$. The excited states differ only by the orientations of transition dipoles, which are along x, y and z axes. The transitions between ns state and $n'p$ states of a higher energy in Rydberg atoms can be modeled this way.

To get the effective Hamiltonian within the first excited manifold $\bar{H}_1$ for N spherically symmetric atoms, we note each spherically symmetric atom is equivalent to three two-level atoms at the same position, with the same transition frequency and transition dipole, and with the orientations of transition dipoles along x, y and z axes. (Note however, this is not true for higher manifolds. Two two-level atoms at the same position can be simultaneously excited, but a single spherically symmetric atom cannot be excited twice.)

$\bar{H}_1$ can be written as

$$\bar{H}_1 \equiv \sum_i \sum_{\xi=x,y,z} (\omega_i - i\gamma_i)\sigma^+_{i\xi}\sigma_{i\xi} + \sum_{i\neq j} \sum_{\xi,\eta=x,y,z} \mathcal{D}_{i\xi,j\eta}\sigma^+_{i\xi}\sigma_{j\eta}, \tag{5.61}$$

where the meaning of $\sigma_{i\xi}$, $\sigma^+_{i\xi}$ and the expression for $\mathcal{D}_{i\xi,j\eta}$ should be clear. From (3.62), there is no dipole-dipole interaction between excited states of the same atom.

Each spherically symmetric atom in ground state is a three-channel scatterer. The mutually orthogonal degenerate eigenchannels of atom i are denoted as $|I_{ix}\rangle$, $|I_{iy}\rangle$, and $|I_{iz}\rangle$. $|I_{ix}\rangle$ is the same as the single eigenchannel of a two-level atom at the same position whose two states are $|g_i\rangle$ and $|e_{ix}\rangle$, etc. They are all photon angular momentum eigenstates with $l = 1$. Each atom behaves like a classical point dipole which is isotropically polarizable along all directions.

The rank of the T-matrix for photon scattering by N spherically symmetric atoms in ground state is $3N$. For a general nonsymmetric small sample of identical proximate atoms not confined to a plane, there are 3 dipole-like, 5 quadrupole-like, $\cdots$, $(2l + 1)$ 2^l-pole-like, $\cdots$ offresonant eigenchannels. To lowest order of x_{ij}, the offresonant widths of the 3 dipole-like offresonant channels are all $N\gamma_0$. The offresonant widths of $2^{(l+1)}$-pole-like eigenchannels

are to the lowest order $\propto x_{ij}^{2l}\gamma_0$.

We study the two identical spherically symmetric atom case in detail. Real and imaginary parts of $\bar{H}_1$ still commute in this case. For two atoms placed on x axis, the six eigenstates of $\bar{H}_1$ are

$$|S_\xi\rangle = \frac{1}{\sqrt{2}}(|e_{1\xi}\rangle + |e_{2\xi}\rangle) \text{ and } |A_\xi\rangle = \frac{1}{\sqrt{2}}(|e_{1\xi}\rangle - |e_{2\xi}\rangle) \ (\xi = x, y, z). \quad (5.62)$$

$|S_y\rangle$ and $|S_z\rangle$, $|A_y\rangle$ and $|A_z\rangle$ are still degenerate. Fig. 5.8 shows the total cross section as a function of incident photon frequency for two identical proximate spherically symmetric atoms. The positions of atoms are the same as in Figs. 5.2 and 4.3. We can only observe 4 resonance peaks because peaks from $|S_y\rangle$ and $|S_z\rangle$, $|A_y\rangle$ and $|A_z\rangle$ add on top of each other. The figure will be exactly the same for scattering of classical radiation waves by two identical proximate point dipoles which are isotropically polarizable.

5.5 Further Topics

In the future, we would like to study photon scattering by atoms initially in a higher manifold $\mathcal{E}_m$ ($m > 1$), i.e., some atoms are already in the excited states initially. One complication here is that the scattering process now has two *interfering* paths. One path is the atoms absorb the incident photon first and

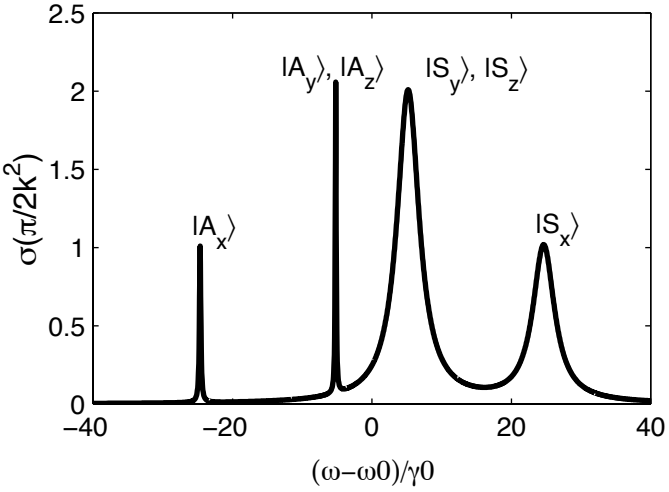

Figure 5.8: Total cross section as a function of incident photon frequency for two spherically symmetric atoms along x axis separated by distance $d = 0.1\lambda_0$. The positions of atoms are the same as in Figs. 4.3 and 5.2. Label(s) atop each peak denote the internal state(s) each resonance corresponds to.

then emit the scattered photon: $|a_m;\nu\rangle \to |a_{m+1};0\rangle \to |a'_m;\nu'\rangle$ ($a_m, a'_m \in \mathcal{E}_m$, and $a_{m+1} \in \mathcal{E}_{m+1}$). The other path is the atoms emit the scattered photon first and then absorb the incident photon: $|a_m;\nu\rangle \to |a_{m-1};\nu\nu'\rangle \to |a'_m;\nu'\rangle$ ($a_{m-1} \in \mathcal{E}_{m-1}$). Our physical intuition tells us that these two paths add up destructively. Photon scattering by atoms in higher manifolds is a multi-photon process. It is related to cascading in superradiance. Its corresponding problem is particle scattering by a group of scatterers in "higher manifolds", i.e., initially some scatterers are already occupied by particles identical to the incident particle. It is a multi-particle process. The quantum mechanical indistinguishability of particles or photons must be taken into account in multi-particle or multi-photon processes.

5.6 Summary

In this chapter, we have first introduced the general formulation of photon scattering by atoms. We have provided an expression relating the T-matrix with the effective Hamiltonian. Each point two-level atom is a single-channel scatterer of photon, just as each s-wave point scatterer is a single-channel scatterer of particle, as discussed in Chapter 2.

The problem of one-photon scattering by a group of point two-level atoms in ground state is parallel to the problem of one-particle scattering by a group of s-wave point scatterers, which we have discussed in Chapter 2. Both problems can be solved from either the effective Hamiltonian point of view or the multiple scattering point of view. The two views are equivalent — the Green's function is simply related to the generalized monopole-monopole or dipole-dipole interaction. The full correspondence between the two problems is summarized in Tables 5.1 and 5.2.

With the knowledge of correspondence, the eigenchannel expansion method and its applications to proximity resonance discussed in Chapter 2 can be directly applied to photon scattering by atoms in ground state as well. The real part of $\bar{H}_1$ determines the positions of resonance peaks and their corresponding internal states. For identical scatterers (atoms), the imaginary part of $\bar{H}_1$ determines the offresonant eigenchannels and their offresonant widths. For a general nonsymmetric system, real and imaginary parts of $\bar{H}_1$ do not commute. This causes the mixing of offresonant channels at resonances and the interferences between resonance peaks. For small samples of proximate scatterers (atoms), the internal state corresponding to the broad peak is the superradiant state. The internal states corresponding to sharp peaks are

Table 5.1: Correspondence between the problem of one-particle scattering by a single s-wave point scatterer and the problem of one-photon scattering by a single point two-level atom in ground state.

	particle scattering by a single scatterer i	photon scattering by a single atom i in ground state
rank of T-matrix	1	1
eigenvalue of T-matrix	$-\frac{\gamma_i}{E-E_i+i\gamma_i}$	$-\frac{\gamma_i}{\omega-\omega_i+i\gamma_i}$
eigenchannel $\|I_i\rangle$	$\langle \boldsymbol{k}\|I_i\rangle \propto \frac{1}{\sqrt{4\pi}} e^{-i\boldsymbol{k}\cdot\boldsymbol{r}_i}$ angular momentum eigenstate for particle with $l=0$	$\langle \nu\|I_i\rangle \propto \frac{1}{\sqrt{\frac{8\pi}{3}}}(\boldsymbol{\epsilon}_\nu \cdot \hat{\boldsymbol{d}}_i) e^{-i\boldsymbol{k}_\nu\cdot\boldsymbol{r}_i}$ angular momentum eigenstate for photon with $l=1$
resonance due to	quasibound state of scatterer	excited state of atom
a resonant scattering process	incident particle trapped inside scatterer, then ejected from scatterer	incident photon absorbed by atom, then a new photon emitted by atom

Table 5.2: Correspondence between the problem of one-particle scattering by a group of s-wave point scatterers and the problem of one-photon scattering by a group of point two-level atoms in ground state.

	particle scattering by N scatterers	photon scattering by N atoms in ground state
rank of T-matrix	N	N
resonances due to	collective quasibound states (internal states)	collective excited states (internal states)
multiple scattering view	particle ejected from one scatterer can be trapped inside another scatterer	photon emitted by one atom can be absorbed by another atom
Green's Function G_{ij} $= \langle I_i \vert O_j \rangle = -A_{ij} + iB_{ij}$ [a]	$\frac{1}{x}e^{ix}$	$\frac{3}{2}\left\{\left(-\frac{1}{x^3}+\frac{i}{x^2}+\frac{1}{x}\right)(\hat{\boldsymbol{d}}_i\cdot\hat{\boldsymbol{d}}_j)+\left(3\frac{1}{x^3}-3\frac{i}{x^2}-\frac{1}{x}\right)(\hat{\boldsymbol{x}}\cdot\hat{\boldsymbol{d}}_i)(\hat{\boldsymbol{x}}\cdot\hat{\boldsymbol{d}}_j)\right\}e^{ix}$
expansion of A_{ij} [a]	$-\frac{1}{x}+\cdots$	$\frac{3}{2}\frac{1}{x^3}-\ldots$ [b]
expansion of B_{ij} [a]	$1-\frac{1}{6}x^2+\frac{1}{120}x^4-\cdots$	$1-\frac{1}{5}x^2+\frac{3}{280}x^4-\ldots$ [b]
effective Hamiltonian $\bar{H}$ for particle inside scatterers or for atoms within $\mathcal{E}_1$	$\sum_i(E_i-i\gamma_i)\sigma_i^+\sigma_i$ $+\sum_{i\neq j}\mathcal{M}_{ij}\sigma_i^+\sigma_j$	$\sum_i(\omega_i-i\gamma_i)\sigma_i^+\sigma_i$ $+\sum_{i\neq j}\mathcal{D}_{ij}\sigma_i^+\sigma_j$
coupling between quasibound states in different scatterers or betwen different atoms	$\mathcal{M}_{ij}=-\sqrt{\gamma_i\gamma_j}G_{ij}$	generalized dipole-dipole interaction $\mathcal{D}_{ij}=-\sqrt{\gamma_i\gamma_j}G_{ij}$

[a] $\boldsymbol{x}=\boldsymbol{x}_{ij}$.

[b] For $\hat{\boldsymbol{d}}_i\|\hat{\boldsymbol{d}}_j$ and $\hat{\boldsymbol{d}}_i,\hat{\boldsymbol{d}}_j\perp\boldsymbol{x}$.

subradiant states. For photon scattering by proximate atoms, the broad superradiant peak is shifted upwards in frequency. The magnitude of the shift is more than that of particle scattering by proximate scatterers. There is also more mixing of offresonant eigenchannels at resonances.

To recover the spatial isotropicity, we have expanded the two-level atom model to the spherically symmetric atom model. In the future, we would like to study both particle and photon scattering in higher manifolds (multi-particle and multi-photon processes).

Chapter 6

Particle and Photon Scattering by Large Samples

In Chapters 2 and 5, we have provided the formulation for particle scattering by a group of s-wave point scatterers and photon scattering by a group of point two-level atoms in ground state, taking all orders of multiple scattering effects into account. We have also studied proximity resonance of small samples, where all scatterers/atoms are proximate, i.e., well within the wavelength of incoming particle/photon in resonance: $x_{ij} \lesssim 1$ for all i, j.

This formulation can also be applied to particle/photon scattering by large samples. In fact, according to [30], with one notable exception [24],

all superradiance experiments deal with something more complex than the idealized small sample case [23]. The theory of wave scattering by a large disordered media, specifically light scattering by atoms (e.g., [48, 49, 50]), have been widely studied. Our study takes into account all orders of multiple scattering effects.

In this chapter, we study particle/photon scattering by large samples of identical scatterers/atoms in 2D. The samples are considered large because not all scatterers/atoms are proximate to each other, i.e., $x_{ij} > 1$ for some pairs. Neighboring scatterers/atoms are still proximate, so we cannot neglect multiple scattering effects.

6.1 Scattering by Random Lattices

In this section, we study the cases of identical scatterers/atoms nearly forming a square lattice in 2D. The samples are generated as follows. A total of $N = N_x \times N_y$ lattice points of a square lattice in 2D (with cell size $a \times a$) are determined. For each lattice point (x_i, y_i), a scatterer/atom is placed within the area $(x_i \pm \frac{v}{2}a, y_i \pm \frac{v}{2}a)$ with uniform probability. The "variability" v is a parameter characterizing the disorderliness of the sample. This kind of

random lattice configuration resembles optical lattices in some experiments. When $N_x k_0 a$ or $N_y k_0 a > 1$, the sample is considered large. The offresonant eigenchannels — eigensystems of matrix B — can no longer be obtained by expanding B into powers of x_{ij} as described in subsections 2.4.3 and 5.4.3. On the other hand, when $k_0 a \lesssim 1$, i.e., neighboring atoms are proximate, we still cannot neglect multiple scattering effects. Fig. 6.1 shows such a random lattice configuration.

6.1.1 Shifts and Widths

We study particle scattering by scatterers first. Fig. 6.2(a) shows the distribution of energy shifts and widths of resonance peaks (or internal states) for the configuration of Fig. 6.1, in the sense of (2.88) and (2.90). This corresponds to diagonalizing the real part of the effective Hamiltonian $\bar{H}$, $\bar{A}$, first. When there is significant overlap between resonances *of similar widths*, individual resonance peaks cannot be resolved. Yet the eigensystem analysis still provide some insights to the scattering spectrum. Fig. 6.2(b) shows the distribution of eigenvalues [$(E - i\Gamma)$'s] of $\bar{H}$. It is different from Fig. 6.2(a) because real and imaginary parts of $\bar{H}$ do not commute. Eigenvalues of $\bar{H}$ ac-

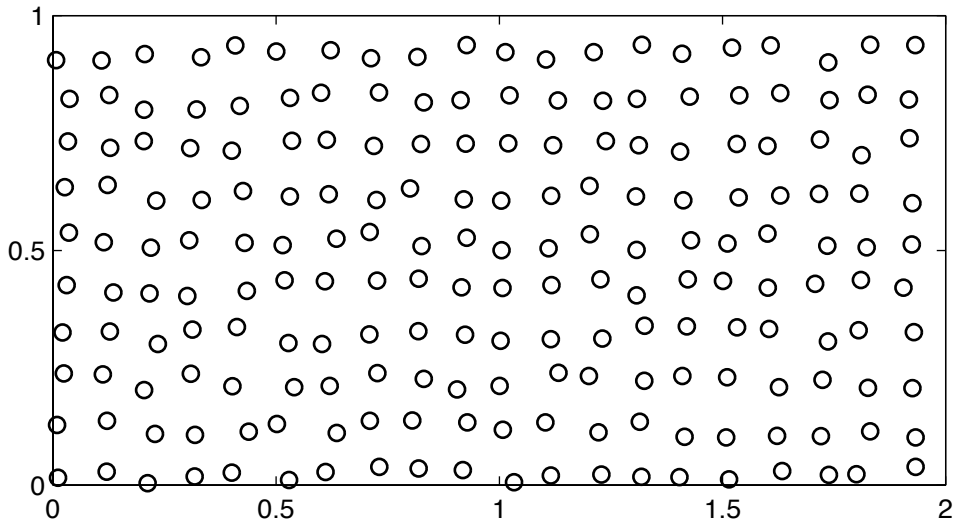

Figure 6.1: A large sample: a 2D random lattice configuration of scatterers/atoms with $N_x = 20$, $N_y = 10$, $a = 0.1\lambda_0$ and $v = 0.4$. (In the figure, distances are in units of λ_0).

tually give a better prediction of the scattering spectrum than E_α's and Γ_α's do (see subsection 6.1.3). However, diagonalization of $\bar{A}$ has the advantage that its corresponding eigenstates, i.e., internal states, have real amplitudes on each scatterer and can be illustrated easily. On the other hand, eigenstates of $\bar{H}$ in general have complex amplitudes. Numerical evidence shows that for all the configurations we study in this section, diagonalizing $\bar{H}$ or $\bar{A}$ gives qualitatively the same distribution of eigensystems, except the values of narrowest widths. We concentrate on the results of diagonalizing $\bar{A}$.

There are some internal states with wide widths ($\Gamma_\alpha > \gamma_0$), and a lot more internal states with narrow widths ($\Gamma_\alpha < \gamma_0$).

Increasing the inter-scatterer distances effectively shrinks the shifts and the widest widths (Fig. 6.3). The widest widths are approximately but slightly less than

$$N_\lambda \gamma_0, \tag{6.1}$$

where N_λ is the number of scatterers within an area of $(\lambda_0/2)^2$. Crudely, as a way to understand scattering by random lattices, we classify that each internal state has either a wide width (which can be thought of as a "superradiant state") or a narrow width (a "subradiant state"). Unlike the small

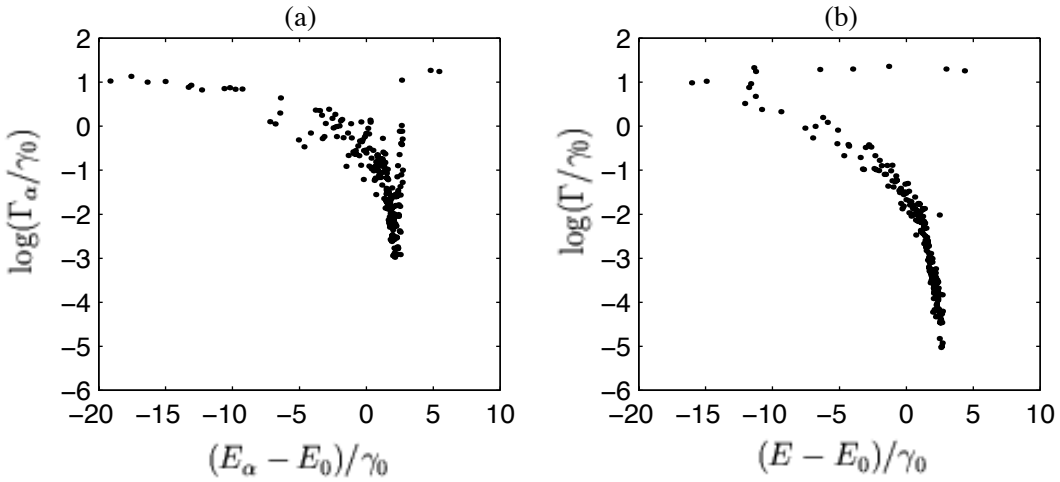

Figure 6.2: Energy shifts and widths for a random lattice of scatterers in Fig. 6.1. (a) Eigenvalues of $\bar{A}$ (E_α's) and their corresponding Γ_α's. (b) Eigenvalues of $\bar{H}$ [$(E - i\Gamma)$'s]. Throughout this chapter, all logarithms in figures are base-10.

sample case where the superradiant state is always shifted lower in energy, superradiant states of a large random lattice can be shifted either lower or higher in energy. We know the wide width ((6.1)). Since the total width is always $N\gamma_0$, assuming the narrow widths are negligible, we can estimate is number of wide widths or superradiant states to be

$$\frac{N}{N_\lambda} = \frac{Na^2}{(\lambda_0/2)^2}. \tag{6.2}$$

The remaining states are subradiant states. Intuitively, this tells us that a large random lattice can be thought of as a sum of areas of $(\lambda_0/2)^2$ (half the resonant wavelength across). Each area can be considered as a small sample, with one superradiant state and the remaining states subradiant states.

Numerical evidence shows that increasing the total number of scatterers does not change the distribution of shifts and widths, but just increases the density of internal states. This can also be explained by the intuitive picture. The distribution of shifts and widths are determined by the properties of the random lattice within the $\lambda_0/2$ range. The Green's function between scatterers can be considered small when they are more than $\lambda_0/2$ apart, compared to the Green's function between neighboring scatterers.

The multiple scattering process of the particle ejected from one scatterer

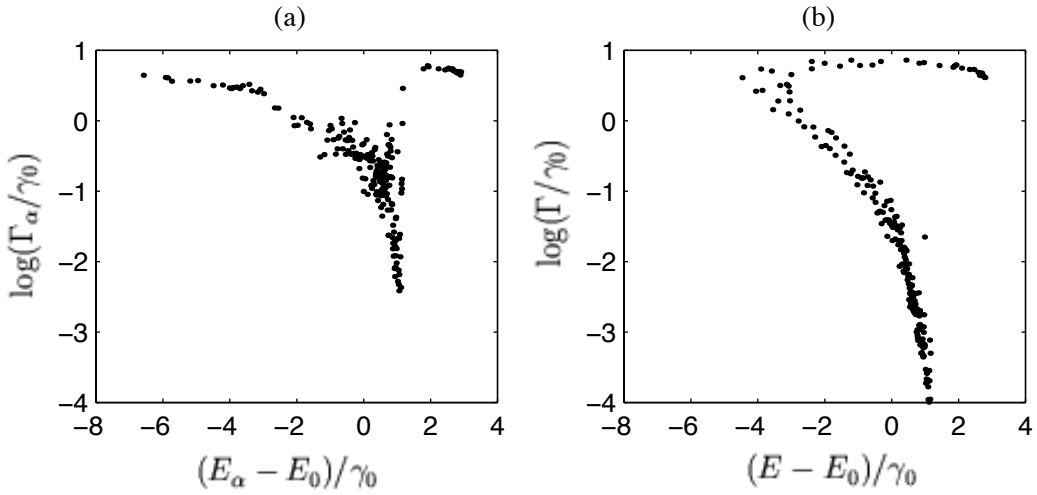

Figure 6.3: Energy shifts and widths for a sparser random lattice of scatterers, with $N_x = 20$, $N_y = 10$, $a = 0.2\lambda_0$ and $v = 0.4$. The difference to Fig. 6.1 is that a is twice as large. (a) E_α's and Γ_α's. (b) Eigenvalues of $\bar{H}$.

being trapped again by another scatterer can be either direct, or indirect — through trapping and ejection by other scatterers. The fact that the Green's function between scatterers more than $\lambda_0/2$ apart can be neglected means that the direct multiple scattering process between two scatterers more than $\lambda_0/2$ apart can be neglected, compared to indirect processes involving multiple scattering through neighboring scatterers.

For random lattices with variability v ranging from 0 to 0.6, the degree of disorder does not affect qualitatively the distribution of energy shifts and widths.

Photon scattering by a large random 2D lattice of atoms in ground state is similar to particle scattering. Again, we assume all atomic dipoles are parallel to each other and perpendicular to the lattice plane. Fig. 6.4(a) shows the distribution of frequency shifts and widths of internal states for the same configuration in Fig. 6.1. It is qualitatively the same as distribution of eigenvalues of $\bar{H}$ (Fig. 6.4(b)), though less accurate in predicting the scattering spectrum.

Crudely, each internal state can be classified as either a superradiant state (having wide width) or a subradiant state (narrow width). Unlike the small sample case where the superradiant state is shifted higher in frequency, su-

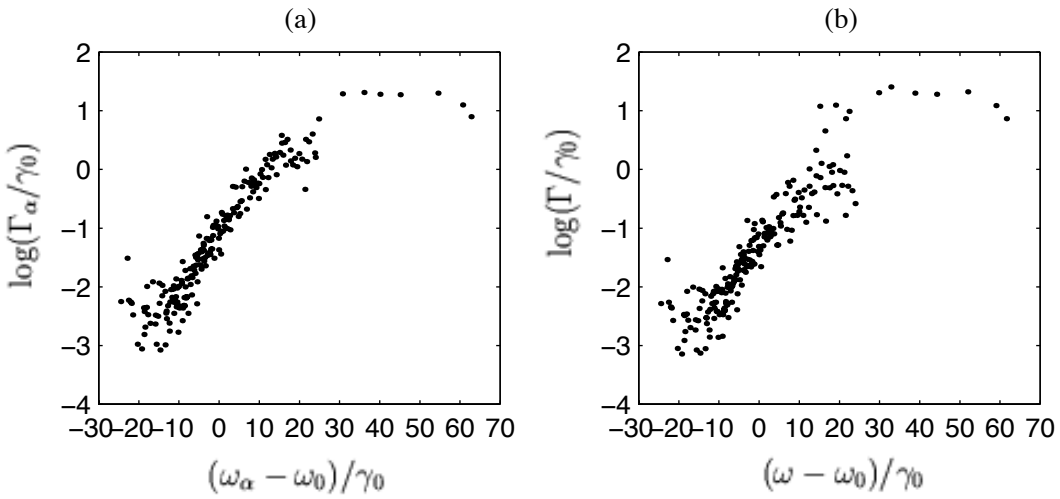

Figure 6.4: Frequency shifts and widths for a random lattice of atoms in Fig. 6.1. (a) ω_α's and Γ_α's. (b) Eigenvalues of $\bar{H}$.

perradiant states for large random lattices might be shifted either higher or lower in frequency. The width of superradiant states is given by (6.1) and the total number of superradiant states is given by (6.2). Intuitively a large random lattice can be thought of as a sum of small-sample areas of $(\lambda_0/2)^2$. The Green's function or generalized dipole-dipole interaction between atoms can be considered small when they are more than $\lambda_0/2$ apart, compared to that between neighboring atoms. In other words, the direct process of a photon emitted by one atom being reabsorbed by another atom if the two atoms are more than $\lambda_0/2$ apart can be neglected, compared to indirect multiple scattering processes involving virtual absorptions and emissions through neighboring atoms.

For the same configuration of scatterers/atoms, the distribution of shifts is wider for photon scattering than for particle scattering. This is understandable because for proximate neighboring scatterers/atoms, the real part of or $\bar{H}$ or Green's function has $\frac{1}{x^3}$ dependence for photon scattering, and $\frac{1}{x}$ dependence for particle scattering (see Table 5.2).

Increasing the interatomic distances effectively shrinks the shifts and the widest widths (Fig. 6.5). Increasing the total number of atoms increases the density of internal states without changing the distribution. Varying the

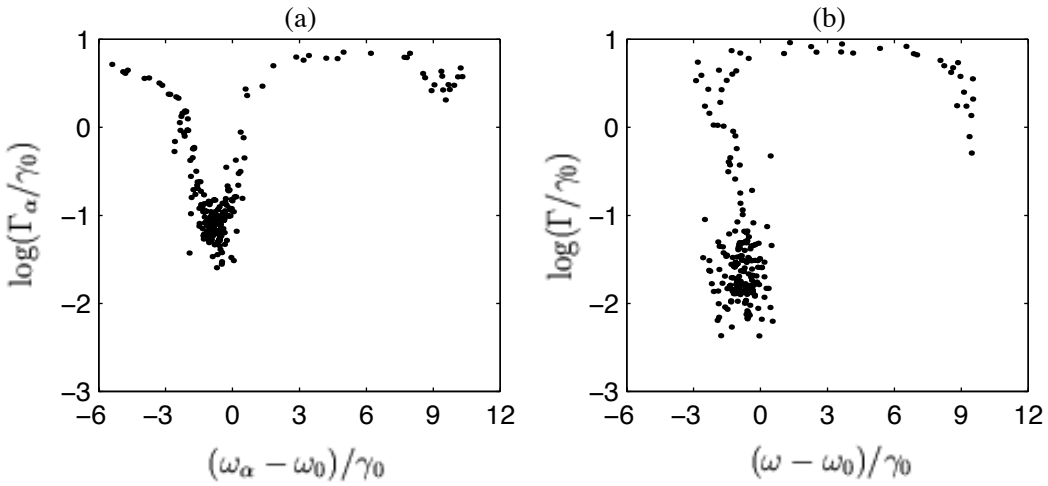

Figure 6.5: Frequency shifts and widths for a sparser random lattice of atoms, with $N_x = 20$, $N_y = 10$, $a = 0.2\lambda_0$ and $v = 0.4$. The difference to Fig. 6.1 is that a is twice as large. (a) ω_α's and Γ_α's. (b) Eigenvalues of $\bar{H}$.

degree of disorder for v ranging from 0 to 0.6 does not qualitatively change the distribution.

6.1.2 Amplitude Distribution of Internal States

We study the amplitude distribution of internal states in this subsection. Internal states can be illustrated by the method similar to the illustration of eigenchannels in Chapters 2 and 5. Each internal state $\vec{q}_\alpha$ can be illustrated

by colored dots at the positions of scatterers/atoms. The color of the dot at the ith scatterer's position is determined by the sign of $\bar{q}_{i\alpha}$, and the radius of the dot is proportional to $|\bar{q}_{i\alpha}|$.

Again, we study particle scattering by scatterers first. All superradiant states are delocalized — the amplitudes spread across particles at different places. Fig. 6.6 shows some typical superradiant states for a random lattice of scatterers in Fig. 6.1. Scatterers with the same sign of amplitudes form domains, i.e., neighboring atoms tend to have the same signs of amplitudes. The energies can be shifted either higher or lower.

Some subradiant states are delocalized (Fig. 6.7). Some subradiant states are *localized* (Fig. 6.8) — the amplitudes are concentrated on scatterers within a small area, or in some cases, several small areas. These long lifetime localized states are similar to Anderson localization [51, 52]. However, in our cases, localization occurs at a length scale less than half the resonant wavelength.

For each internal state $\vec{\bar{q}}_\alpha$, we can define the inverse participation ratio (IPR) as

$$R_\alpha \equiv \sum_i \bar{q}_{i\alpha}^4. \tag{6.3}$$

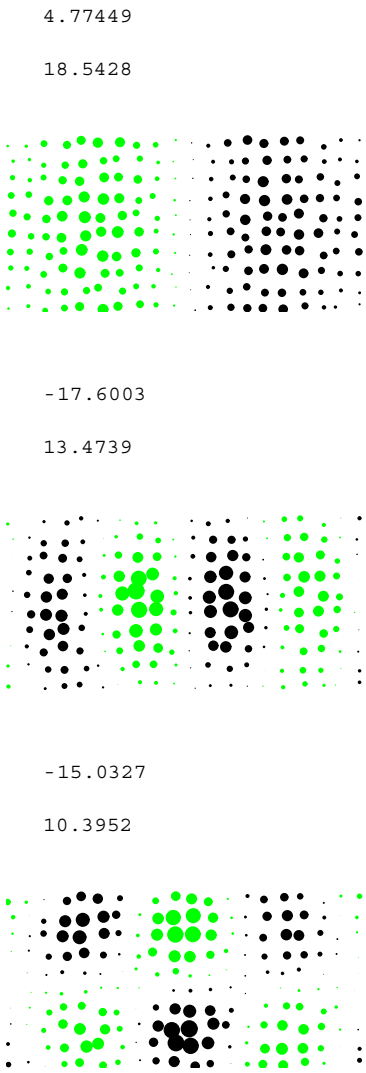

Figure 6.6: Typical superradiant states for a random lattice of scatterers in Fig. 6.1. The two numbers above each illustration are $(E_\alpha - E_0)/\gamma_0$ and Γ_α/γ_0 respectively (same for later illustrations of internal states).

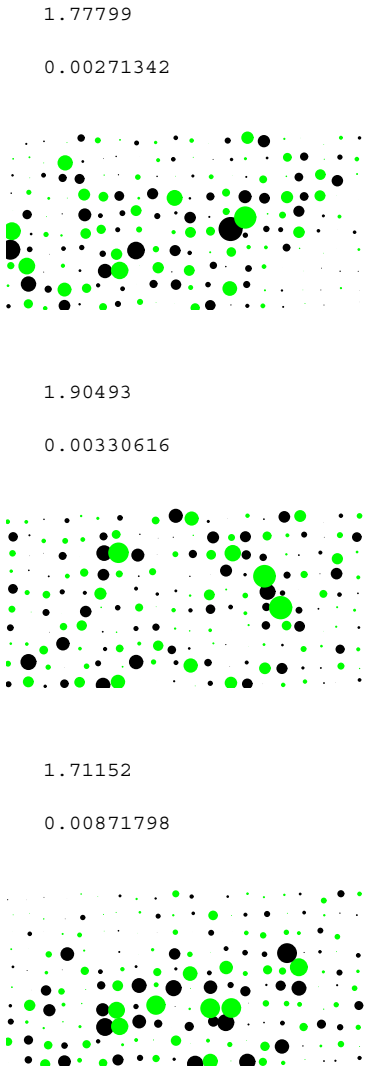

Figure 6.7: Typical delocalized subradiant states for a random lattice of scatterers in Fig. 6.1.

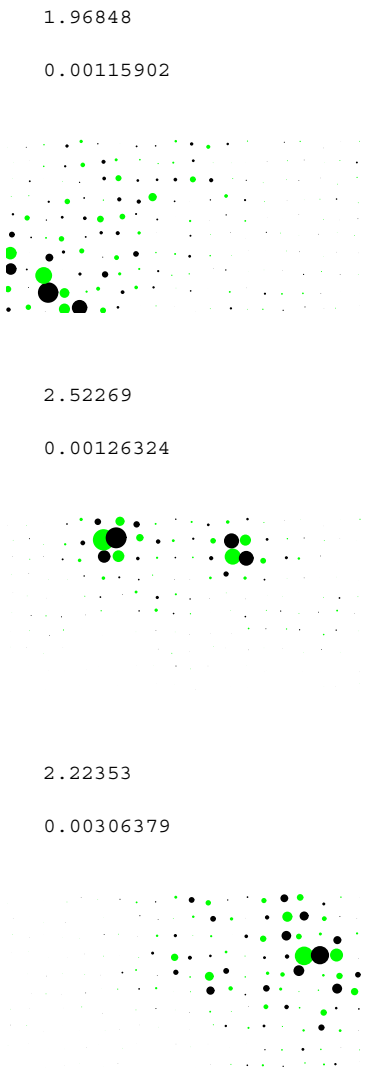

Figure 6.8: Typical localized subradiant states for a random lattice of scatterers in Fig. 6.1. (A dot of the same radius in this figure represents a larger amplitude on a scatterer than in Figs. 6.6 and 6.7. If we used the same scale, the dots in this figure would overlap heavily.)

(Note $\sum_i \bar{q}_{i\alpha}^2 = 1$.) The IPR characterizes the degree of concentration of amplitudes on scatterers. A larger IPR implies a more concentrated amplitude distribution. The extreme cases are as follows. The total angular momentum eigenstates in Dicke model has equal absolute value of amplitude on each scatterer, and has the minimum possible IPR of $\frac{1}{N}$. The quasibound state of a single scatterer has a maximum possible IPR of 1. The inverse of IPR can be thought of as the number of scatterers participating in the formation of the internal state. Thus the name "inverse participation ratio".

A localized state has a large IPR. However, a large IPR does not necessarily imply localization, because the amplitudes can be concentrated on scatterers at different areas. We find numerically that IPR qualitatively characterizes the degree of localization in the samples we study. Fig. 6.9 shows the distribution of IPRs and widths of internal states for the random lattice of scatterers in Fig. 6.1. From the figure we see all superradiant states are delocalized (minimum possible IPR is $\frac{1}{200} = 0.005$), while subradiant states are either delocalized or localized.

For a more disordered random lattice (larger v), there are more localized subradiant states, and the degree of localization is higher (larger IPR) (Fig. 6.10). This is in agreement with the conventional wisdom for Anderson

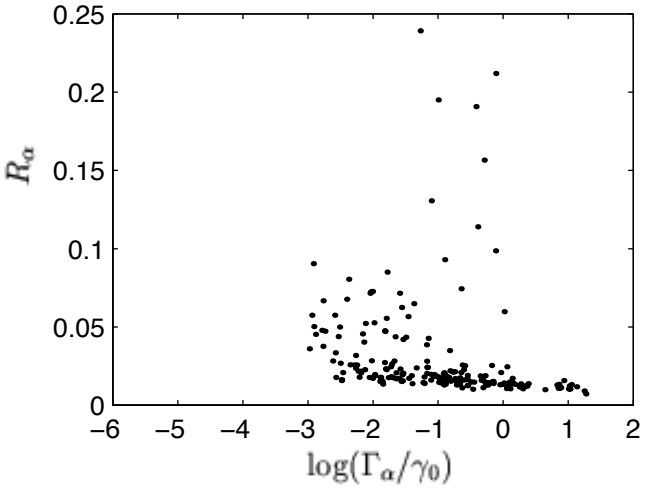

Figure 6.9: IPRs and widths of internal states for a random lattice of scatterers in Fig. 6.1. The minimum possible IPR for 200 scatterers is 0.005. A larger IPR implies a larger degree of localization.

localization.

Photon scattering by a random lattice of atoms in ground state is similar to particle scattering. For photon scattering by atoms of the same configuration in Fig. 6.1, all superradiant states are delocalized and have domains of atoms with the same signs of amplitudes (Fig. 6.11). They can be shifted either higher or lower in frequency. Subradiant states can be either delocalized (Fig. 6.12) or localized (Fig. 6.13). Compared to particle scattering by scatterers in the same configuration, there are more localized states and the degree of localization is higher for internal states of atoms (Fig. 6.14). This is because for photon scattering, the real part of $\bar{H}$ or Green's function between atoms has the $\frac{1}{x^3}$ dependence on interatomic distances, much more sensitive than the $\frac{1}{x}$ dependence on inter-scatterer distances for particle scattering. Also for photon scattering by a more disordered random lattice, there are more localized subradiant states, and the degree of localization is higher (Fig. 6.15).

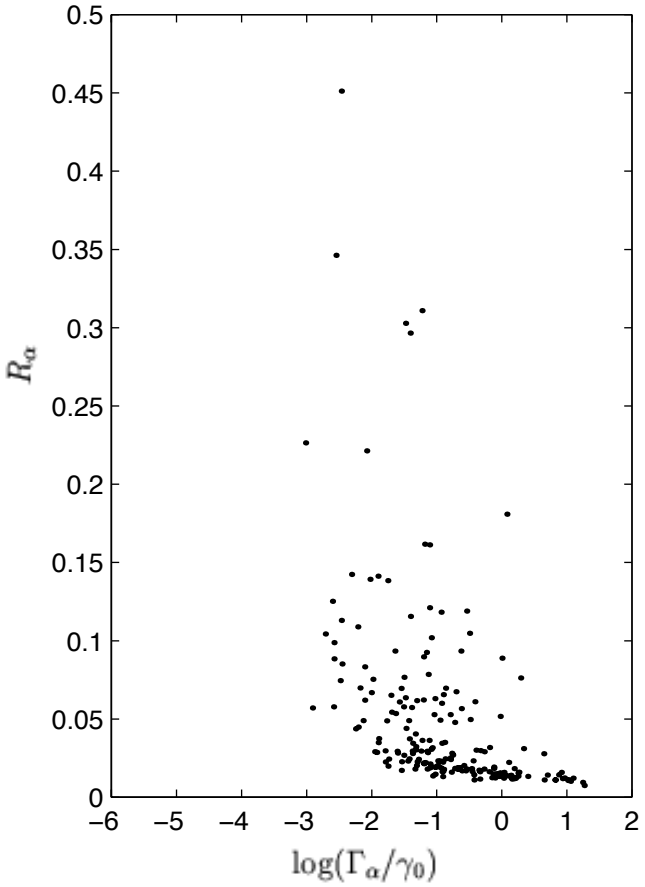

Figure 6.10: IPRs and widths of internal states for a more disordered random lattice of scatterers, with $N_x = 20$, $N_y = 10$, $a = 0.1\lambda_0$ and $v = 0.6$. The difference to Fig. 6.1 is that v is larger.

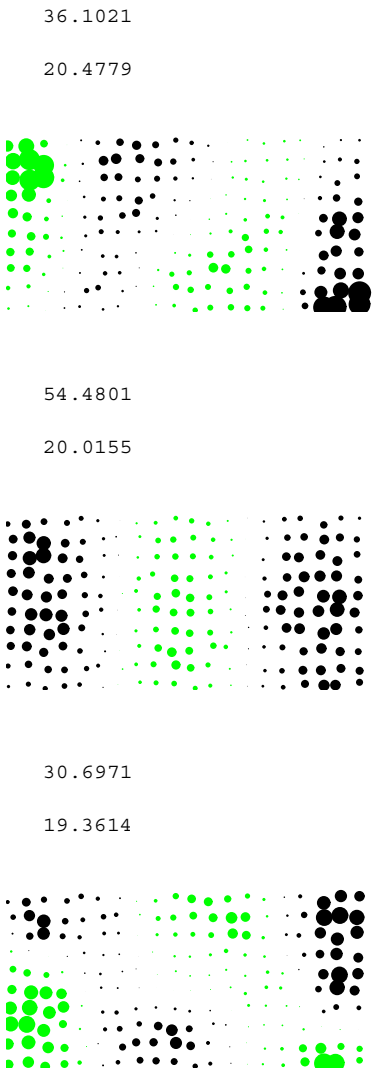

Figure 6.11: Typical superradiant states for a random lattice of atoms in Fig. 6.1. The two numbers above each illustration are $(\omega_\alpha - \omega_0)/\gamma_0$ and Γ_α/γ_0 respectively (same for later illustrations of internal states).

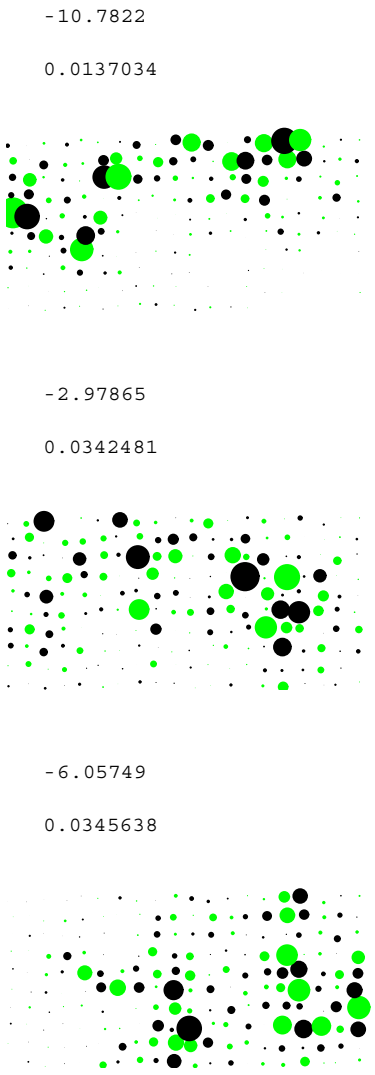

Figure 6.12: Typical delocalized subradiant states for a random sample of atoms in Fig. 6.1.

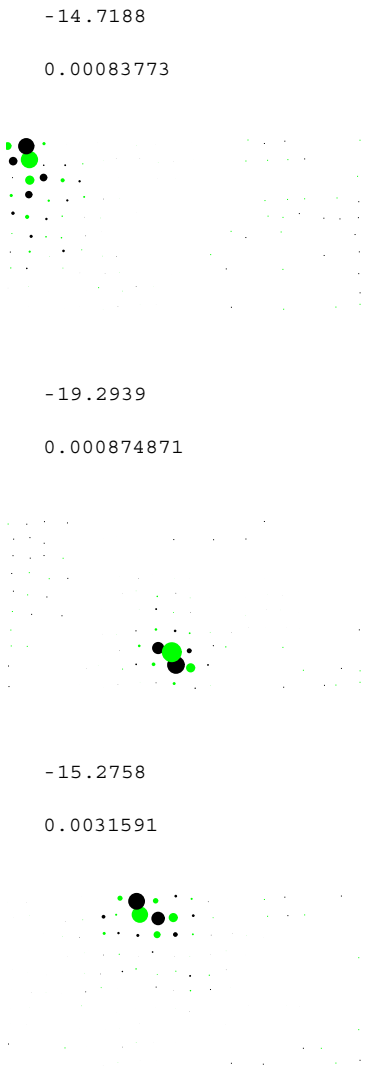

Figure 6.13: Typical localized subradiant states for a random lattice of atoms in Fig. 6.1. (A dot of the same radius in this figure represents a larger amplitude on an atom than in Figs. 6.11 and 6.12.)

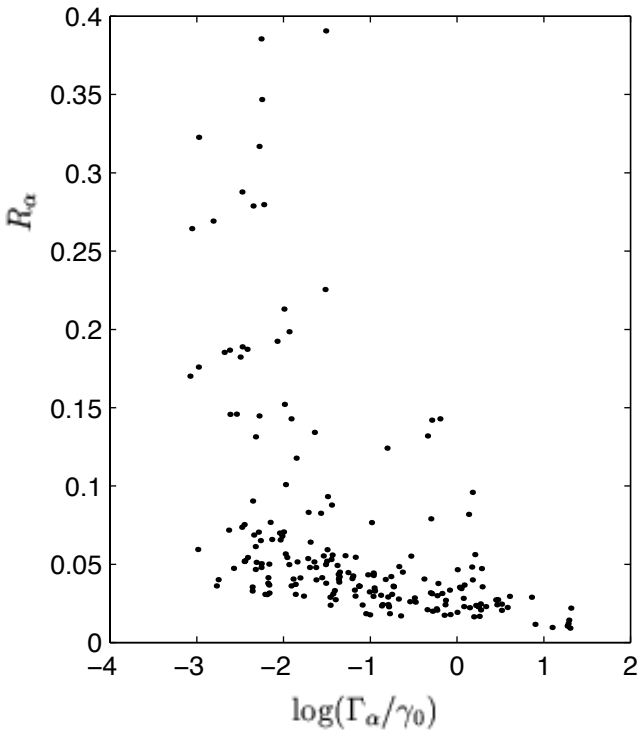

Figure 6.14: IPRs and widths of internal states for a random lattice of atoms in Fig. 6.1.

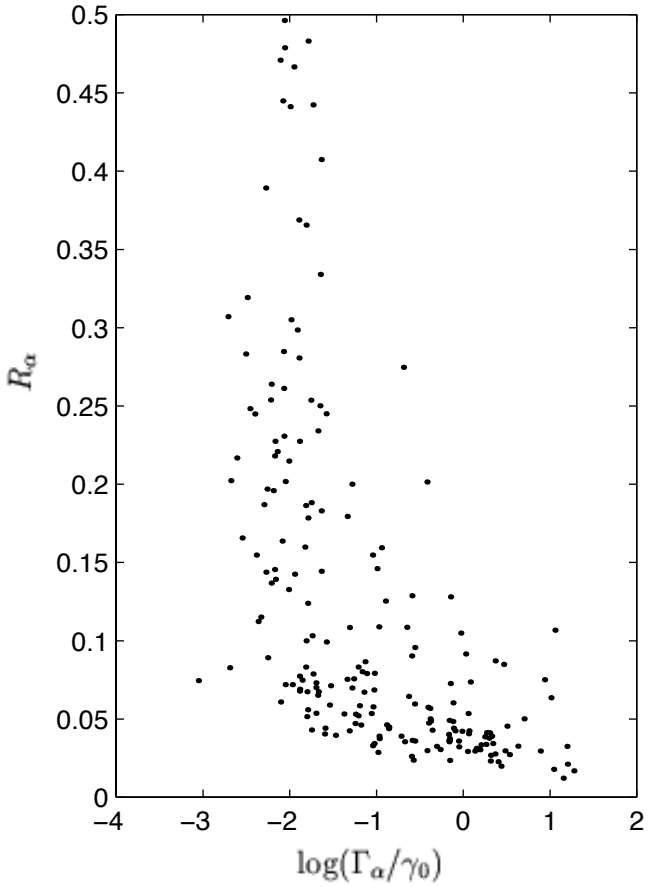

Figure 6.15: IPRs and widths of internal states for a more disordered random lattice of atoms, with $N_x = 20$, $N_y = 10$, $a = 0.1\lambda_0$ and $v = 0.6$. The difference to Fig. 6.1 is that v is larger.

6.1.3 Scattering Spectra

In this subsection, we show the scattering spectra (total cross section as a function of incident particle/photon energy) for scattering by large random lattices. Fig. 6.16(a) shows the total cross section as a function of incident particle energy for the random lattice of scatterers in Fig. 6.1. There are significant overlaps between superradiant peaks so individual peaks cannot be resolved. Collectively the "superradiant states" provide a background which is mostly shifted lower in energy. Most of the "subradiant peaks" do not overlap with each other, so they give narrow peaks based on the background (Fig. 6.16(b)). Since they do not overlap, these narrow peaks do indicate long-lifetime subradiant states.

Fig. 6.17(a) shows the prediction of scattering spectrum for the random lattice of scatterers in Fig. 6.1 from diagonalization of $\bar{A}$. It is obtained by assuming each internal state $\vec{\bar{q}}_\alpha$ gave a Lorentzian peak at E_α whose width is Γ_α, and there were *no* interferences between Lorentzians. It is very different from the actual scattering spectrum (Fig. 6.16, note the scales of vertical axes in Figs. 6.16(a) and 6.17 are different), because real and imaginary parts of $\bar{H}$ do not commute. However, E_α's and Γ_α's (Fig. 6.2(a)) do predict

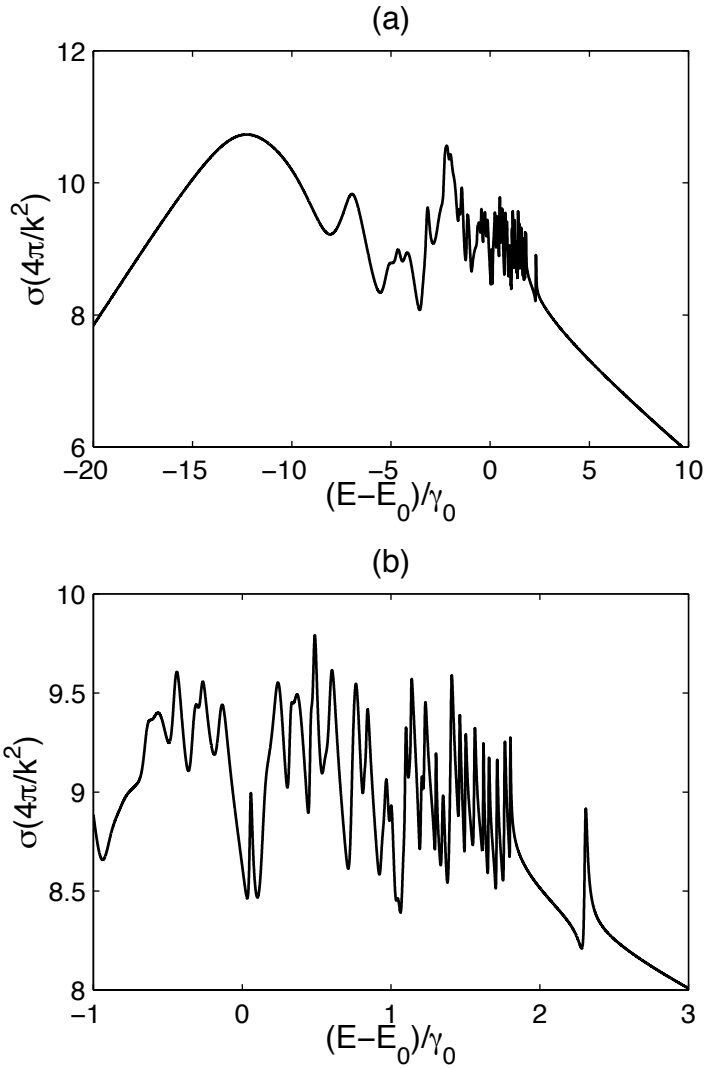

Figure 6.16: (a) Total cross section as a function of incident particle energy for a random lattice of scatterers in Fig. 6.1. (b) An enlargement of some of the subradiant peaks in (a).

qualitatively correctly the positions of narrow subradiant peaks. This is because for subradiant states, the imaginary part of $\bar{H}$ is small and indeed can be considered as a small correction to the real part.

Fig. 6.17(b) shows the prediction of the scattering spectrum from diagonalization of $\bar{H}$. It is obtained by assuming each eigenvalue of $\bar{H}$, $E-i\Gamma$, gave a Lorentzian peak at E whose width is Γ, and there were *no* interferences between Lorentzians (or eigenstates of $\bar{H}$ were orthogonal to each other). It is better than the prediction from diagonalization of $\bar{A}$.

Increasing the total number of scatterers increases the density of internal states and causes more subradiant peaks to overlap with each other. Increasing the inter-scatterer distances (thus shrinking the spread of energy shifts) also causes more subradiant peaks to overlap, making them less resolved (Fig. 6.18).

Fig. 6.19 shows the total cross section as a function of incident photon frequency for the same random lattice of atoms in ground state in Fig. 6.1. The superradiant peaks overlap significantly with each other and collectively provide a background which is mostly shifted higher in frequency. Most of the subradiant peaks do not overlap with each other. The narrow subradiant peaks based on the background indicate the long-lifetime subradiant states.

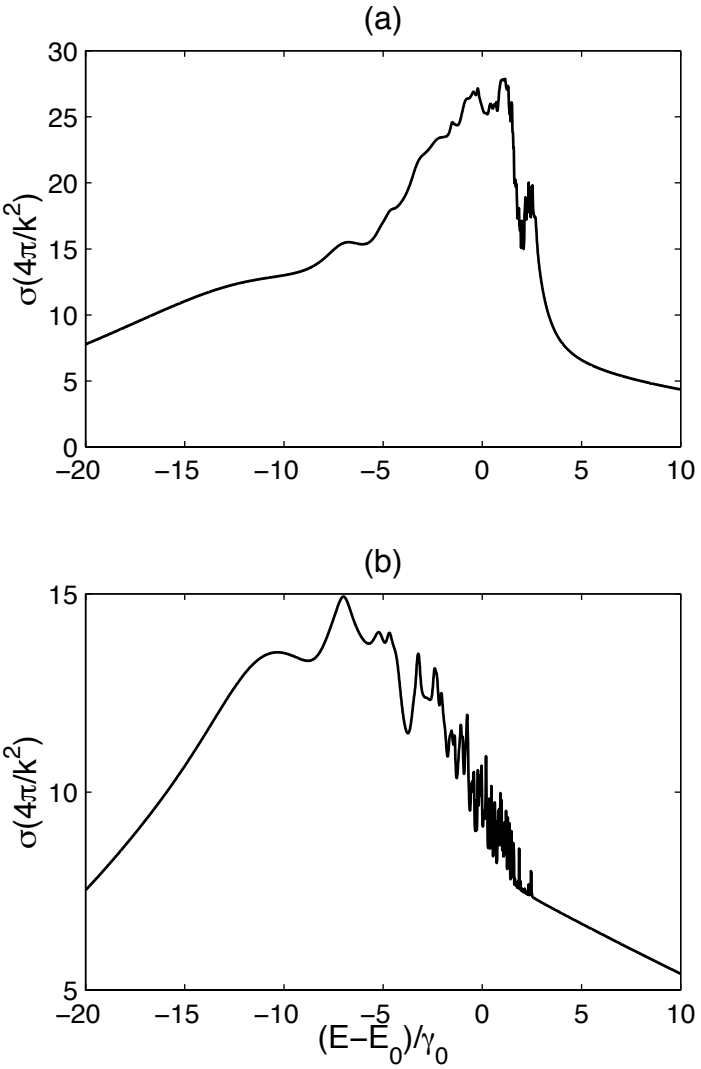

Figure 6.17: Approximate scattering spectra for a random lattice of scatterers in Fig. 6.1. (a) Prediction from eigenvalues of $\bar{A}$ (E_α's) and their corresponding Γ_α's. (b) Prediction from eigenvalues of $\bar{H}$.

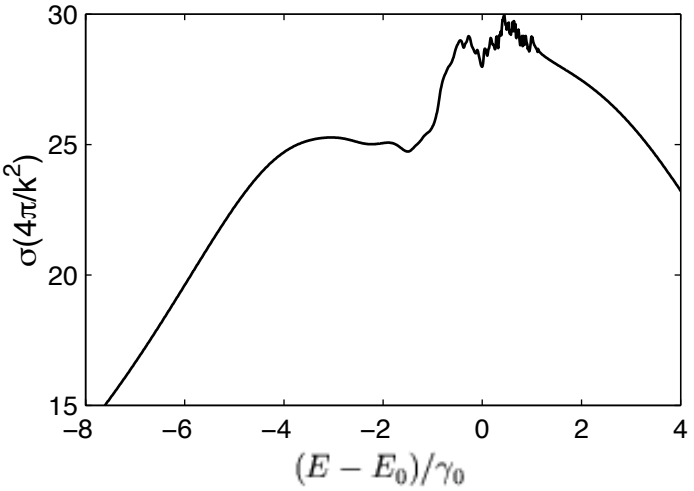

Figure 6.18: Scattering spectrum for a sparser random lattice of scatterers, with $N_x = 20$, $N_y = 10$, $a = 0.2\lambda_0$ and $v = 0.4$. The difference to Fig. 6.1 is that a is twice as large.

For the same configuration of scatterers/atoms, the subradiant peaks are more separate and resolved for photon scattering than for particle scattering. This is because the shifts are spread over a larger range. The individual subradiant peaks for the random lattice of atoms are much narrower than the resonance peak of a single atom. They might be useful in precision measurement of frequency.

Fig. 6.20(a) shows the prediction of the scattering spectrum for the random lattice of atoms from diagonalization of $\bar{A}$. Fig. 6.20(b) shows the prediction of the scattering spectrum from diagonalization of $\bar{H}$. It is better than the prediction from diagonalization of $\bar{A}$. Both predicts the scattering spectrum better than their counter parts for particle scattering by scatterers. Again, this is because the shifts are more spread out for photon scattering by atoms, and there is less overlap or interference between individual peaks.

Increasing the total number of atoms increases the density of internal states and causes more subradiant peaks to overlap. Increasing the interatomic distances (thus shrinking the spread of frequency shifts) also causes more subradiant peaks to overlap, making them less resolved (Fig. 6.21).

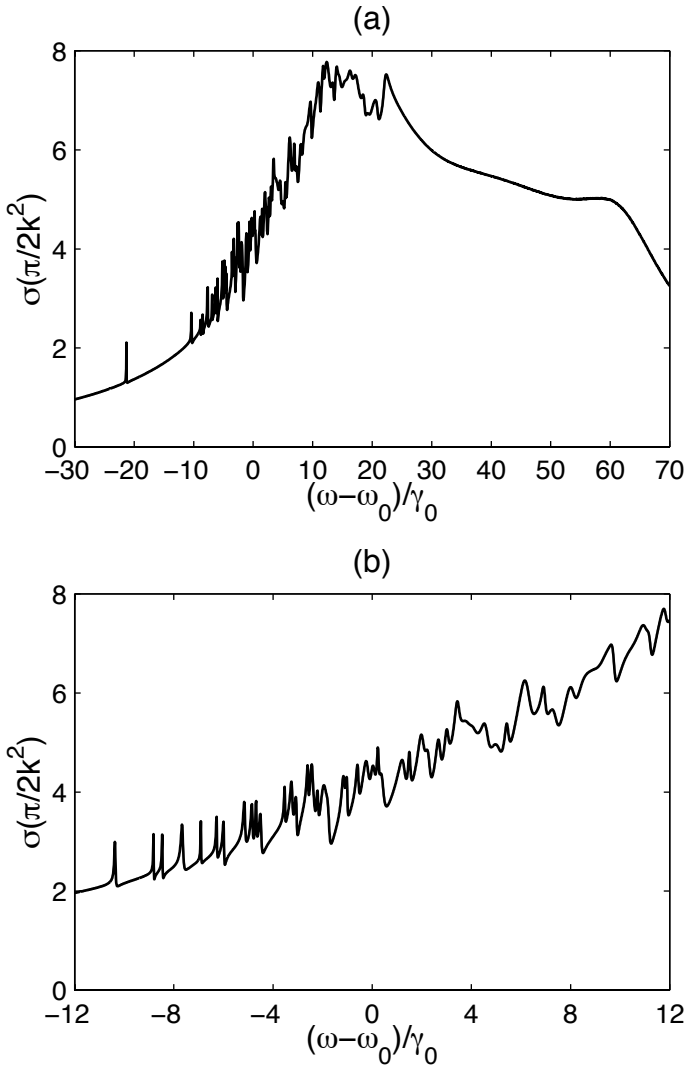

Figure 6.19: (a) Total cross section as a function of incident photon frequency for a random lattice of atoms in Fig. 6.1. (b) An enlargement of some of the subradiant peaks in (a).

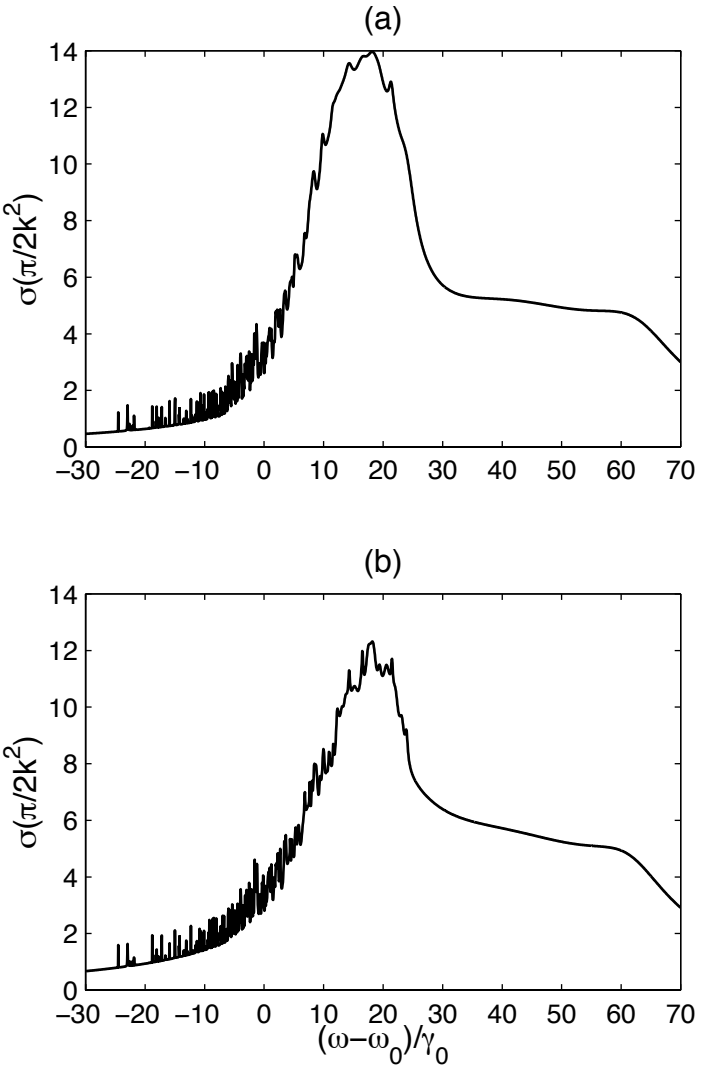

Figure 6.20: Approximate scattering spectra for a random lattice of atoms in Fig. 6.1. (a) Prediction from eigenvalues of $\bar{A}$ (ω_α's) and their corresponding Γ_α's. (b) Prediction from eigenvalues of $\bar{H}$.

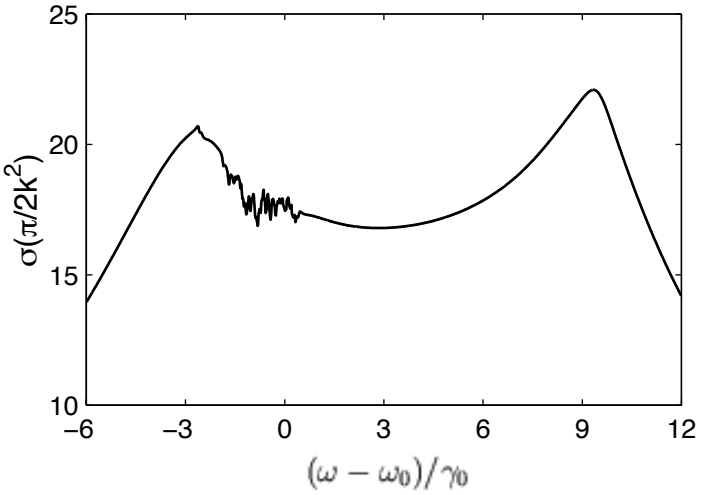

Figure 6.21: Scattering spectrum for a sparser random lattice of atoms, with $N_x = 20$, $N_y = 10$, $a = 0.2\lambda_0$ and $v = 0.4$. The difference to Fig. 6.1 is that a is twice as large.

6.2 Further Topics

6.2.1 Validity of Markov Approximation

In this subsection, we discuss the validity of Markov approximation for particle and photon scattering by random 2D lattices. In previous section, we have shown that the Green's function between scatterers/atoms more than $\lambda_0/2$ apart can be neglected compared to the Green's function between neighboring scatterers/atoms, if neighboring scatterers/atoms are proximate. For $a < (\lambda_0/2)$, the random lattice and be thought of as a sum of small-sample areas of $(\lambda_0/2)^2$. Similar to small-sample cases discussed in Chapters 2 and 5, the validity condition is

$$N_\lambda \left\langle \frac{1}{x} \right\rangle \gamma_0 \ll E_0 \tag{6.4}$$

for particle scattering and

$$N_\lambda \left\langle \frac{1}{x^3} \right\rangle \gamma_0 \ll \omega_0 \tag{6.5}$$

for photon scattering. N_λ is the number of scatterers/atoms within an area of $(\lambda_0/2)^2$, and $\left\langle \frac{1}{x} \right\rangle$ and $\left\langle \frac{1}{x^3} \right\rangle$ are taken within a square area of $(\lambda_0/2)^2$.

For sparser lattices where $a \gtrsim (\lambda_0/2)$, the eigenchannels at each energy (and thus internal states, eigenchannels at their respective peaks) are

very sensitive to the energy of incident particle/photon. This is because the Green's function has the factor of $e^{ikr_{ij}}$ which is very sensitive to k when r_{ij} is large. However, the Green's function itself is small when scatterers/atoms are more than half the wavelength apart, and multiple scattering effects are not important. For sparse lattices, the internal states have small shifts and widths $\sim \gamma_0$. The scattering spectrum is not affected by Markov approximation, as long as Markov approximation is valid for a single scatterer/atom.

6.2.2 Scattering by Samples with More Disorder

For the random lattices we have studied in previous section, if we increase the variability to $v \gtrsim 1$, the sample cannot be considered as a "lattice" any more. For photon scattering by atoms in ground state, the scattering spectrum is *qualitatively* different. Superradiant peaks are less wide and less delocalized. There are more localized subradiant states and the degree of localization is much higher. In addition, some pairs of atoms may be very proximate to each other. Due to the $\frac{1}{x^3}$ dependence on the interatomic distance for the real part of Green's function or generalized dipole-dipole interaction, internal states localized on these pairs have huge shifts compared to the shifts

of internal states for regular random lattices. Intuitively, these very proximate pairs of atoms can be considered as "molecules", which have multiple excited states at different energies. The whole sample includes nonidentical molecules. For particle scattering by scatterers, the "molecule forming effects" are much less pronounced. This is because the real part of Green's function has $\frac{1}{x}$ dependence on inter-scatterer distance, less sensitive than for photon scattering.

6.3 Summary

In this chapter, we have studied particle or photon scattering by large random lattices of s-wave point scatterers or point two-level atoms in ground state. Intuitively, each large sample can be thought of as a sum of small-sample areas of $(\lambda_0/2)^2$. All superradiant states are delocalized. In the scattering spectrum, their peaks overlap significantly and collectively give a background, mostly shifted lower in energy for particle scattering and higher in frequency for photon scattering. Subradiant states can be either delocalized or localized. They give narrow resonance peaks on top of the background.

Increasing the total number of scatterers/atoms increases the density of

internal states. Increasing the inter-scatterer/atom distances shrinks the spread of shifts and the superradiant peak widths. Increasing the the degree of disorder of the random lattice increases the localization of subradiant states. For samples with more disorder, the scattering spectra become qualitatively different from random lattices.

Bibliography

[1] L.S. Rodberg and R.M. Thaler, *Introduction to the Quantum Theory of Scattering* (Academic, New York, 1967).

[2] M.L. Goldberger and K.M. Watson, *Collision Theory* (Wiley, New York, 1964).

[3] S. Albeverio, F. Geszetsky, R. Høegh-Krohn, and H. Holden, *Solvable Models in Quantum Mechanics* (Springer-Verlag, Berlin, 1989).

[4] Yu.N. Demkov and V.N. Ostrovskii, *Zero-range Potentials and Their Applications in Atomic Physics* (Plenum, New York, 1988).

[5] J.S. Hersch, Ph.D. Thesis (Harvard University, Cambridge, MA, 1999).

[6] M. Rusek, J. Mostowski, and A. Orłowski, Phys. Rev. A **61**, 022704 (2000).

[7] B.A. Lippmann and J. Schwinger, Phys. Rev. **79**, 469 (1950).

[8] V.V. Sokolov and V.G. Zelevinsky, Nucl. Phys. A **504**, 562 (1989).

[9] V.V. Sokolov and V.G. Zelevinsky, Ann. Phys. (N.Y.) **216**, 323 (1992).

[10] I. Tolstoy, J. Acoust. Soc. Am. **80**, 282 (1986).

[11] I. Tolstoy, J. Acoust. Soc. Am. **83**, 2086 (1988).

[12] C. Feuillade, J. Acoust. Soc. Am. **98**, 1178 (1995).

[13] E.J. Heller, Phys. Rev. Lett. **77**, 4122 (1996).

[14] R. Szmytkowski and C. Szmytkowski, Phys. Lett. A **235**, 217 (1997)

[15] J.S. Hersch and E.J. Heller, Phys. Rev. Lett. **81**, 3059 (1998).

[16] U. Fano, Phys. Rev. **124**, 1866 (1961).

[17] U. Fano and J.W. Cooper, Rev. Mod. Phys. **40**, 441 (1968).

[18] M.H. Anderson, J.R. Ensher, M.R. Matthews *et al.*, Science **269**, 198 (1995).

[19] D.G. Fried, T.C. Killian, L. Willmann *et al.*, Phys. Rev. Lett. **81**, 3811 (1998).

[20] A. Robert, O. Sirjean, A. Browaeys *et al.*, Science **292**, 461 (2001).

[21] D. Jaksch, C. Bruder, J.I. Cirac *et al.*, Phys. Rev. Lett. **81**, 3108 (1998).

[22] R.H. Dicke, Phys. Rev. **93**, 99 (1954).

[23] M. Gross and S. Haroche, Phys. Rep. **93**, 301 (1982).

[24] R.G. DeVoe and R.G. Brewer, Phys. Rev. Lett. **76**, 2049 (1996).

[25] P. Mataloni, E. De Angelis, and F. De Martini, Phys. Rev. Lett. **85**, 1420 (2000).

[26] P.D. Drummond and H.J. Carmichael, Opt. Commun. **27**, 160 (1978).

[27] R.G. Brewer, Phys. Rev. Lett. **77**, 5153 (1996).

[28] H.T. Dung and K. Ujihara, Phys. Rev. Lett. **84**, 254 (2000).

[29] G.S. Agarwal and A.K. Patnaik, Phys. Rev. A **63**, 043805 (2001).

[30] J.P. Clemens and H.J. Carmichael, Phys. Rev. A **65**, 023815 (2002).

[31] S. Schneider and G.J. Milburn, Phys. Rev. A **65**, 042107 (2002).

[32] C. Cohen-Tannoudji, J. Dupont-Roc and G. Grynberg, *Atom-photon Interactions: Basic Processes and Applications* (Wiley, New York, 1992).

[33] L. Allen and J.H. Eberly, *Optical Resonance and Two-level Atoms* (Dover, New York, 1987).

[34] A.A. Belavin, B.Ya. Zeldovich, A.M. Perelomov *et al.*, Sov. Phys. JETP **56**, 264 (1969).

[35] R.H. Lemberg, Phys. Rev. A **2**, 883 (1970).

[36] G.S. Agarwal, Phys. Rev. A **2**, 2038 (1970).

[37] G.S. Agarwal, *Quantum Statistical Theories of Spontaneous Emission and Their Relation to Other Approaches*, Springer Tracts in Modern Physics Vol. 70: Quantum Optics (Springer-Verlag, Berlin, 1974).

[38] J.D. Jackson, *Classical Electrodynamics* 3ed. (Wiley, New York, 1999).

[39] F. Friedberg and S.R. Hartmann, Opt. Commun. **10**, 298 (1974).

[40] K.M. Watson, J. Math. Phys. **10** 688 (1969).

[41] G.S. Agarwal, A.C. Brown, L.M. Narducci *et al.*, Phys. Rev A **15**, 1613 (1977).

[42] M.O. Scully and K. Drühl, Phys. Rev. A **25**, 2208 (1982).

[43] M.G. Moore and P. Meystre, Phys. Rev. Lett. **25** 5202 (1999).

[44] P. de Vries, D.V. van Coevorden, and A. Lagendijk, Rev. Mod. Phys **70**, 447 (1998).

[45] P. Meystre and M. Sargent III, *Elements of Quantum Optics* (Springer-Verlag, Berlin, 1991).

[46] A. Cives-Esclop, A. Luis, and L.L. Sánchez-Soto, J. Mod. Opt. **46**, 639 (1999).

[47] E.M. Purcell and C.R. Pennypacker, Astrophys. J. **186**, 705 (1973).

[48] D. Sornette and B. Souillard, Europhys. Lett. **7** 269 (1988).

[49] T.M. Nieuwenhuizen, A. Burin, Y. Kagan *et al.*, Phys. Lett. A **184** 360 (1994).

[50] C.A. Müller and C. Miniatura, J. Phys. A **35** 10163 (2002).

[51] P.W. Anderson, Phys. Rev. **109** 1492 (1958).

[52] P.W. Anderson, Rev. Mod. Phys. **50** 191 (1978).